

*Institute of Paper Science and Technology
Atlanta, Georgia*

SLIDE MATERIAL

To The

PAPERMAKING

And

PROCESS SIMULATION AND CONTROL

PROJECT ADVISORY COMMITTEE

March 22, 1994

INSTITUTE OF PAPER SCIENCE AND TECHNOLOGY PURPOSE AND MISSION STATEMENT

The Institute of Paper Science and Technology is a unique organization whose charitable, educational, and scientific purpose evolves from the singular relationship between the Institute and the pulp and paper industry which has existed since 1929. The purpose of the Institute is fulfilled through three missions, which are:

- to provide high quality students with a multidisciplinary graduate educational experience which is of the highest standard of excellence recognized by the national academic community and which enables them to perform to their maximum potential in a society with a technological base; and
- to sustain an international position of leadership in dynamic scientific research which is participated in by both students and faculty and which is focused on areas of significance to the pulp and paper industry; and
- to contribute to the economic and technical well-being of the nation through innovative educational, informational, and technical services.

ACCREDITATION

The Institute of Paper Science and Technology is accredited by the Commission on Colleges of the Southern Association of Colleges and Schools to award the Master of Science and Doctor of Philosophy degrees.

NOTICE AND DISCLAIMER

The Institute of Paper Science and Technology (IPST) has provided a high standard of professional service and has put forth its best efforts within the time and funds available for this project. The information and conclusions are advisory and are intended only for internal use by any company who may receive this report. Each company must decide for itself the best approach to solving any problems it may have and how, or whether, this reported information should be considered in its approach.

IPST does not recommend particular products, procedures, materials, or service. These are included only in the interest of completeness within a laboratory context and budgetary constraint. Actual products, procedures, materials, and services used may differ and are peculiar to the operations of each company.

In no event shall IPST or its employees and agents have any obligation or liability for damages including, but not limited to, consequential damages arising out of or in connection with any company's use of or inability to use the reported information. IPST provides no warranty or guaranty of results.

The Institute of Paper Science and Technology assures equal opportunity to all qualified persons without regard to race, color, religion, sex, national origin, age, handicap, marital status, or Vietnam era veterans status in the admission to, participation in, treatment of, or employment in the programs and activities which the Institute operates.

INSTITUTE OF PAPER SCIENCE AND TECHNOLOGY

Atlanta, Georgia

SLIDE MATERIAL

PAPERMAKING

And

PROCESS SIMULATION AND CONTROL

March 22, 1994

ADVANCES IN IMPULSE DRYING RESEARCH

SLIDE MATERIAL

FOR

PROJECT 3470

March 22, 1994
Institute of Paper Science and Technology
Atlanta, Georgia

Project Title:	FUNDAMENTALS OF DRYING
Project Staff:	David Orloff
Budget (FY93-94):	\$207,000
Reporting Period:	March 1993 - March 1994
Division:	Engineering and Paper Materials
Project Code:	DRYING
Project No.	3470

OBJECTIVE

To develop an understanding and a database for commercialization of advanced water removal systems, based on high intensity drying principles. This new technology will reduce capital costs, increase machine productivity, reduce the amount of energy used, and improve properties.

GOAL

To commercialize the impulse drying process by 1998.

SUMMARY

Over the past year we have focused on mechanical design issues as well as process issues.

Key accomplishments for the reporting period include:

°Union Camp, Beloit and the Institute have agreed, "in principle", to jointly commercialize impulse drying for board grades.

°Experiments on Beloit's batch-pilot extended-nip shoe press confirmed the conditions under which multi-ply/recycle containing linerboard could be successfully impulse dried and printed. Sheet sticking problems were resolved by insuring the smoothness of the surface of the press roll.

°A numerical model of a proposed controlled-crown impulse drying press roll was initiated in order to explore design parameters that optimize energy utilization and to predict stress within the impulse drying press roll.

°A high speed test stand, to document the long term durability of impulse drying press roll coatings, has been designed. The hydraulics and controls of the Institutes' impulse drying simulator have been improved to allow better control of press pulse shape.

SUMMARY (CONTINUED)

° Student work is being completed, to determine the interdependency of the "thermal mass" of the heated press roll surface and press impulse on impulse drying performance.

° Student work to measure heat and mass transfer to a sheet during steam box operation has begun with the design and construction of an apparatus that can operate at speeds of 2500 feet per minute.

° Student work to investigate ways of opening the operating window of impulse drying have begun with the design of an apparatus to determine the effect of nip opening pressure on flash evaporation and sheet delamination.

DISCUSSION OF KEY RESULTS

Commercialization Of Impulse Drying For Board Grades

Agreement is being finalized.

A proposal to DOE is in preparation.

Batch-Pilot Extended-Nip Shoe Press Experiments At the Beloit Corporation

Sheet Sticking:: Previously observed high temperature sheet sticking was due to excessive press roll surface roughness.

Press Roll Surface Strength: The IPST "C" roll coating was susceptible to chipping under shear, while the Beloit "A" roll did not chip.

Critical Impulse Drying Temperature : Critical impulse drying temperature was confirmed to depend on the hydrodynamic specific surface of the heated layer of the sheet and was higher for the "low thermal mass" IPST "C" press roll than for the "higher thermal mass" Beloit "A" press roll. Felt choice influenced critical temperature.

DISCUSSION OF KEY RESULTS

Batch-Pilot Extended-Nip Shoe Press Experiments At the Beloit Corporation

Press Dryness: Press dryness decreased when the hydrodynamic specific surface of the sheet increased. Impulse dried dryness was generally higher than that achieved by double-felted pressing. The Beloit "A" roll yielded higher press dryness than the IPST "C" roll, even though it was generally operated at lower temperature.

STFI Compression Strength : The Geometric mean STFI compression strength of impulse dried sheets were consistently higher than that obtained by double-felted pressing. No substantial strength difference was observed comparing sheets impulse dried with the Beloit "A" roll to those dried using the IPST "C" press roll.

Sheet Surface Roughness: Impulse dried samples were smoother than single-felted pressed samples, which were smoother than double-felted pressed samples.

Printability: Selected samples were printed on a commercial flexographic printing press and evaluated for print quality. Double felted pressed sheets tended to have the worst mottle, while the mottle exhibited by impulse dried sheets was equal to or less than that exhibited by single felted pressed sheets.

DISCUSSION OF KEY RESULTS

A Numerical Model Of A Proposed Controlled-Crown Impulse Drying Press Roll

The long term durability of press roll surfaces requires study. Hence, an analytical modeling effort was initiated that will eventually lead to the prediction of stress and temperature as a function of position and time in the various layers of a commercial impulse drying press roll.

As a first step, a closed form model of lubrication and heat transfer at the boundary between the internal hydrostatic shoe and the inside of the roll shell was undertaken. The objective of the analysis was to predict pressure and temperature distributions at this interface. Once accomplished, these distributions will act as boundary conditions to a finite element model of the varied layer press roll. An additional objective of the lubrication and heat transfer models was to provide design assistance to Beloit.

DISCUSSION OF KEY RESULTS

Design Of A High Speed Press Roll Durability Test Stand

Through an EPRI grant IPST has designed a modification to the existing pilot impulse dryer to allow it to function as a press roll durability test stand. The design calls for removing the second nip and installing the induction heater on the first nip in place of the infrared heater. With some additional drive changes, this will allow test stand to operate at speeds of 2500 fpm.

6 DOE will fund the construction, instrumentation and operation of the durability test stand. Three test coatings will be tested at the same time. The coated roll will be heated, by induction, to 250°C, will be driven at 2500 fpm and will be loaded against a wet felt acting as a heat sink. The roll surface will be continuously monitored by infrared thermography to detect the onset of surface flaws in the coating and surface strain will be measured using three dimensional speckle interferometry. Experimental surface strains will be compared to the predictions of the finite element model.

DISCUSSION OF KEY RESULTS

Interdependency Of "Thermal Mass" And Press Impulse

Laboratory experiments were conducted to determine the interdependency of the "thermal mass" of the heated press roll surface and press impulse on impulse drying performance. Process conditions were chosen that were similar to the conditions used for the Beloit batch-pilot extended-nip shoe press experiments, providing laboratory confirmation of the results. The IPST "C" surface coating and an alternate coating IPST "A" were used as well as a mild steel surface for contrast, all platens having surface thermocouples mounted to record surface energy transfer. Each surface coating was tested at a constant dwell time of 40 ms and pressures of 6000, 7500, and 9000 pli using extra sheets of furnishes FD5 (100% OCC @ 450 ml CSF) and FD6 (740 virgin Kraft top ply with 50/50 blend of virgin Kraft and OCC bottom ply), left over from the pilot trials.

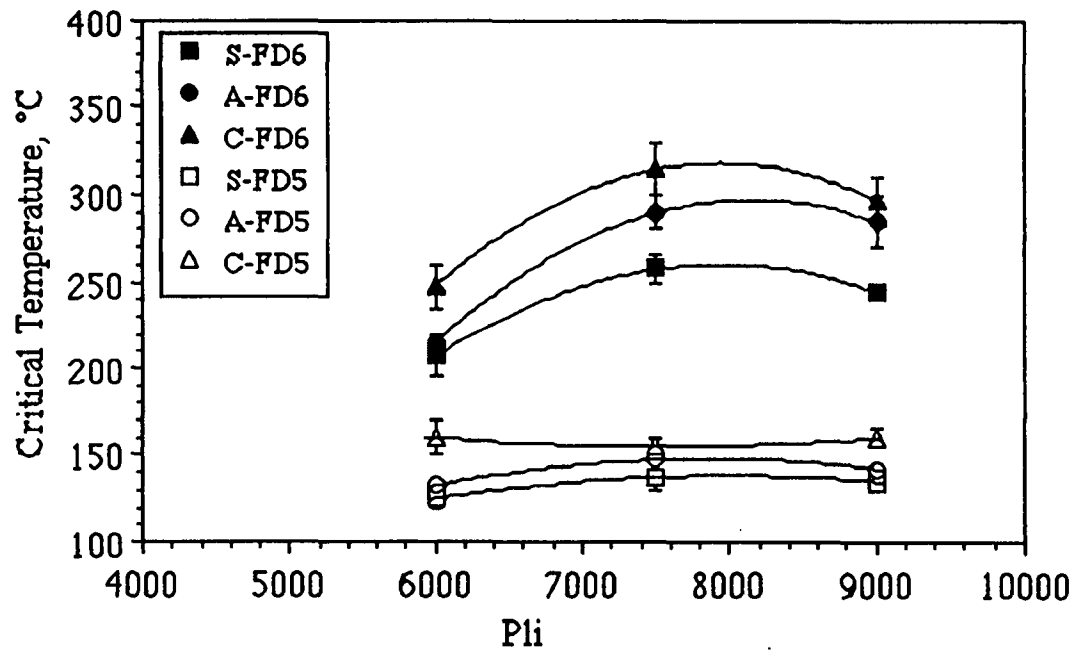
"Thermal mass" values for each coating type

<u>Temperature</u> (°C)	<u>IPST "A"</u>	<u>IPST "C"</u>	<u>Mild Steel</u>
100	3260	1973	7211
200	3619	2050	7729
300	3949	2084	8178
400	4633	2091	8624

DISCUSSION OF KEY RESULTS

Interdependency Of "Thermal Mass" And Press Impulse

Critical impulse drying temperatures were substantially higher for FD6 sheets having hydodynamic specific surface of $1.3 \text{ m}^2/\text{g}$ than for FD5 sheets having hydodynamic specific surface of $10.5 \text{ m}^2/\text{g}$. Use of platens with lower "Thermal Mass" resulted in higher critical temperatures. For the FD6 sheets, increased press loading increases critical temperature until a maximum is reached at about 8000 pli.

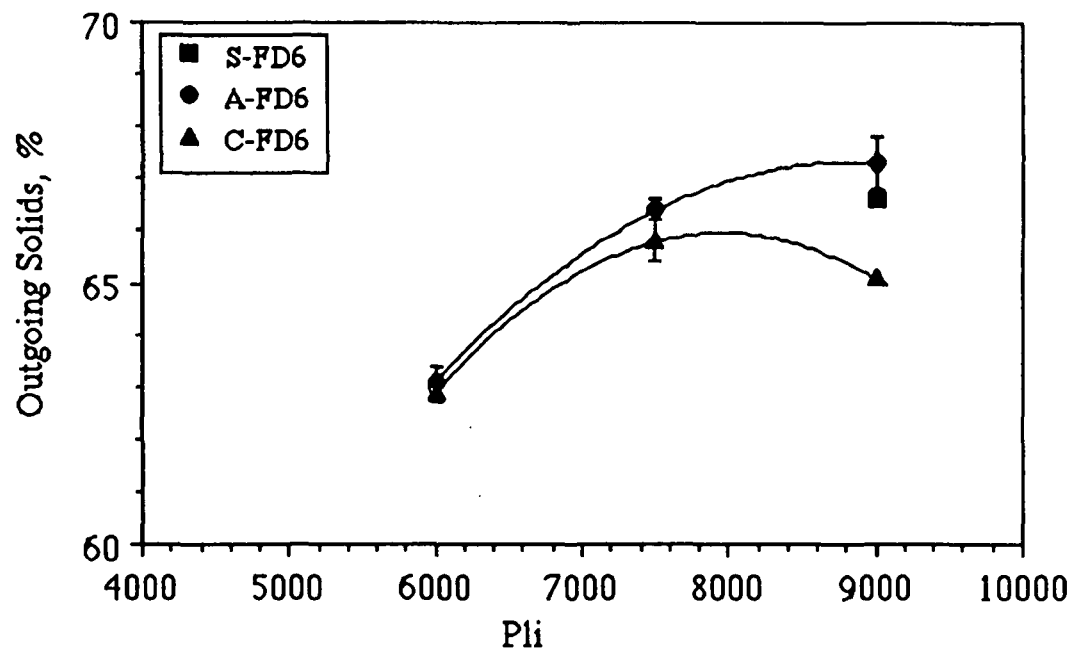


Critical Impulse Drying Temperature As A Function Of Pli

DISCUSSION OF KEY RESULTS

Interdependency Of "Thermal Mass" And Press Impulse

Limited outgoing solids data suggests that even though the IPST "C" roll operated at higher temperature than the IPST "A" surface, outgoing solids were higher for the IPST "A" case than the IPST "C" case. For the IPST "A" surface, outgoing solids was highest at the highest press load of 9000 pli, while the IPST "C" surface yielded maximum outgoing solids at about 8000 pli.

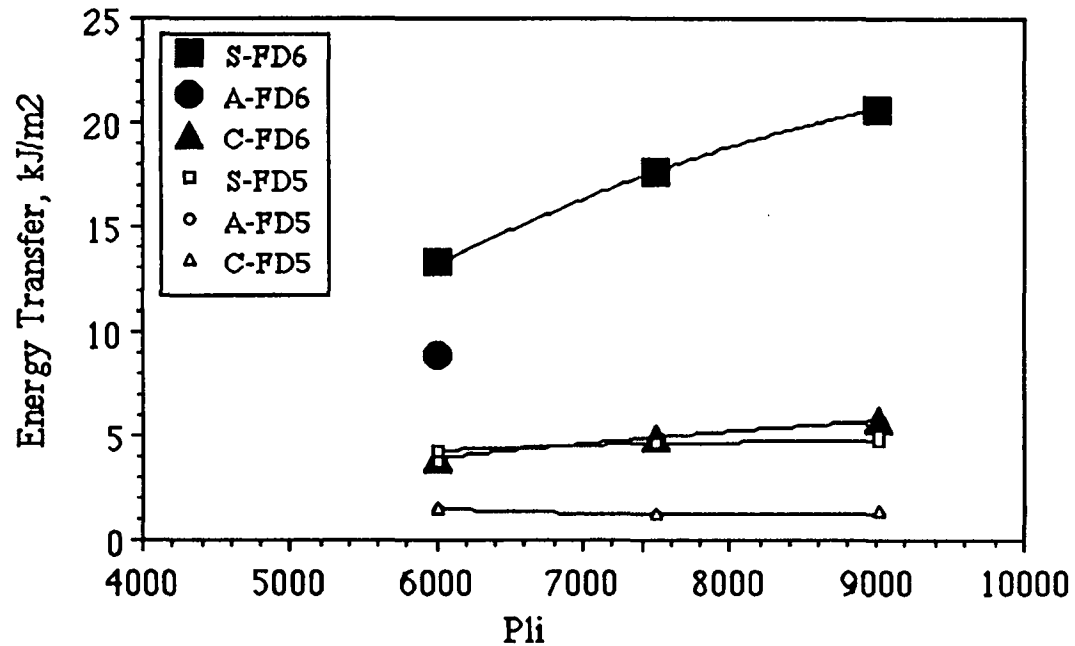


Outgoing Solids As A Function Of Pli

DISCUSSION OF KEY RESULTS

Interdependency Of "Thermal Mass" And Press Impulse

The IPST "C" roll surface is relatively independent of press load, while the IPST "S" roll surface is highly dependent on press load. Unfortunately, we do not have sufficient energy data for the IPST "A" surface to show its press load dependency. It is interesting to note the similar sheet impulse dried at the same impulse but with different press roll surfaces delaminated at different amounts of energy transfer. This suggests that we examine differences in the permeability of the heated layer of sheets to explain this dissimilarity. At the time of this writing, we have initiated these measurements.

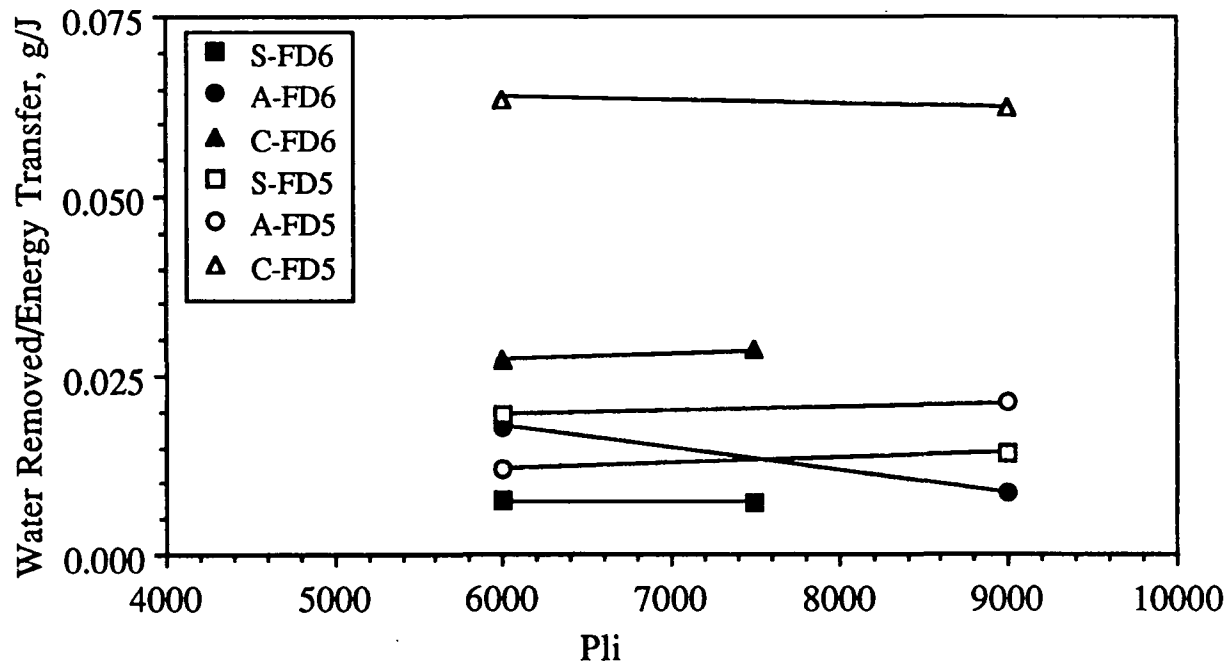


Energy Transfer To The Sheet During Impulse Drying As A Function Of Pli

DISCUSSION OF KEY RESULTS

Interdependency Of "Thermal Mass" And Press Impulse

The ratio of water removed to energy transferred during impulse drying is plotted, as a function of press load, in the figure below. The data confirms, that the IPST "C" roll surface results in more water removal for a given amount of energy transfer to the sheet.



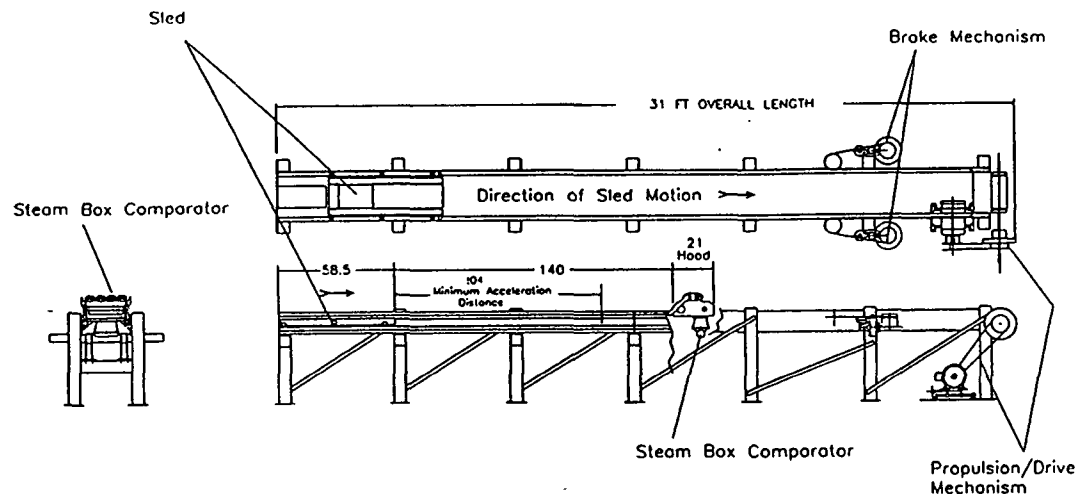
The Ratio Of Water Removed To Energy Transferred As A Function Of Pli

DISCUSSION OF KEY RESULTS

Heat And Mass Transfer To A Sheet During Steam Box Operation

Impulse drying performance is maximized when the sheet has been preheated as close to 100°C as possible. To ensure optimum performance of impulse drying, as well as conventional pressing, steam boxes may be used to preheat paper webs. Published heat and mass transfer correlations, allowing the accurate sizing of steam boxes, is scarce. There are disagreements as to the relative benefits of various commercial designs and operating conditions. There is no data to predict steam box performance as a function of sheet structure/permeability.

Two student projects have been initiated to develop instrumentation to measure temperature and moisture profiles, through sheets traversing under pilot steam boxes at commercial speeds. The apparatus to accelerate and decelerate an instrumented paper web under an instrumented pilot steam box has been constructed as shown below.



The IPST Steam Box Comparator - "Rocket Sled"

GOALS FOR FY: 1994-1995

The Institute will complete the formation of the agreement to commercialize impulse drying. Once formed, and funded by DOE, the Institutes dues' funded impulse drying work will concentrate aspects which will expand the usefulness of impulse drying technology to grades outside the scope of the commercialization agreement.

Work planned for FY'94-95 will focus on these major objectives.

Complete the numerical model of a proposed controlled-crown impulse drying press roll to explore design parameters that optimize energy utilization and to predict stress and temperature within the impulse drying press roll during typical operation.

Construct and use the high speed test stand to document the long term durability of impulse drying press roll coatings.

Complete student work to determine the interdependency of the "thermal mass" of the heated press roll surface and press impulse on impulse drying performance.

Complete student work to measure heat and mass transfer to a sheet during steam box operation.

Complete student work to investigate ways of opening the operating window of impulse drying.

FUNDAMENTALS OF COATING SYSTEMS

SLIDE MATERIAL

FOR

PROJECT 3674

March 22, 1994
Institute of Paper Science and Technology
Atlanta, Georgia

**Progress Report
to the
Research Advisory Committee**

on Project 3674

Fundamentals of Coating Systems

by

**Cyrus K. Aidun
Associate Professor**

**Institute of Paper Science and Technology
A privately funded non-profit graduate university**

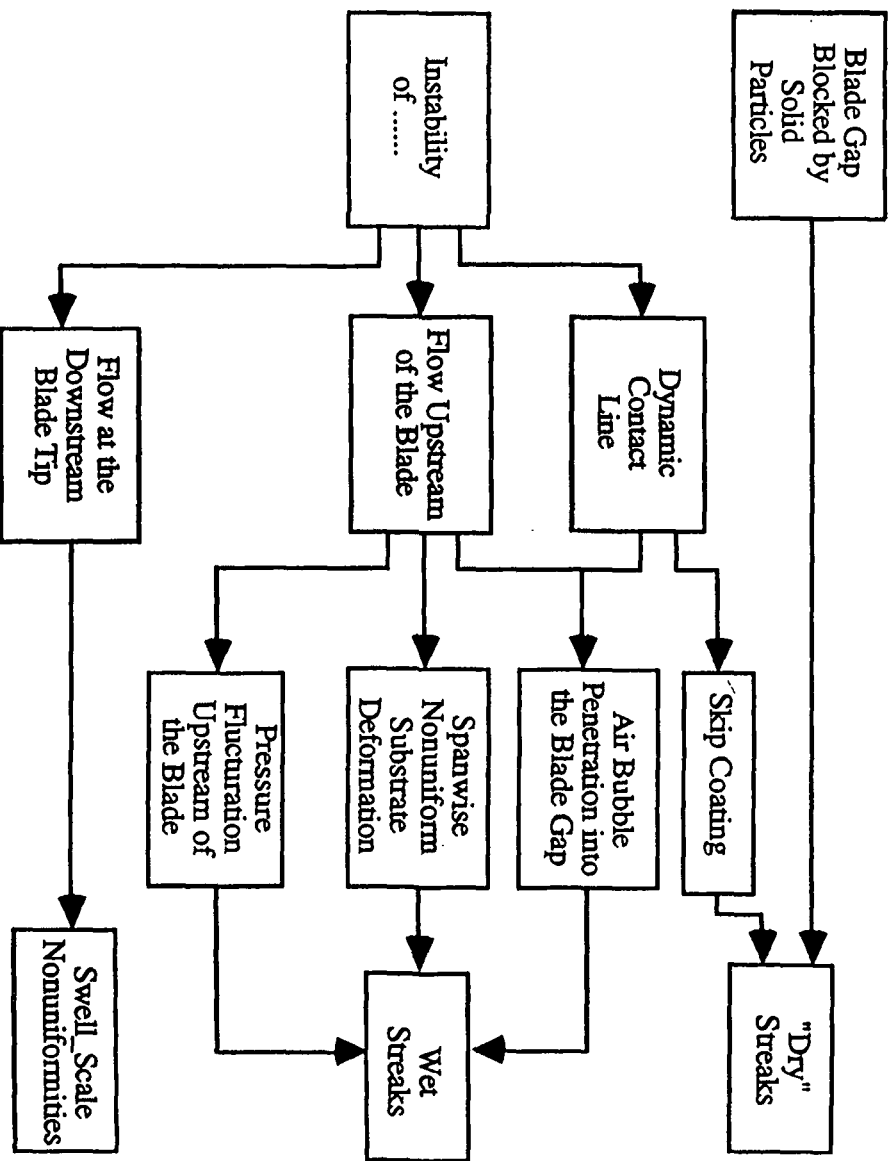
OBJECTIVES

- 1. Investigate the Cause and Origin of Problems with High-Speed Blade Coaters**
- 2. Design a Superior Coating Application System**

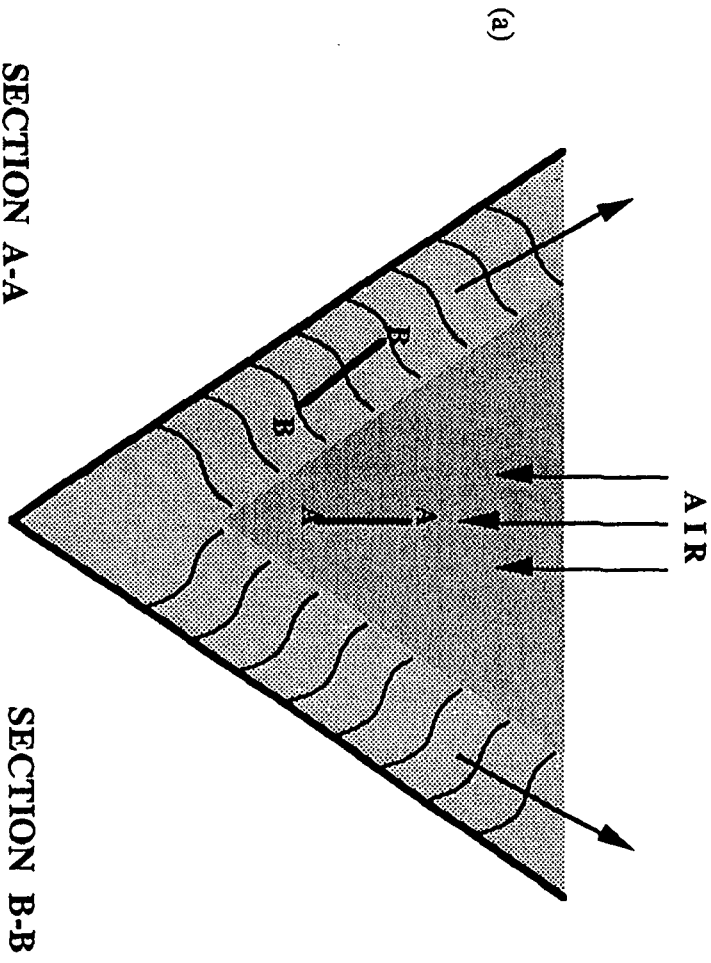
ORGANIZATION OF PRESENTATION

- **Studies of Coat-Weight Nonuniformities
(Wet Streaks)**
- **A Superior Short-Dwell Blade Coater**
- **Computational Fluid Dynamic Analysis of
Coating and Other Papermaking Processes**

COATING DEFECT MECHANISMS

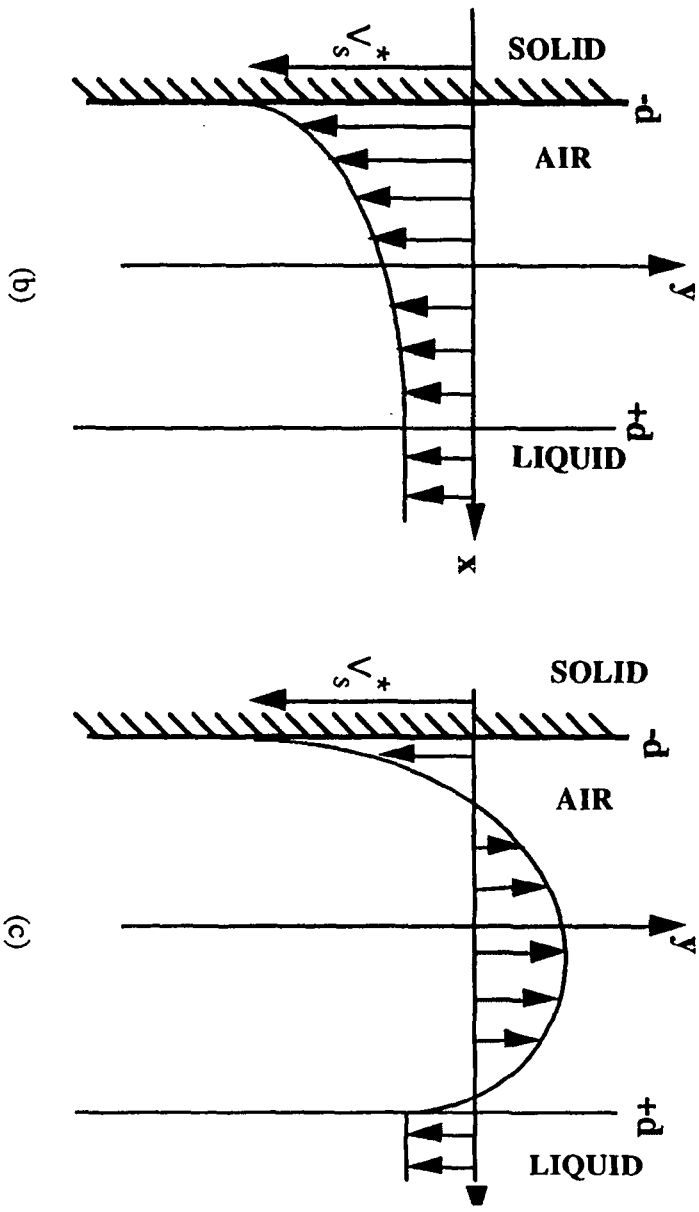


AIR ENTRAINMENT MECHANISM IN COATING



SECTION A-A

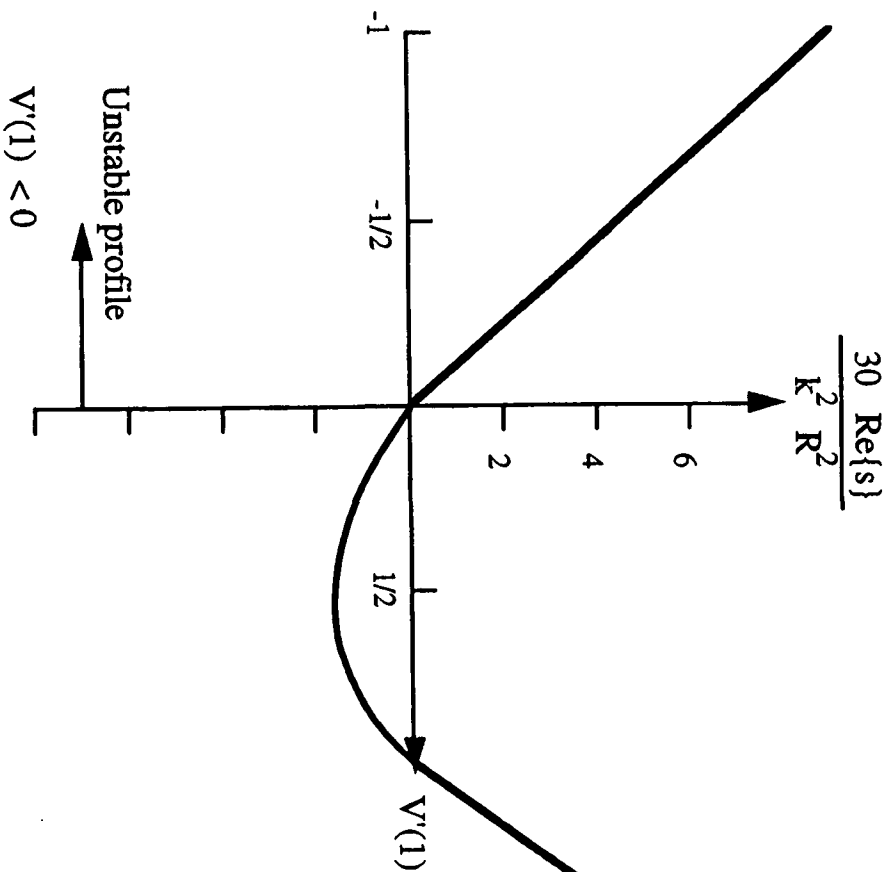
SECTION B-B



(b)

(c)

STABILITY ANALYSIS OF AN AIR/LIQUID INTERFACE



$$\text{Growth rate, } \text{Re}\{s\} = \frac{R^2}{30} \left\{ 4 \left[\frac{1}{2} - V'(1) \right]^2 - 1 \right\} k^2 + O(k^3)$$

$$\text{Phase speed, } \phi = -\text{Im}\{s\}/k = (k-1)R V'(1) + O(k^2) \quad , \quad k \ll 1$$

STABILITY ANALYSIS OF AN AIR/LIQUID INTERFACE

The stability analysis of an air/liquid interface assuming Newtonian liquid shows:

- (1) Increasing the shear viscosity of the liquid enhances interfacial instability and consequently air entrainment
- (2) The phase speed of the waves at the interface agree with experimental observations

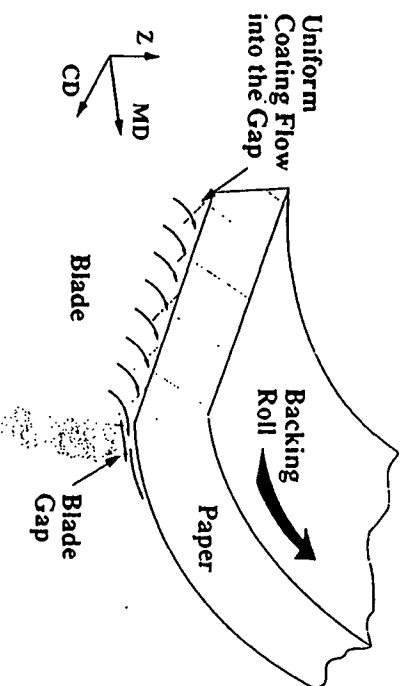


Figure 6.

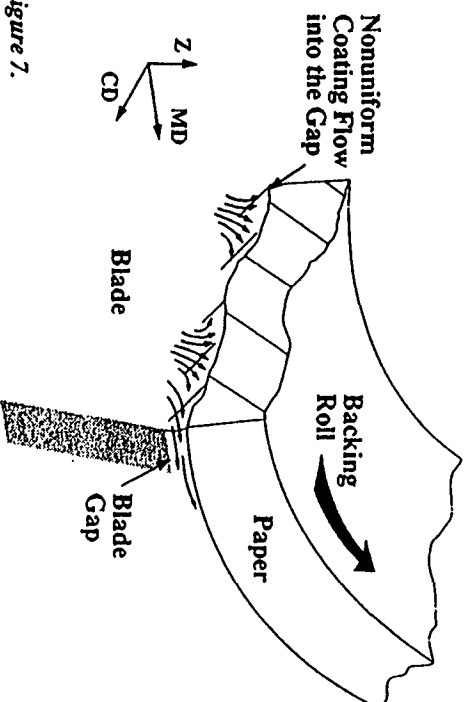


Figure 7.

Short-Term Research Plans

1. Dynamic Contact Line

A fundamental study of the interaction of the coating fluid coming into contact with a moving surface at velocities of up to 2000 m/min. The extensional stress levels experienced by the coating fluid in the neighborhood of the dynamic contact line.

2. Air Entrainment

Mechanism of air entrainment at high-speed

Effects of air entrainment on surface properties

How would the rheological characteristics of the fluid influence air entrainment into the system from the contact line.

3. Rheological Characterization

Identify the key rheological characteristics of coating colors which can explain the problem with runnability of certain formulations.

Devise a model or theory that can provide a prediction of the rheological data to coater performance.

Establish a consistent rheological constitutive model for use in computational analysis and optimization.

	U_p	L_{in}	L_{gap}	$\varphi = \frac{2U_p L_{in}}{3}$	U_w	surf.tens	μ_x viscosity	μ_o viscosity	K	ρ density	n	COM- MENTS
Run	m/s	m	m	l/s/m	m/s	kg/s ²	kg/(m s)	kg/(m s)		kg/m ³		
C1	3.0	0.0025	50 10 ⁻⁶	5.00	20.0	0.05	0.05	1.00	0.01	1200	0.65	<-- S
C2					30.0							S
C3					40.0							S
C11	5.0	0.0025	50 10 ⁻⁶	8.33	20.0	0.05	0.05	1.00	0.01	1200	0.65	S
C12	8.0			13.33								S
C13	12.0			20.0								S
C14	16.0			26.67								A
C15	20.0			33.33								<-- A

INPUT PARAMETERS FOR THE SIMULATION OF NON-NEWTONIAN FLOW (Carreau Model)

TABLE 1.

A, Attached Flow
S, Separated Flow

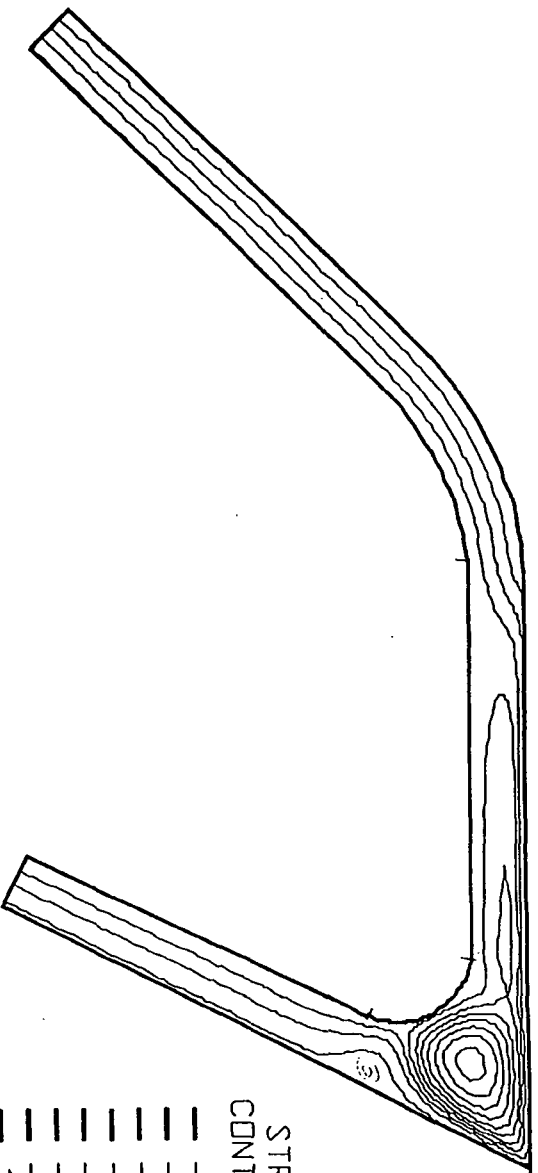
	U_b	L_{in}	L_{gap}	q pumped	q	U_w	surf.tens	μ_x viscosity	μ_o viscosity	K	ρ density	n	COM- MENTS
Run	m/s	m	m	l/s/m	l/s/m	m/s	kg/s ²	kg/(m s)	kg/(m s)		kg/m ³		
NB51	5.0	0.0025	50 10 ⁻⁶	0.0	6.25	30.0	0.05	0.05	1.00	0.01	1200	0.65	S
NB52	5.0			2.5	8.75								S
NB53	5.0			5.0	11.25								S
NB54	10.0			0.0	12.50								S
NB55	10.0			5.0	17.50								<-- A
NB61	5.0	0.0025	50 10 ⁻⁶	5.0	11.25	40.0	0.05	0.05	1.00	0.01	1200	0.65	S
NB62	10.0			5.0	17.50								A
NB63	15.0			5.0	23.75								A

INPUT PARAMETERS FOR THE SIMULATION OF NON-NEWTONIAN FLOW (Carreau Model)

TABLE 2.

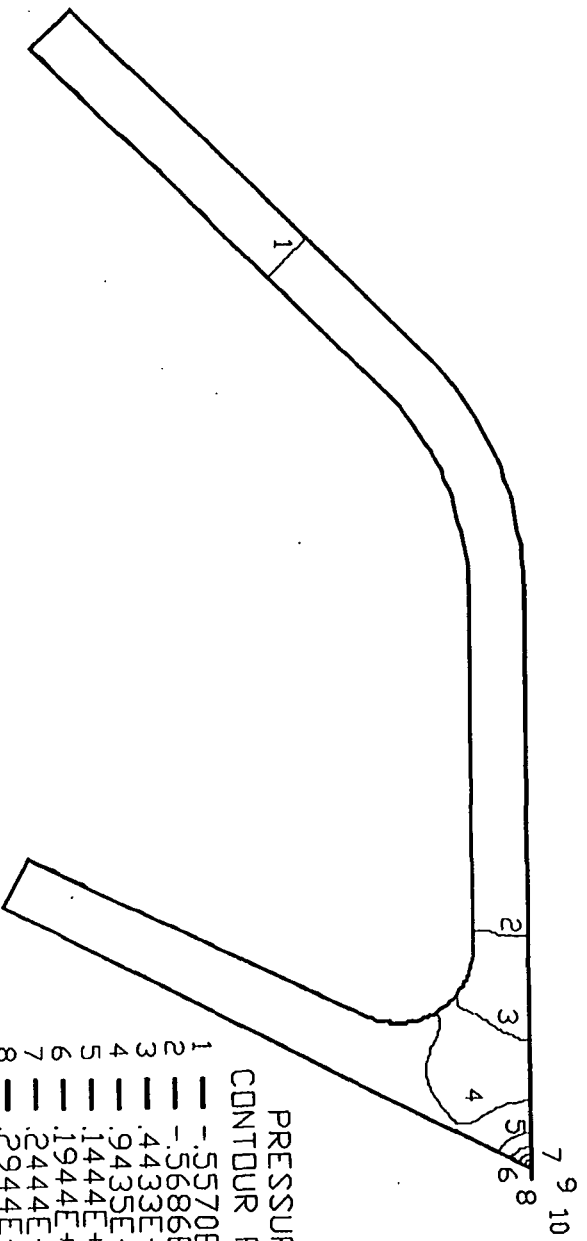
A, Attached Flow
S, Separated Flow

C1



STREAMLINE
CONTOUR PLOT

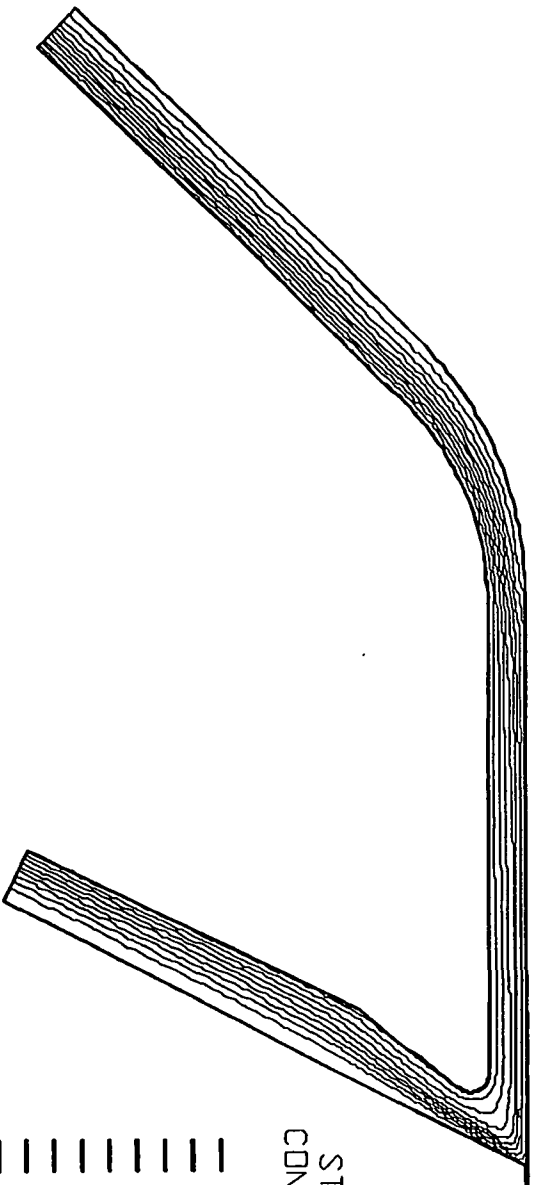
---	-1.402E+01
---	-.1185E+01
---	-.9669E+00
---	-.7491E+00
---	-.5313E+00
---	-.3135E+00
---	-.9572E-01
---	.1221E+00
---	.3399E+00
---	.5577E+00



PRESSURE
CONTOUR PLOT

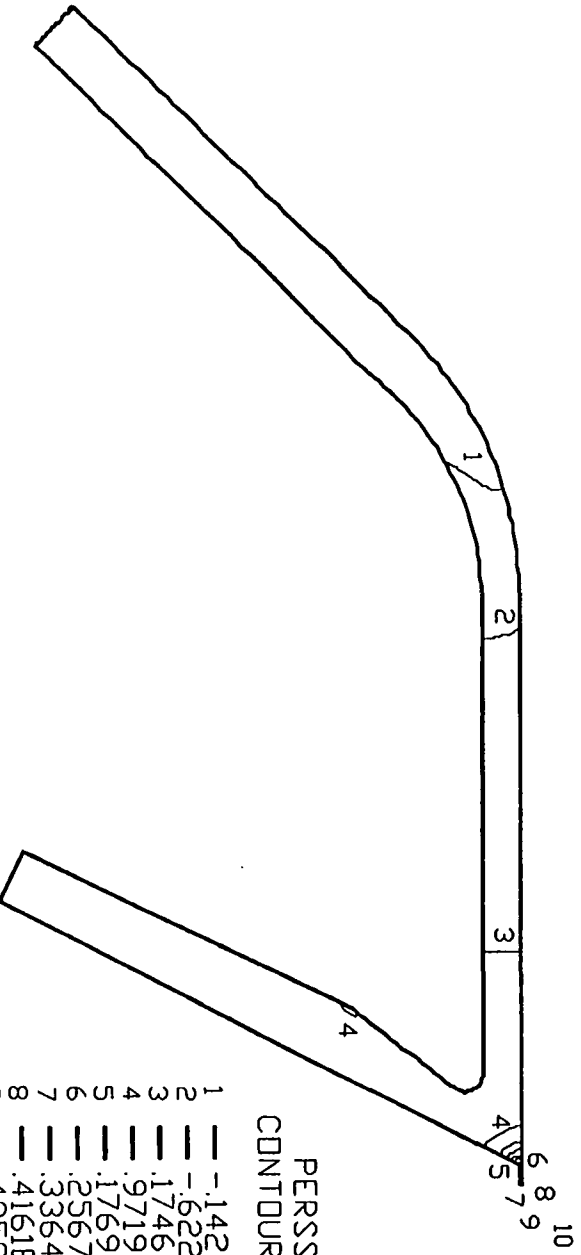
---	-5.5570E+01
---	-.5686E+00
---	.4433E+01
---	.9435E+01
---	.1444E+02
---	.1944E+02
---	.2444E+02
---	.2944E+02
---	.3444E+02
---	.3944E+02

NB55



STREAMLINE
CONTOUR PLOT

---	.2945E-01
---	.1000E+00
---	.1706E+00
---	.2414E+00
---	.3117E+00
---	.3823E+00
---	.4529E+00
---	.5235E+00
---	.5940E+00
---	.6646E+00



PRESSURE
CONTOUR PLOT

---	1	-.1420E+01
---	2	-.6228E+00
---	3	.1746E+00
---	4	.9719E+00
---	5	.1769E+01
---	6	.2567E+01
---	7	.3364E+01
---	8	.4161E+01
---	9	.4959E+01
---	10	.5756E+01

LONG-TERM OBJECTIVES

1. Develop a new high-speed coating system to provide acceptable coat-weight uniformities in both macroscopic and microscopic scales at machine speeds up to 2400 m/min with a broad spectrum of coating formulations.
2. Assist in the development of an improved short-dwell coater to allow a wide operating window in terms of coating formulations.
3. Develop on-line instrumentation for rheological characterization and control of coating colors.

AIR/SHEET INTERACTIONS

SLIDE MATERIAL

FOR

PROJECT 3730

March 22, 1994
Institute of Paper Science and Technology
Atlanta, Georgia

**Progress Report
to the
Research Advisory Committee**

on Project 3730

Air/Sheet Interactions

by

**Cyrus K. Aidun
Associate Professor**

Institute of Paper Science and Technology

A privately funded non-profit graduate university

GOALS

- (1) to investigate and optimize the paper and board formation process, and**
- (2) to develop new ideas and innovative methods to improve the design of the current forming technology**

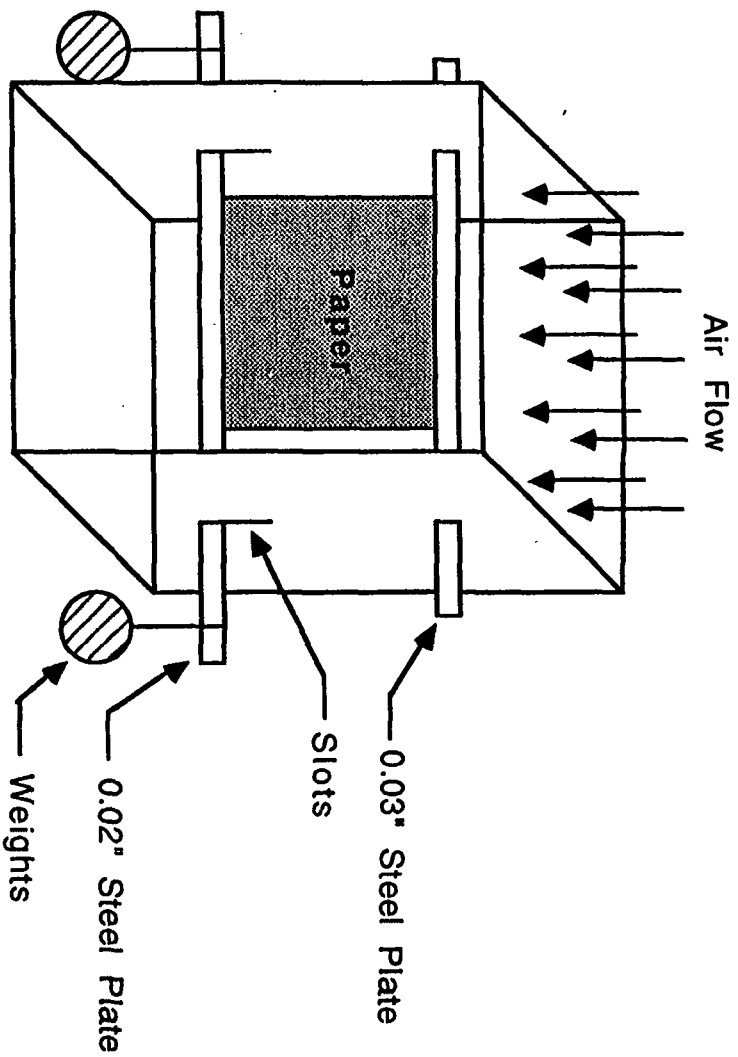
SHORT-TERM OBJECTIVES ARE TO:

- **investigate the effect of various parameters on cross- stream and secondary flow in the forming section and effects on fiber orientation and mass formation, and**
- **optimize the influx of the flow into the headbox to reduce cross-stream flow and eliminate nonuniformities in fiber orientation and mass formation**

LONG-TERM OBJECTIVES ARE TO:

- **analyze the jet/wire interactions and effects on formation**
- **investigate the drainage characteristics on the wire and effects on fine particle distribution**
- **explore new and improved design concepts**

SCHEMATIC OF THE TEST SECTION



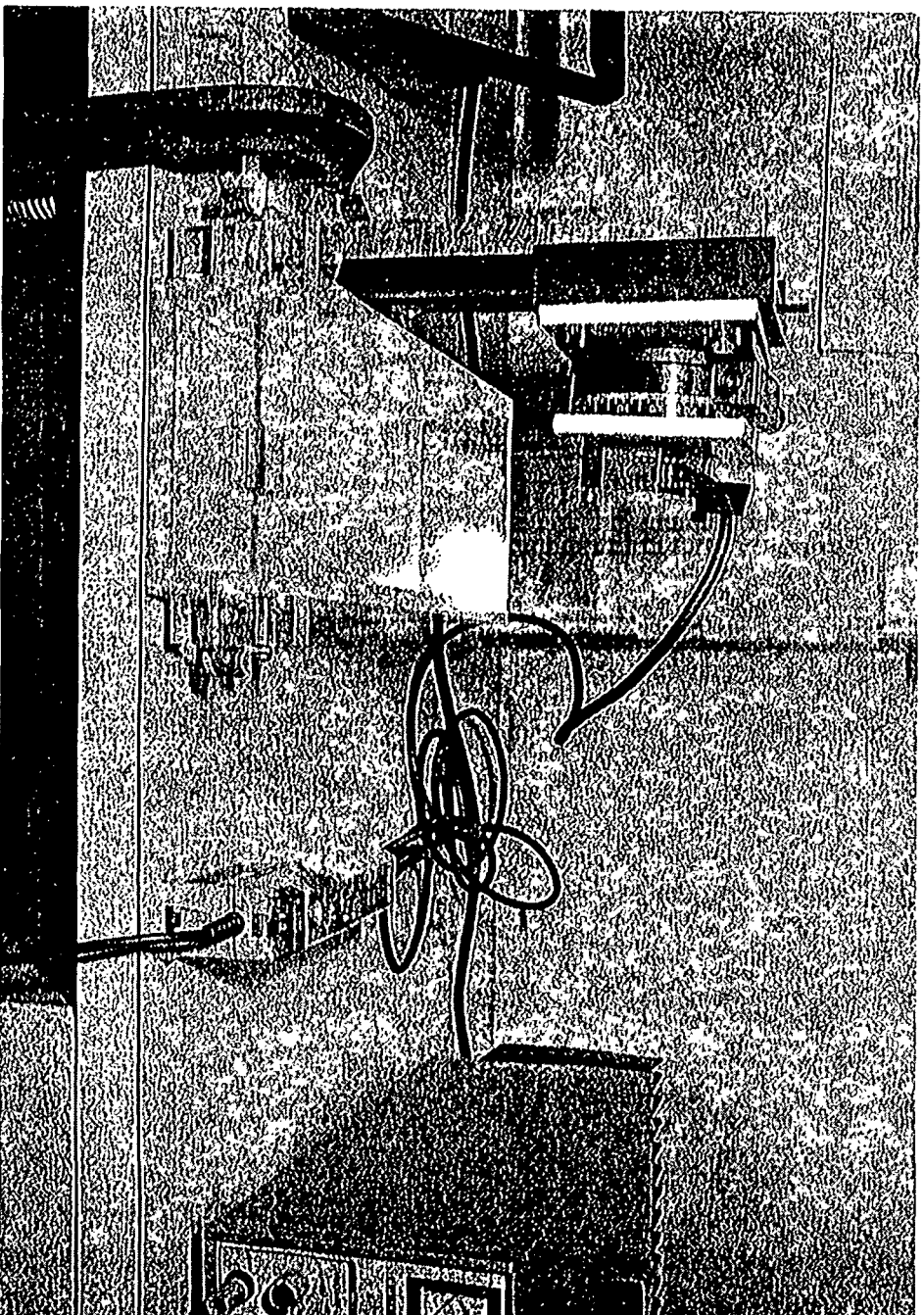
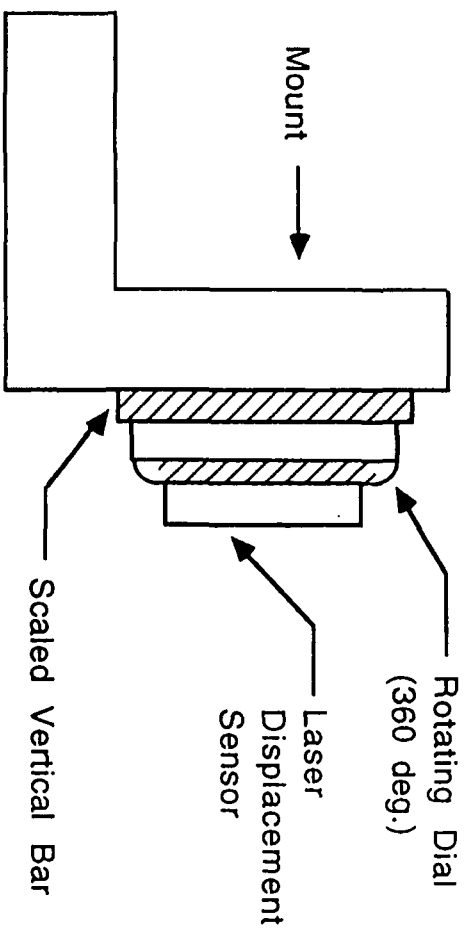
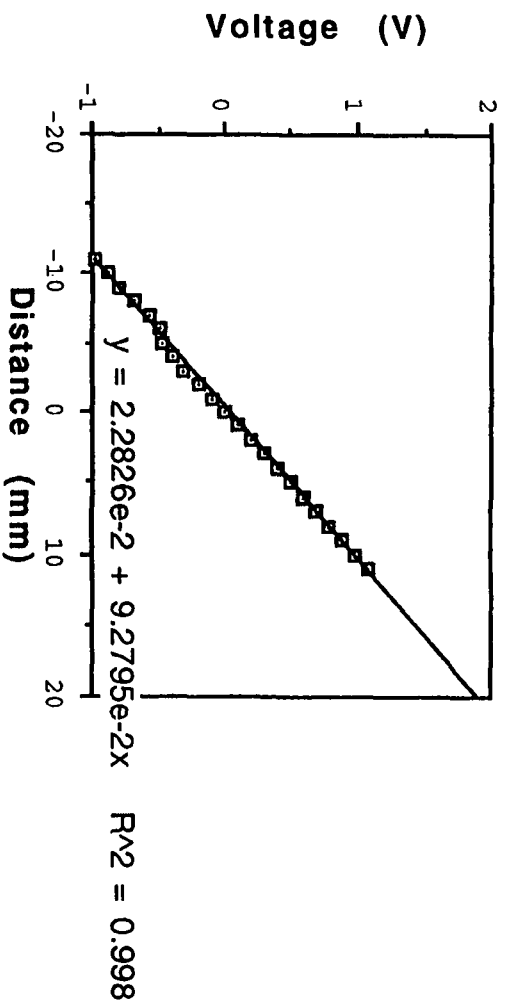
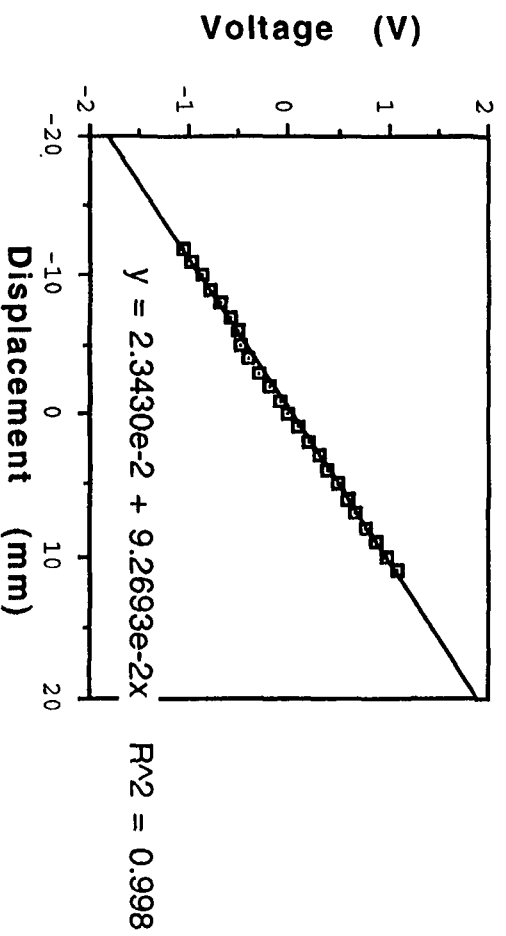


Figure 2. Calibration for the Laser Displacement Sensor.

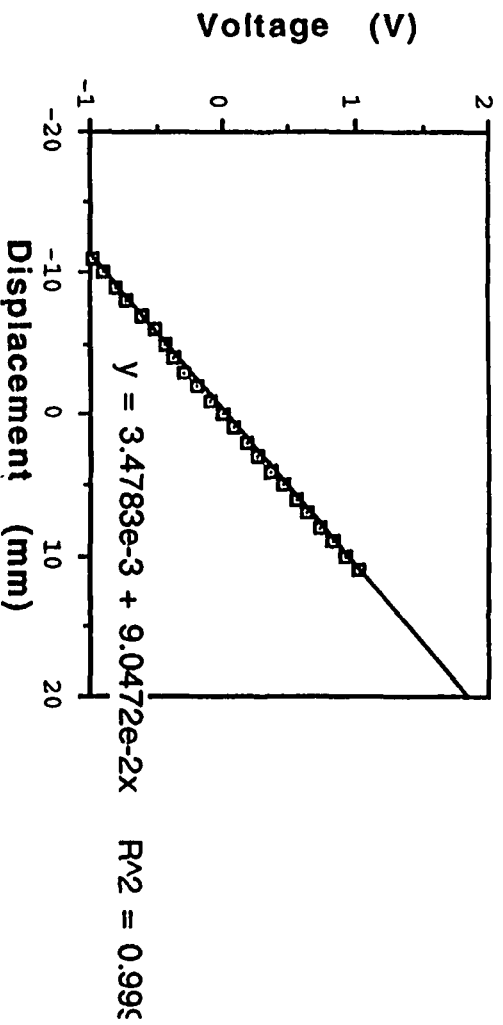
(a) Bond #4 Paper



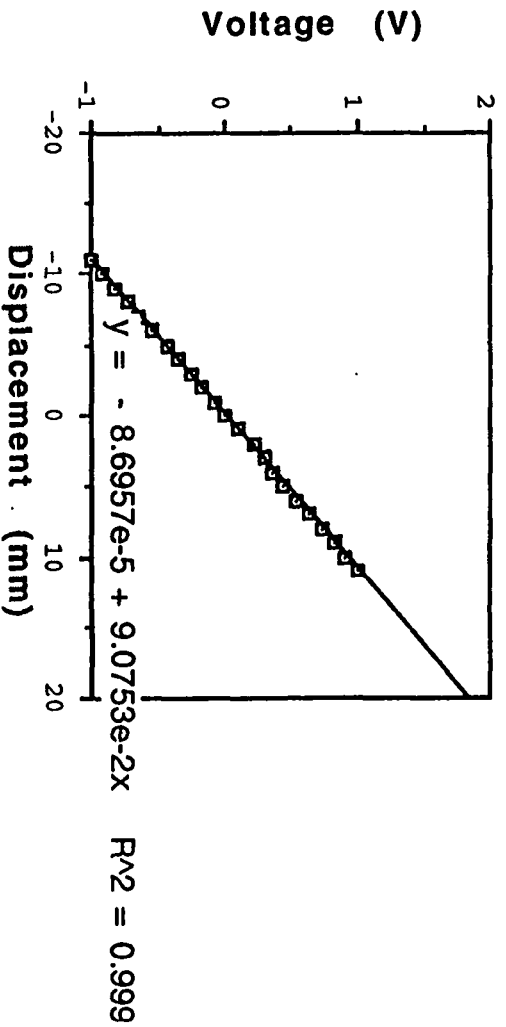
(b) Letter Paper



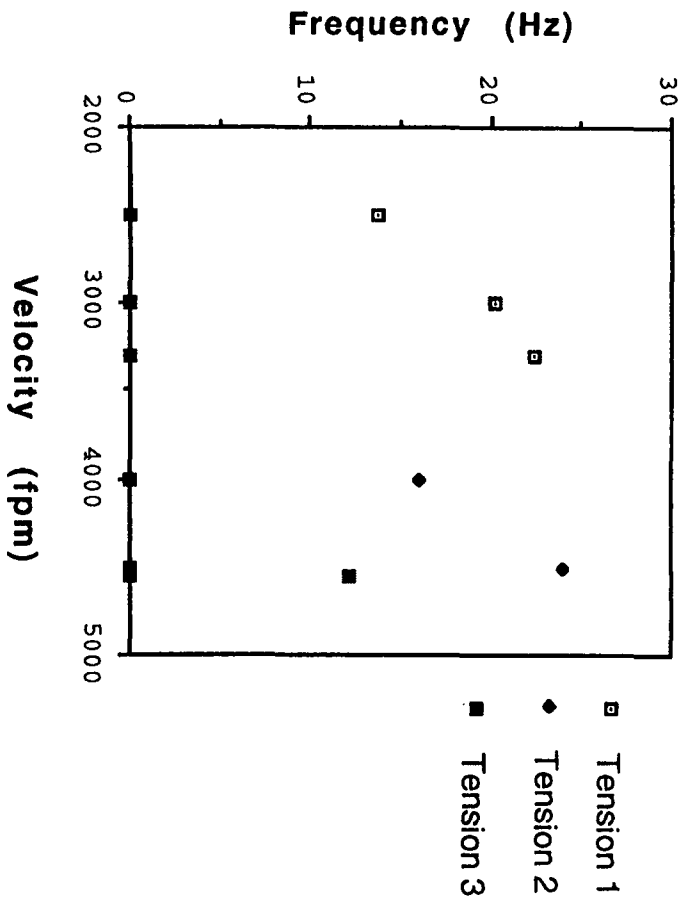
(c) Corrugating Medium (unbleached paperboard)



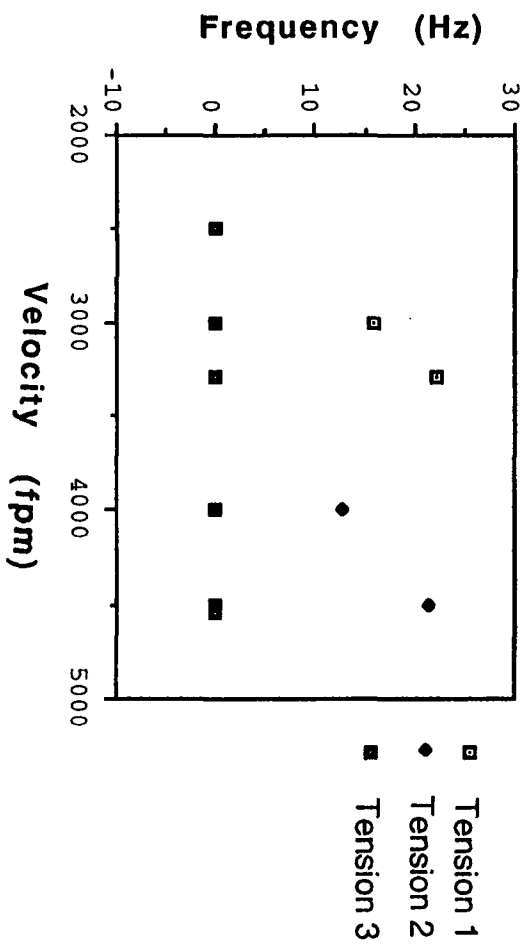
(d) Trace Paper



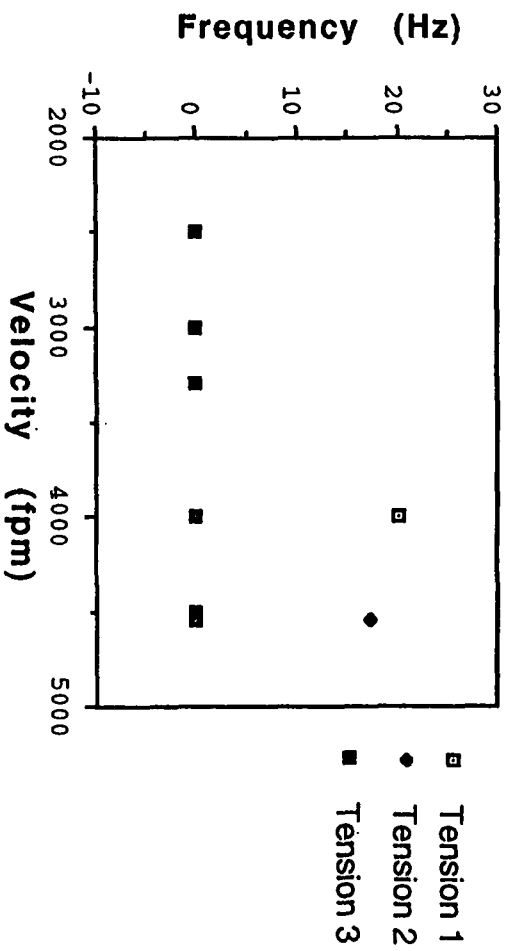
(a) Bond #4 paper



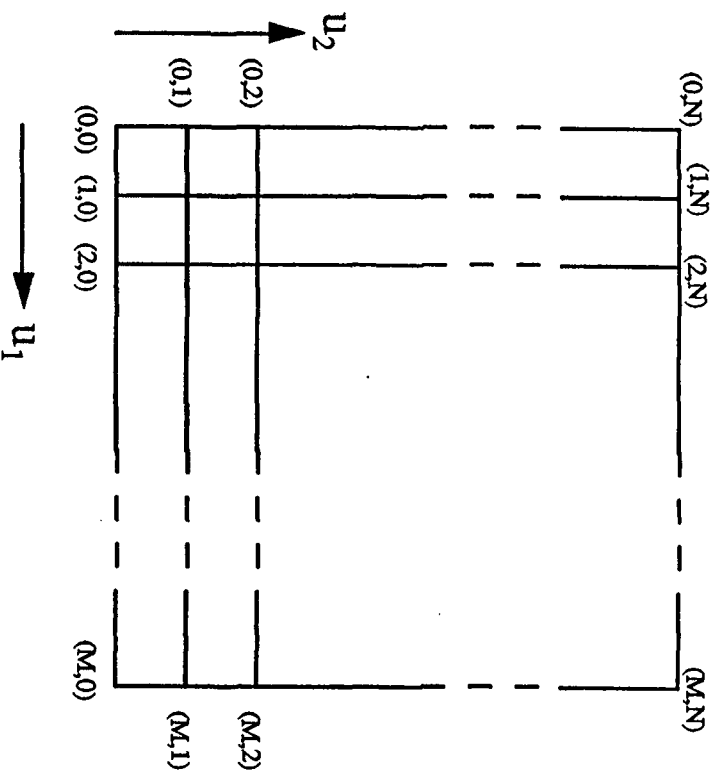
(b) Letter Paper



(c) Corrugating Medium (unbleached paperboard)



CONTROL POINT POSITIONS AND MATERIAL COORDINATE



FUTURE GOALS and TASKS:

1. Wind Tunnel Experiments

- Measurement of the onset of sheet flutter and its frequency as a function of air velocity and tension.

FUTURE GOALS and TASKS (cont'd)

2. Analyses:

- a. Continue the implementation of a thin shell finite element code (steady state, 3-dimensional, linear, isotropic material behavior) with sheet under tension on bottom and top edges and subject to gravity.
- b. Modification of part (a) to consider non-linear and non-isotropic material behavior.

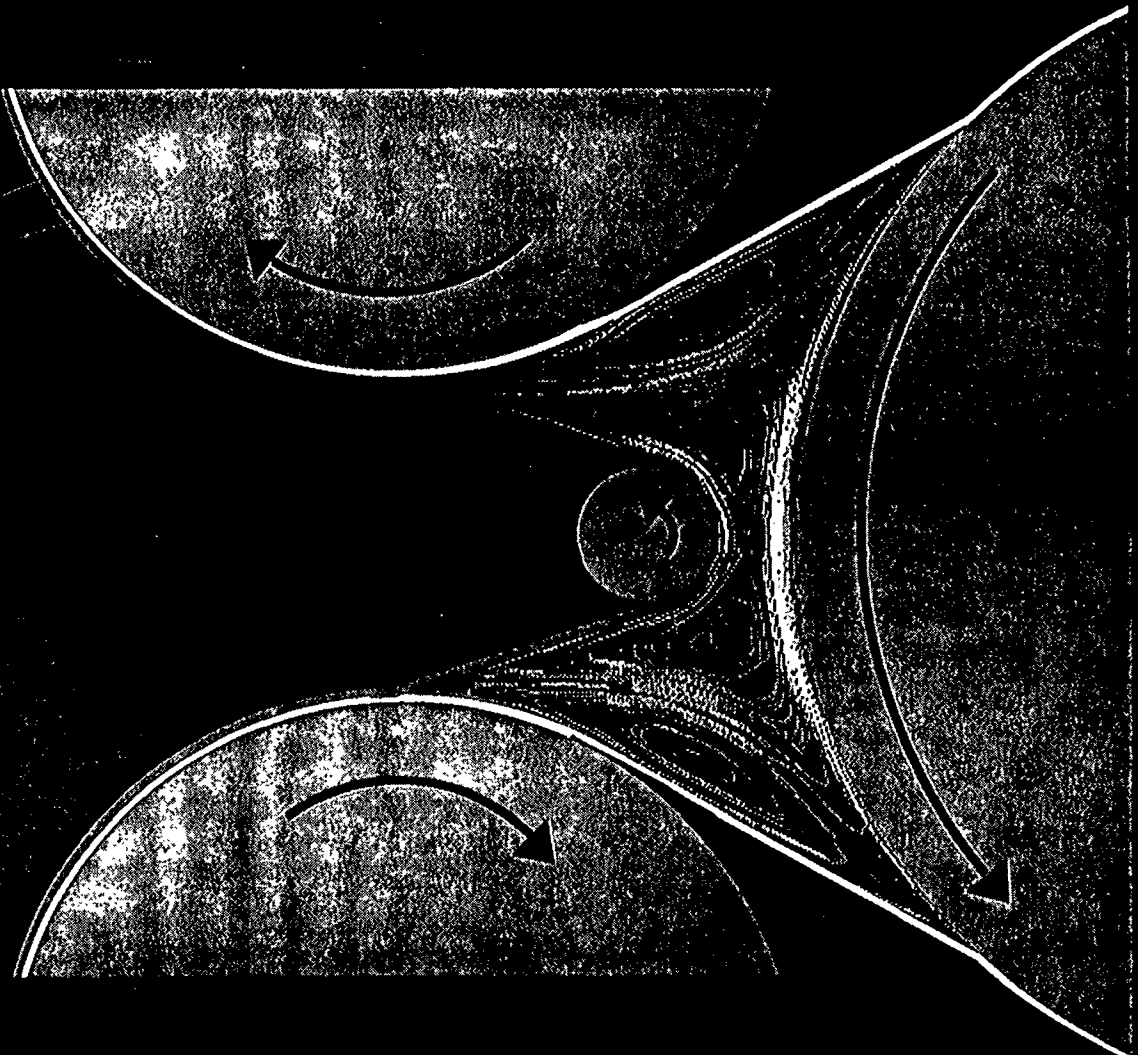
FUTURE GOALS and TASKS (cont'd)

2. Analyses (cont'd)

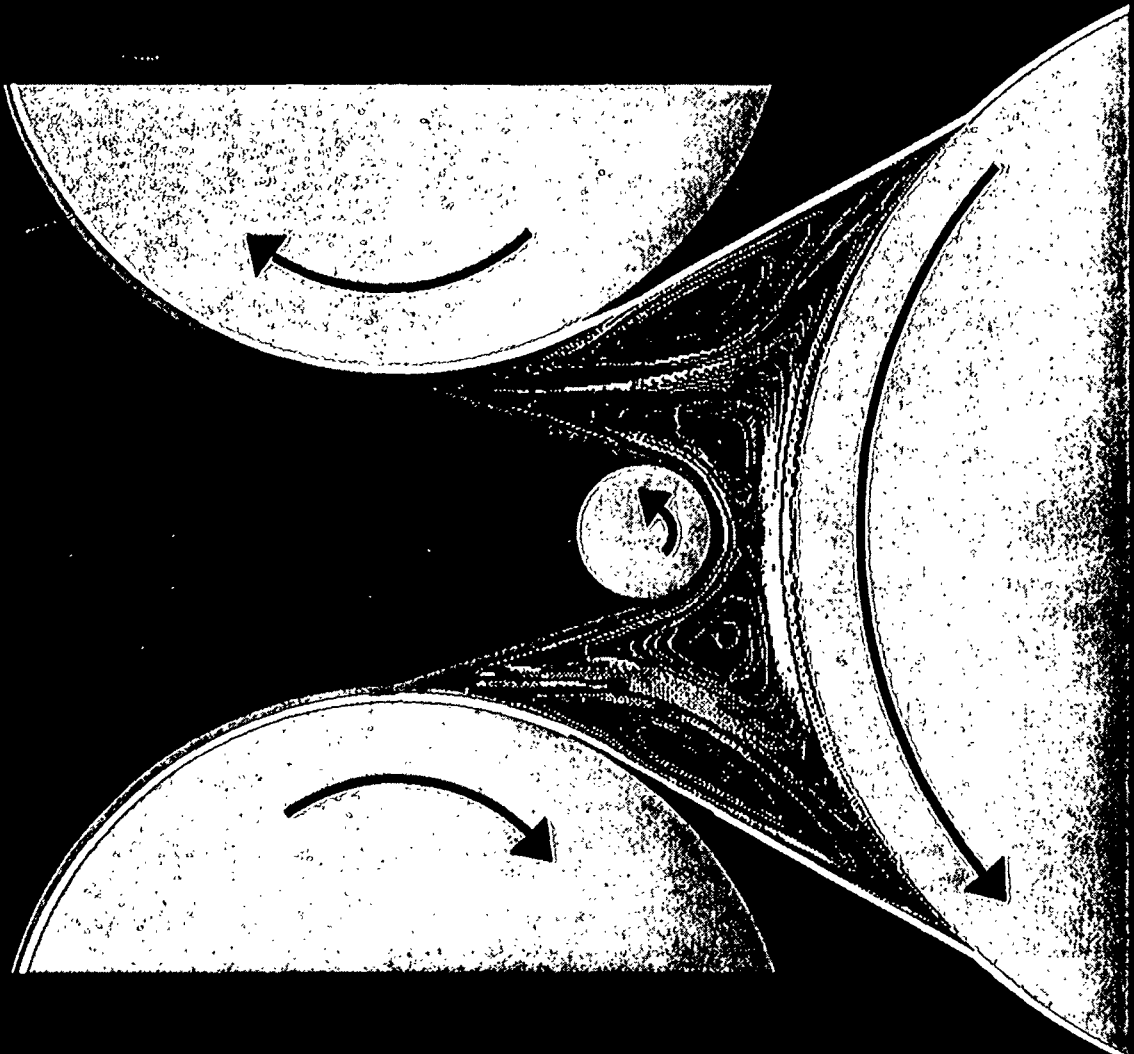
- c. Analysis of the effects of time-dependent boundary conditions.
- d. Fluid dynamics analysis and computation of lift and drag on surface with varying angles.
- e. Coupling of the solid-fluid effects. The excitation force is replaced by a lift and drag induced force.

3. Optimization

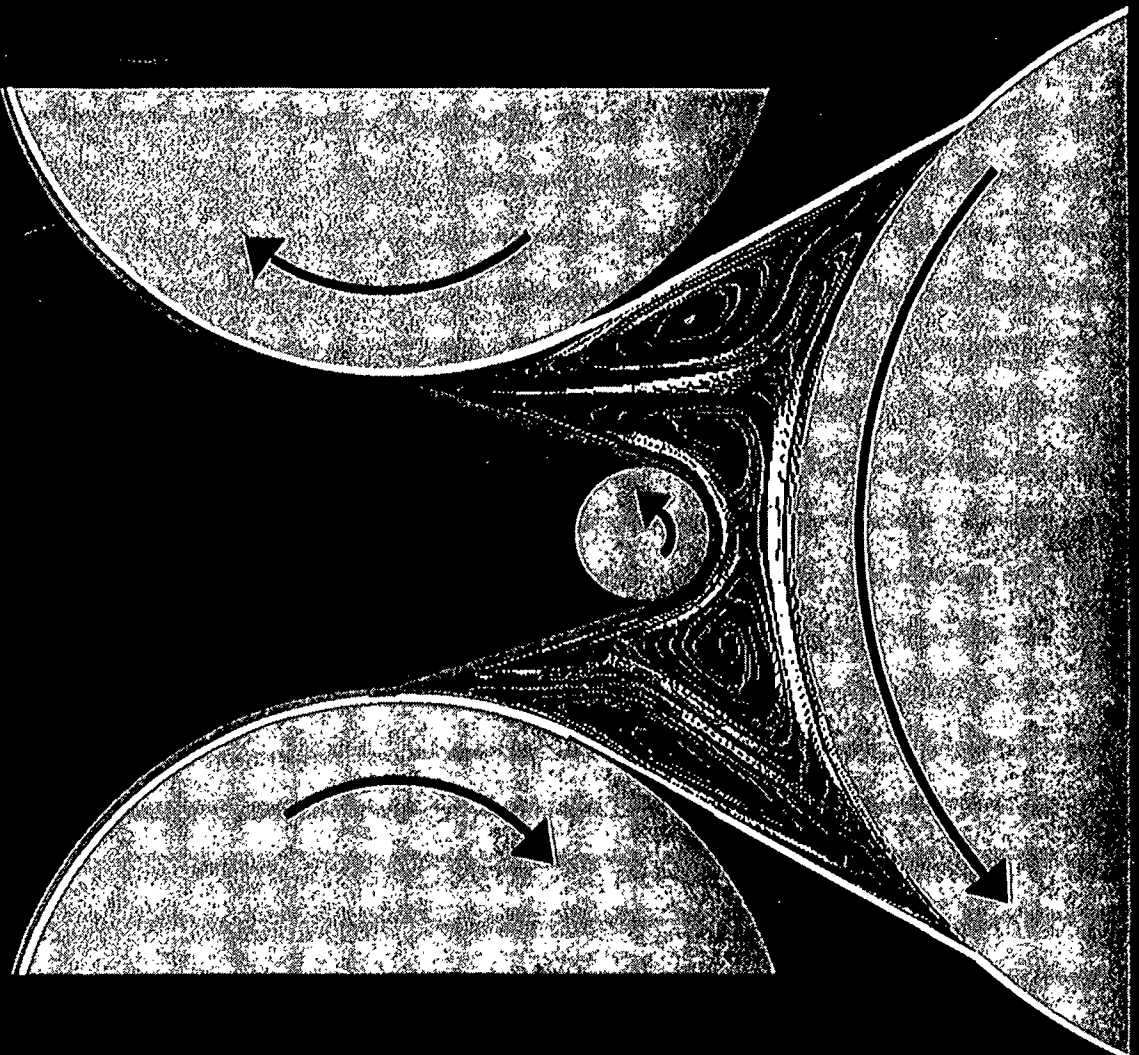
Velocity Streamlines for $Re=7$



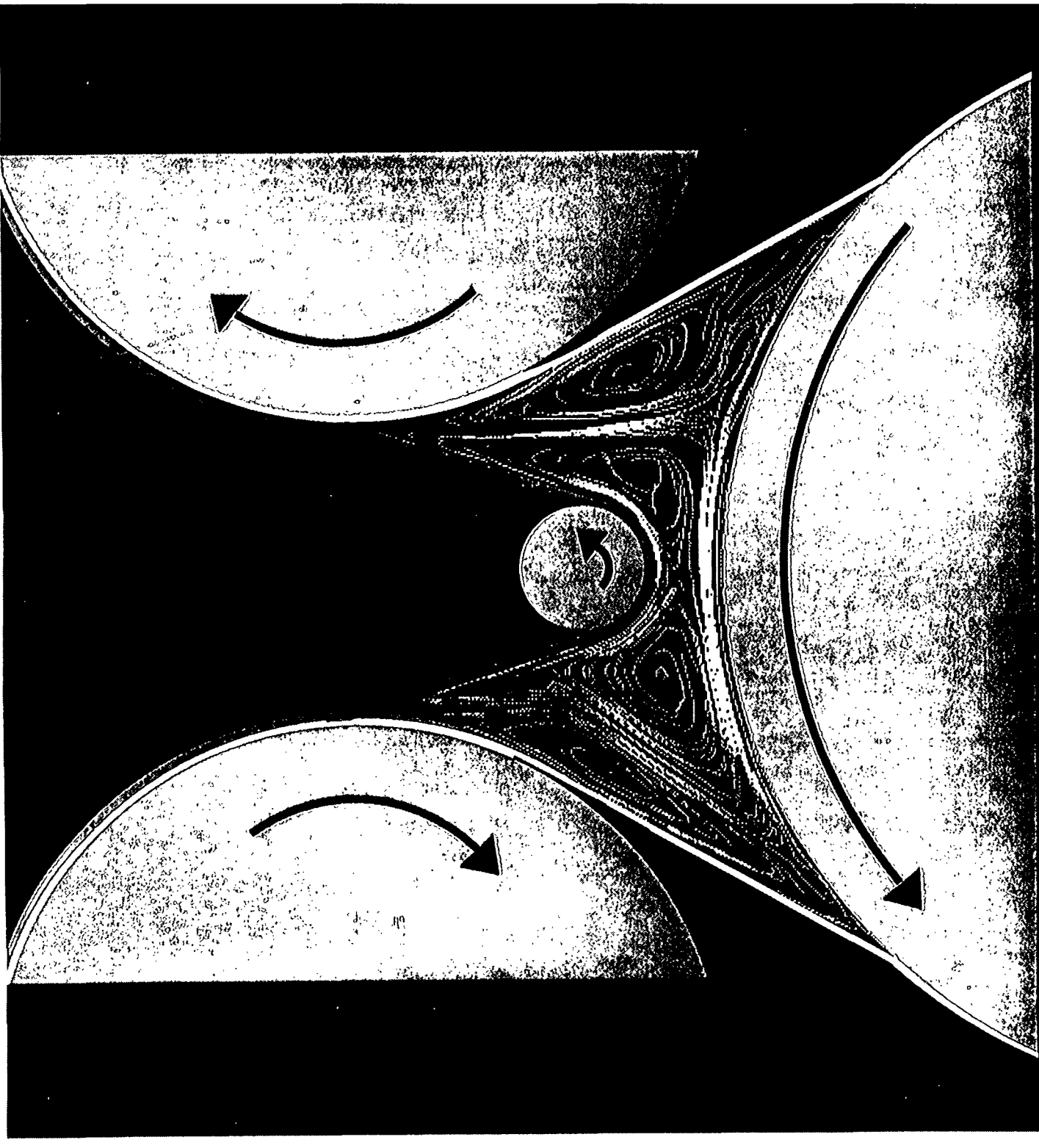
Velocity Streamlines for $Re=70$



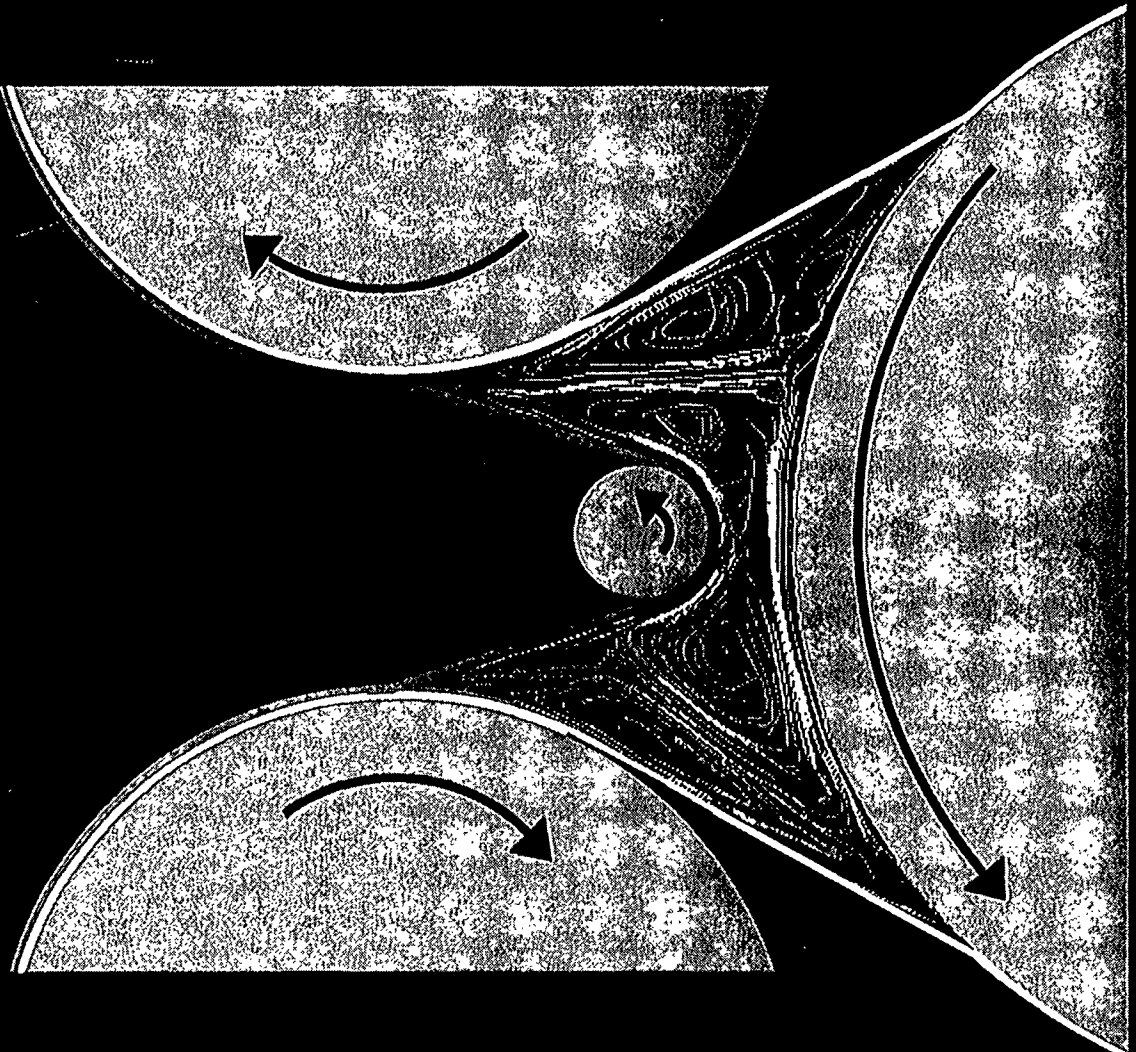
Velocity Streamlines for $Re=210$



Velocity Streamlines for $Re=350$



Velocity Streamlines for $Re=700$



FUNDAMENTALS OF WATER REMOVAL PROCESSES

SLIDE MATERIAL

FOR

PROJECT 3480

March 22, 1994
Institute of Paper Science and Technology
Atlanta, Georgia

Project 3480

**Fundamentals of Water
Removal**

Jeffrey D. Lindsay

Inertial Effects in Fibrous Media

- Nonlinear relationship between pressure drop and flow rate at high fluid velocity
- Important for drainage on the wire, through drying, possible displacement dewatering
- Usually not a factor in wet pressing
- Important for filter products

Relation Between Flow and Pressure Drop

$$\frac{\Delta P}{L} = \frac{90\mu v_{avg}(1-\epsilon)^2}{D_f^2 \epsilon^3} + \frac{\sqrt{90I}(1-\epsilon)p_{avg} v_{avg}^2}{D_f \epsilon^3}$$

ϵ = porosity

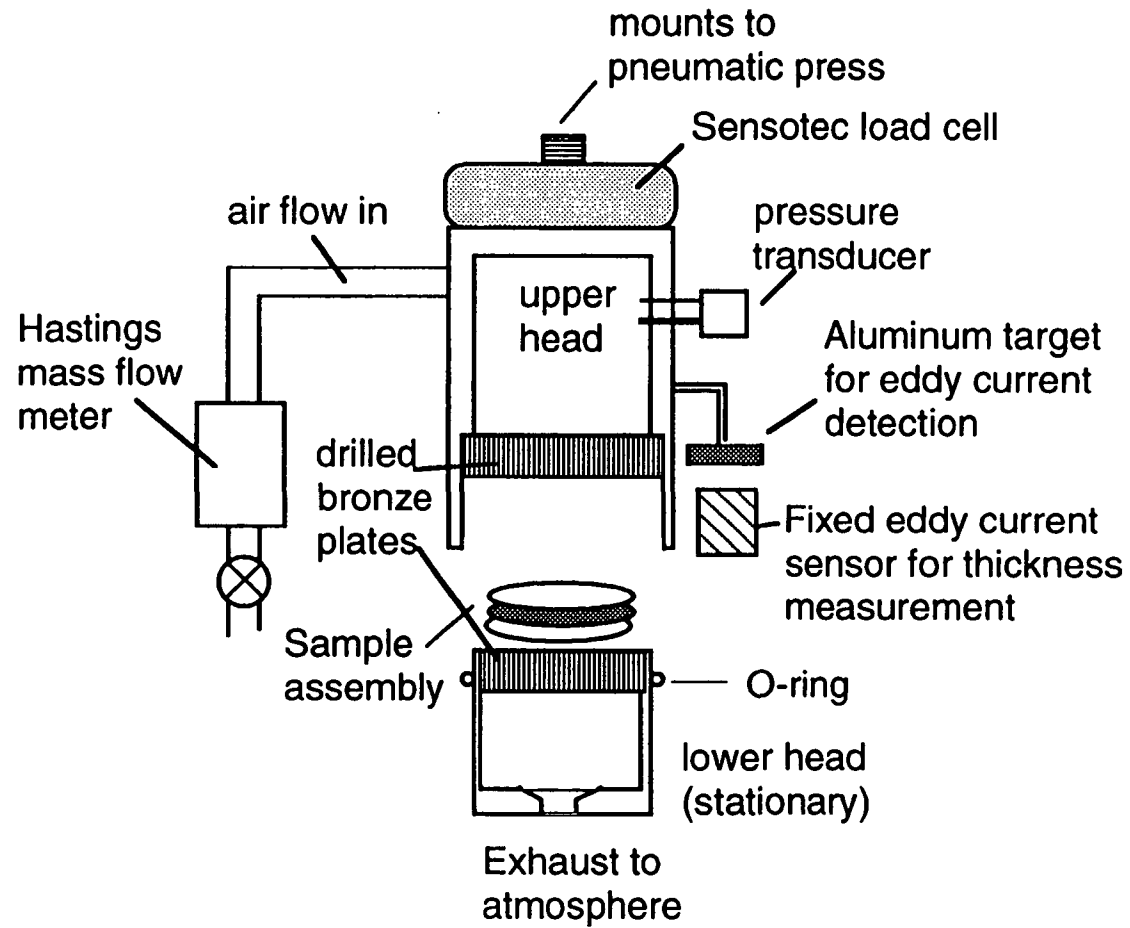
D_f = fiber diameter

v = superficial velocity

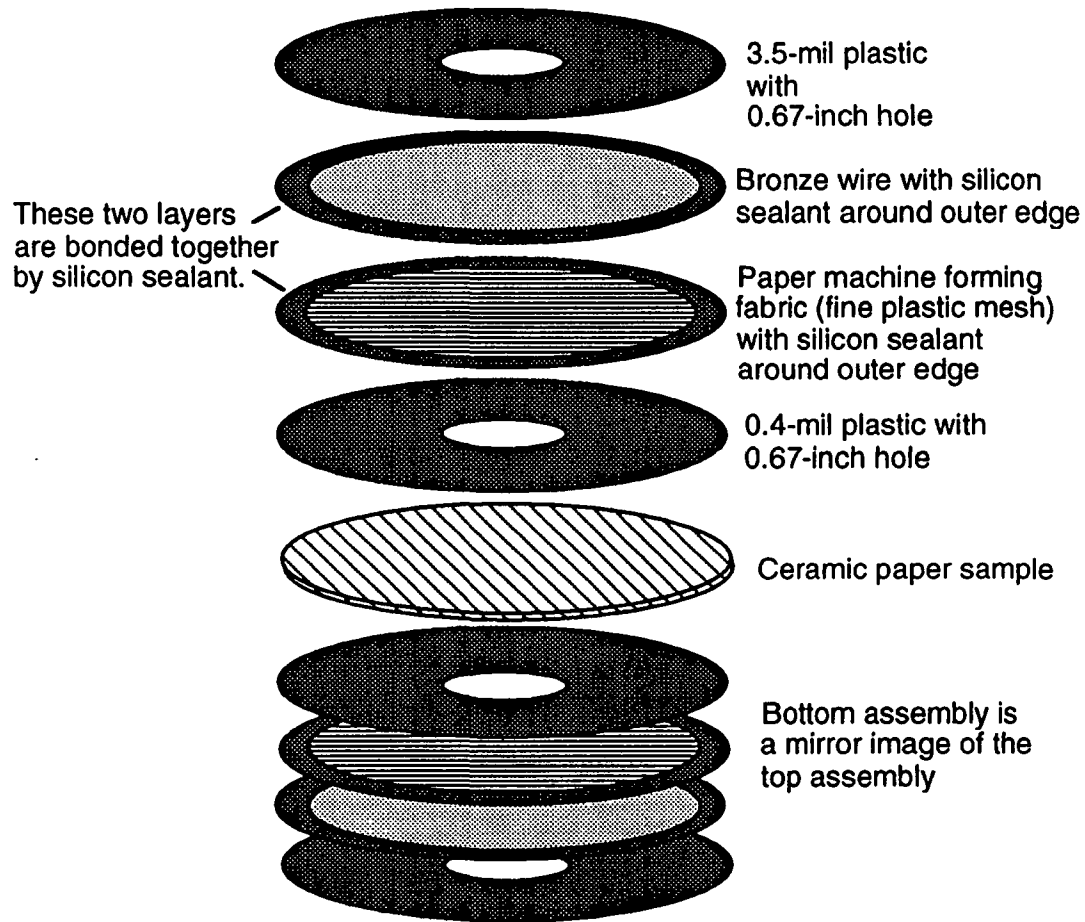
μ = viscosity

$\Delta P/L$ = pressure loss per unit length

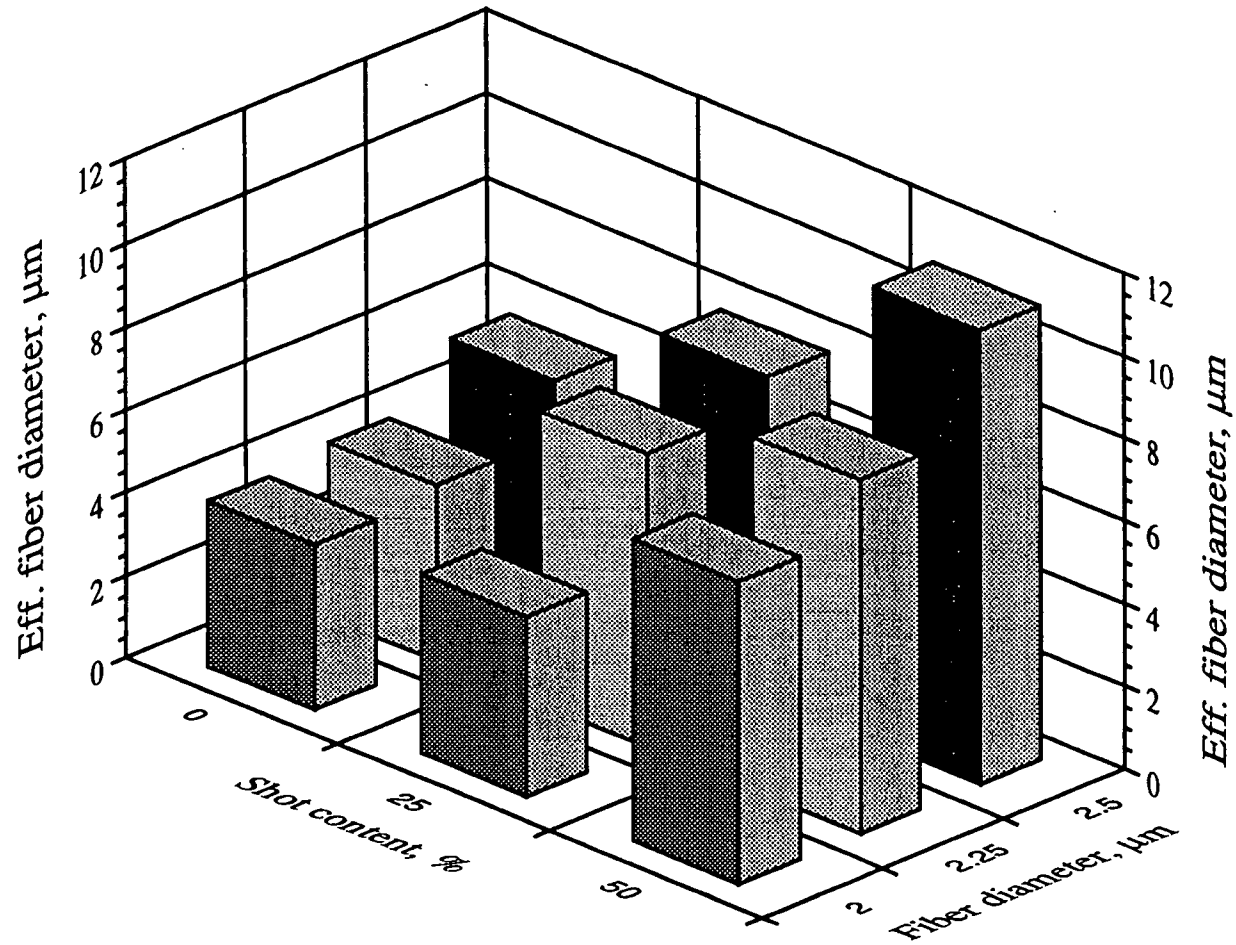
I = inertial parameter



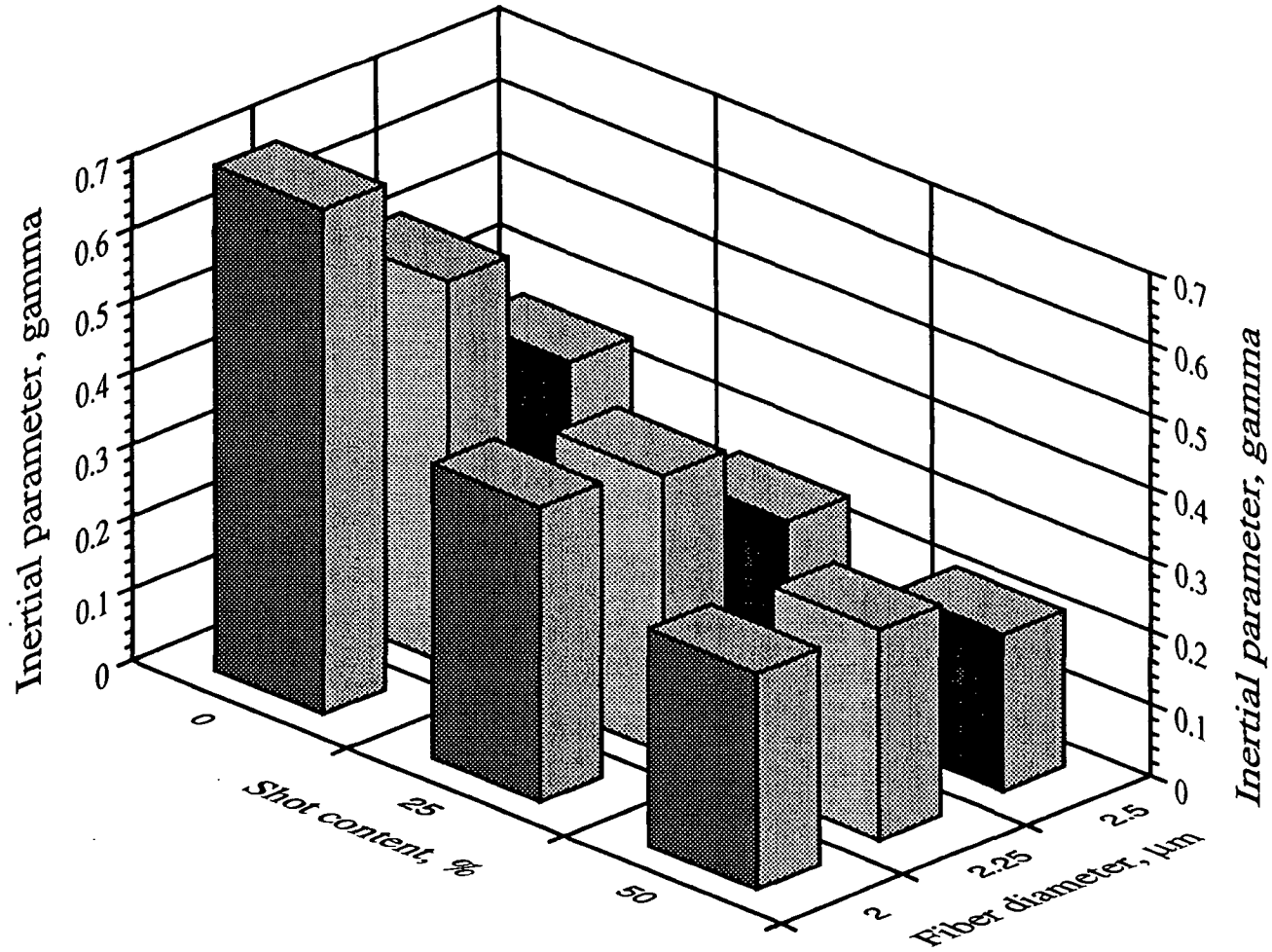
Air flow apparatus for measurements in ceramic paper.



Sample assembly for air flow measurements.



Effective fiber diameter as a function of shot content and fiber diameter.



Inertial coefficient as a function of shot content and fiber diameter.

A Fundamental Question:

How much of the pore space in paper is open to flow?

Relative Flow Porosity

- Definition:

- Fraction of the total pore space that is open to flow

- Example:

- A value of 0.5 means half of the pores are closed to flow

Pores Closed to Flow

- Dead-end extrafiber pores
- Micropores in the cell wall
- Lumens (not all)
- Stagnant zones behind fibers

Porosity Definitions

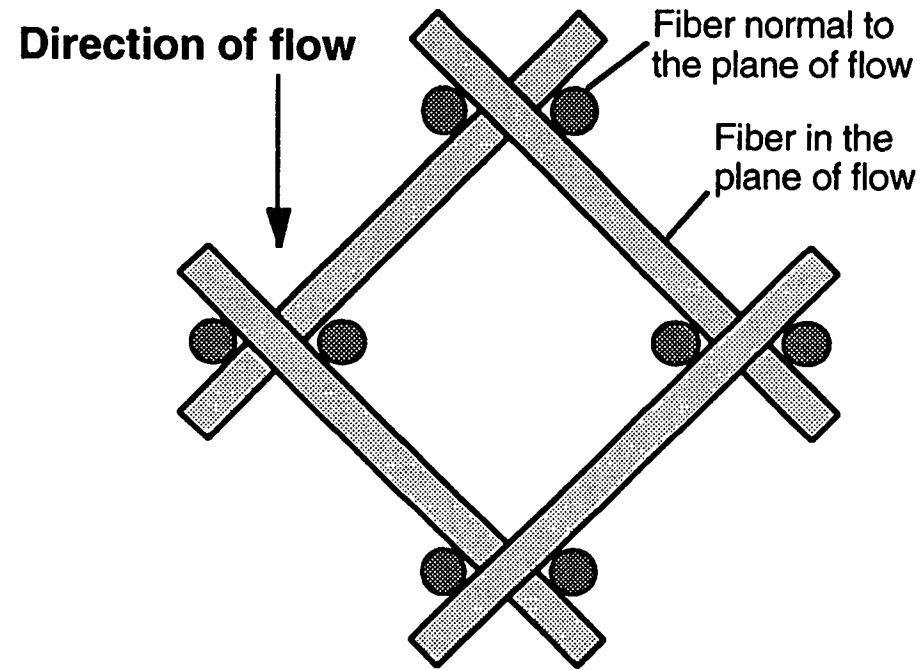
Term	Definition
Total porosity, ε	Volume fraction of pore space, or 1 - volume fraction of solid matrix
Effective flow porosity, ε_{eff}	Volume fraction of pore space open to flow
Relative flow porosity, ε_{rel}	Ratio of pore space open to flow to total pore space: $\varepsilon_{\text{rel}} = \varepsilon_{\text{eff}}/\varepsilon$
Extrafiber porosity, ε_0	Volume fraction of pore space between swollen fibers, or 1 - volume fraction of swollen fibers

Extrafiber Pore Space

- Pore space between swollen fibers
- Excludes lumens, associated water, micropores in cell wall
- Simplest assumption: relative porosity equals extrafiber porosity / total porosity.

Estimates of Extrafiber Pore Space

- Water retention values
- Specific volume from Kozeny-Carman approach (permeability data)
- Solute exclusion methods
- Other techniques

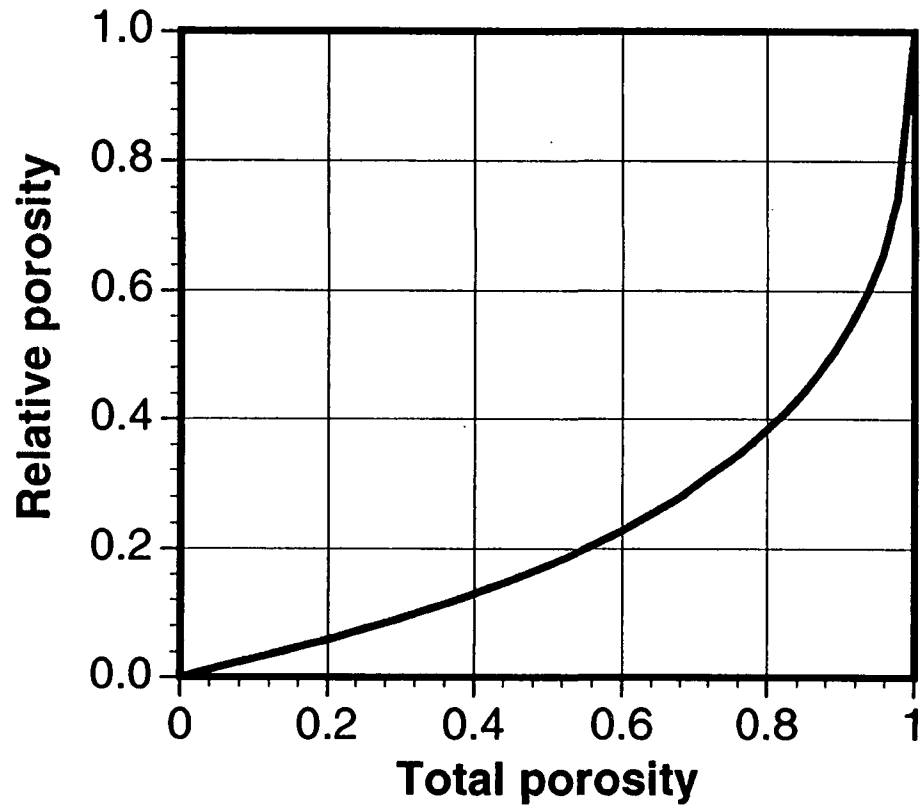


Unit cell of a fibrous medium used in the analysis of Kyan et al.

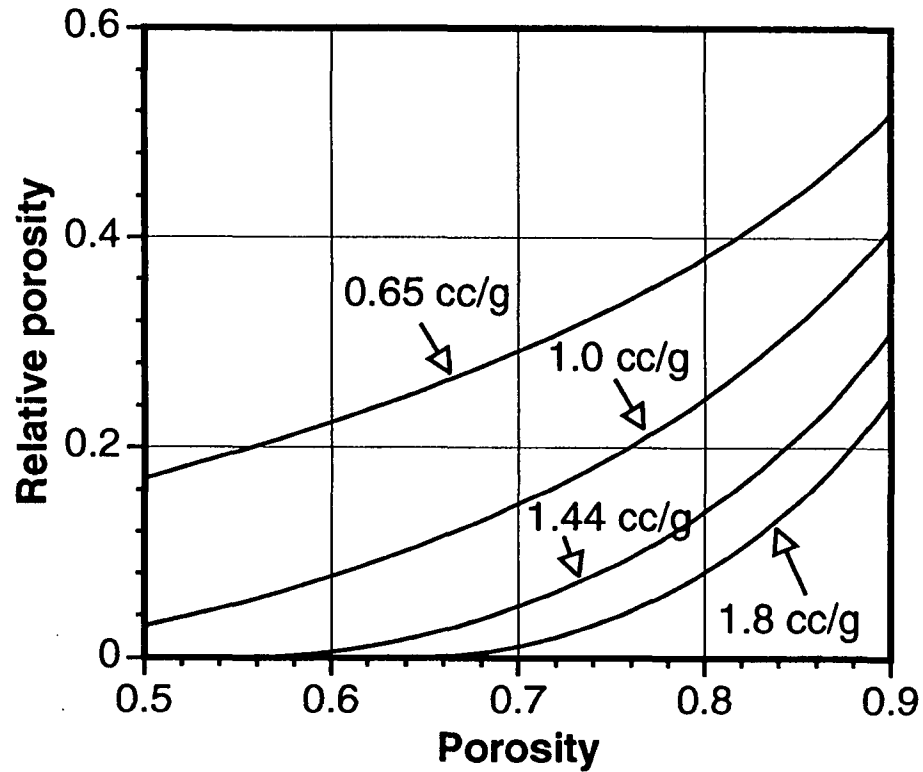
The Geometric Model of Kyan, et al.

$$\varepsilon_{\text{eff}} = N_e^2 (1 - \varepsilon) (0.5/\pi)$$

$$N_e = \left(\frac{\pi}{0.5(1 - \varepsilon)} \right)^{1/2} - 2.5$$



Predicted relative porosity based on the approach of Kyan et al.



Relative porosity results based on a combination of Kyan's model and extrafiber porosity analysis. Unhydrated fiber corresponds to $\alpha = 0.65$ cc/g.

Water Retention Approach

$$\epsilon_{\text{rel}} = 1 - \text{WRR} \frac{\rho_s}{\rho_l} \left(\frac{1 - \epsilon}{\epsilon} \right)$$

Darcy's Law

$$v = \frac{K}{\mu} \frac{\Delta P}{L}$$

Kozeny-Carman Approach

$$\varepsilon_o = 1 - \alpha C$$

$$K = \frac{1}{5.55 S_o^2} \frac{(1 - \alpha C)^3}{\alpha^2 C^2}$$

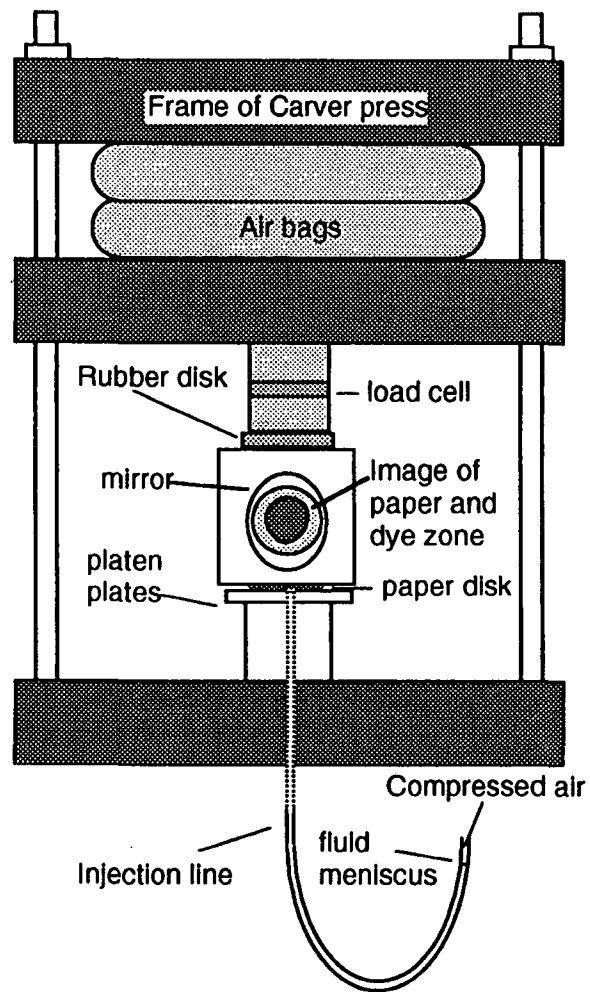
Use of Specific Volume Data

$$\epsilon_{\text{rel}} \approx \frac{\epsilon_0}{\epsilon} = \frac{1 - \alpha c}{\epsilon} = \frac{1 - \alpha \rho_s (1 - \epsilon)}{\epsilon}$$

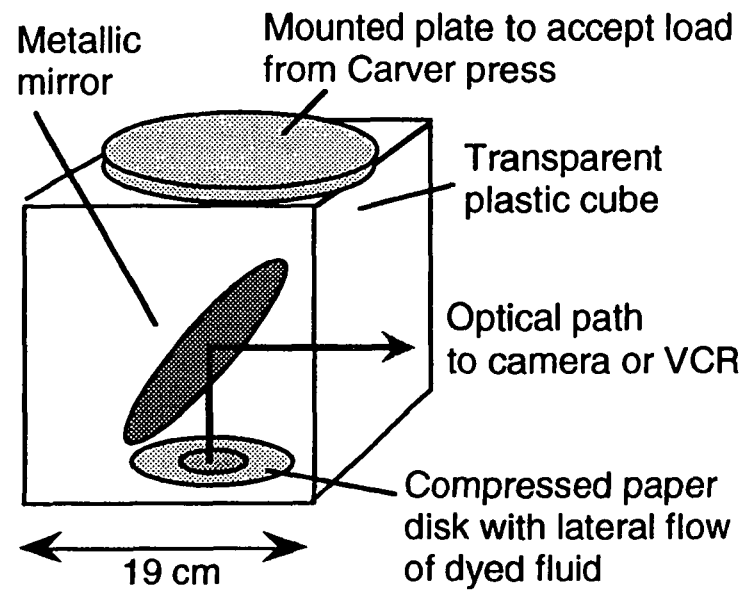
- α = specific volume, cc/g fiber
- c = fiber concentration, g/cc
- ρ = density of pure solid, g/cc

Experimental Approach

- In-plane dye injection
- Measure growth rate of dye zone
- Measure volume of dye injected
- Measure sheet thickness and basis weight to get total porosity
- Compare volume of dyed zone to volume of dye injected.



Modified lateral flow apparatus for dye injection tests.



Plastic pressing block with mirror for optical access to a compressed sheet.

Problems to Consider

- Dispersion of the dye
- Z-direction gradients
- Dye-specific artifacts

Never-Dried Bleached Softwood Kraft

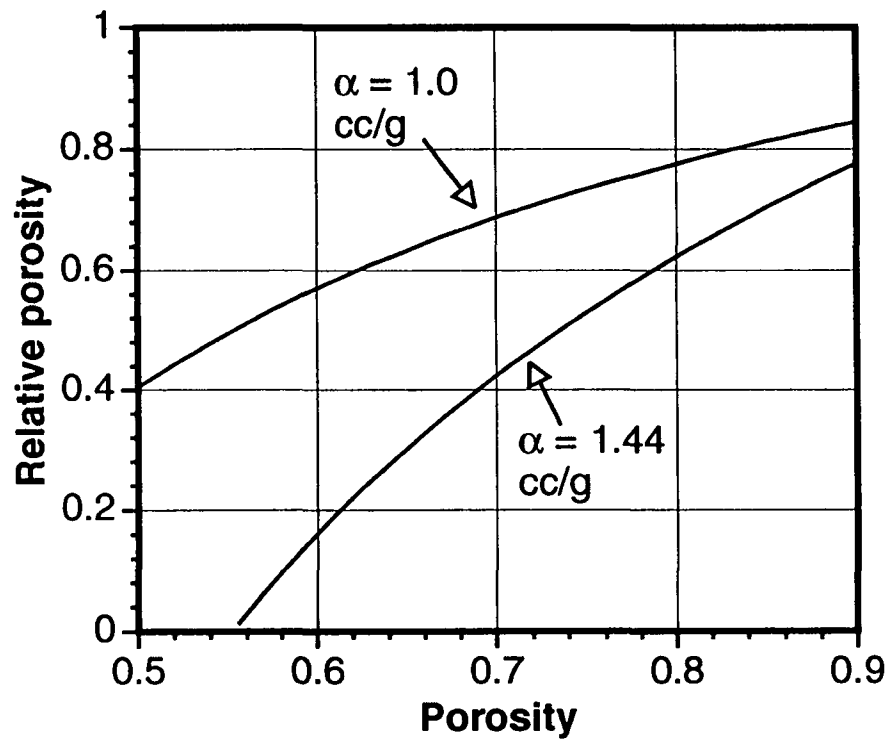
Total porosity	Relative porosity
0.814	0.471
0.817	0.454
0.815	0.446
0.817	0.465
0.812	0.458
AVG:	0.459

Ceramic Papers

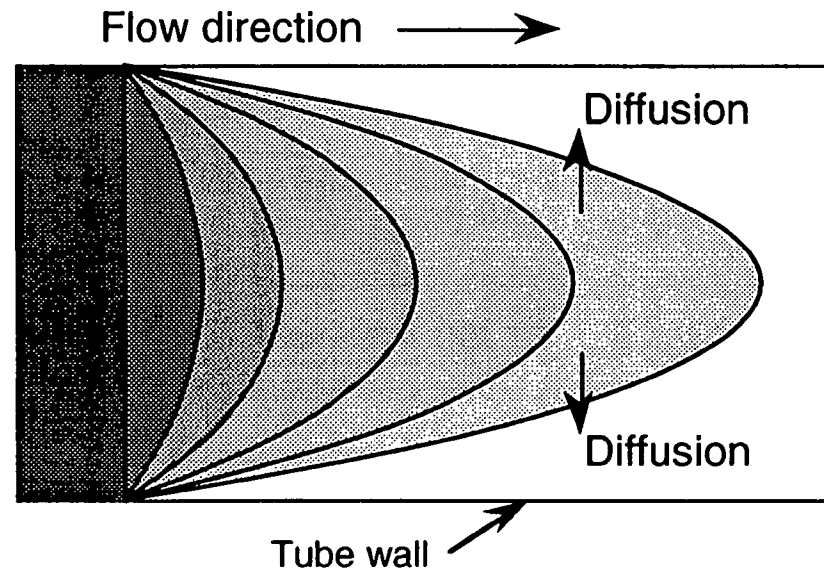
- Relative porosity measured at 90% or above

Results for Dry Blotter Paper

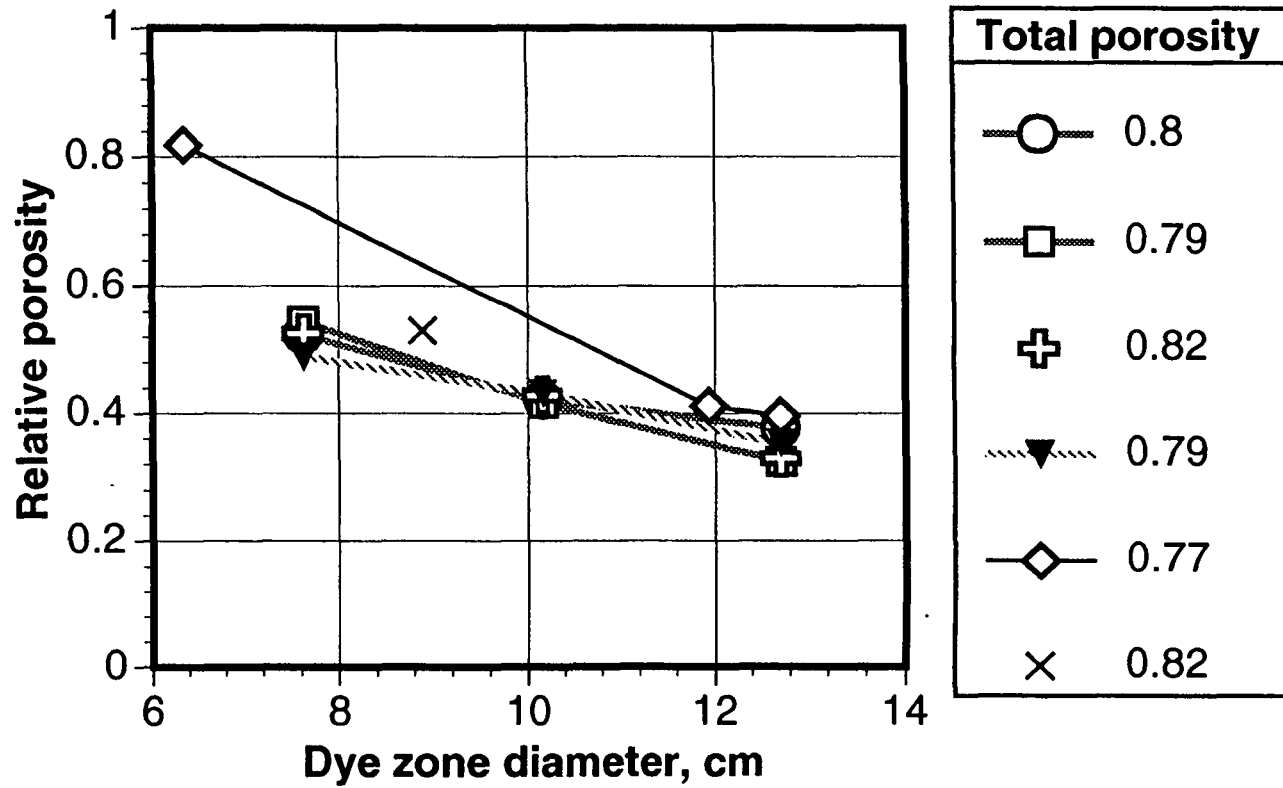
Series I		Series II		Series III	
ϵ	Dry ϵ_{rel}	ϵ	Dry ϵ_{rel}	ϵ	Dry ϵ_{rel}
0.771	0.936	0.778	0.583	0.649	0.699
0.773	0.836	0.777	0.712	0.647	0.854
0.769	0.974	0.782	0.747	0.656	0.891
0.771	1.004	0.777	0.668	0.648	0.801
0.772	0.933	0.778	0.803	0.649	0.962
0.768	0.810				
AVG:	0.916	AVG	0.703	AVG	0.841



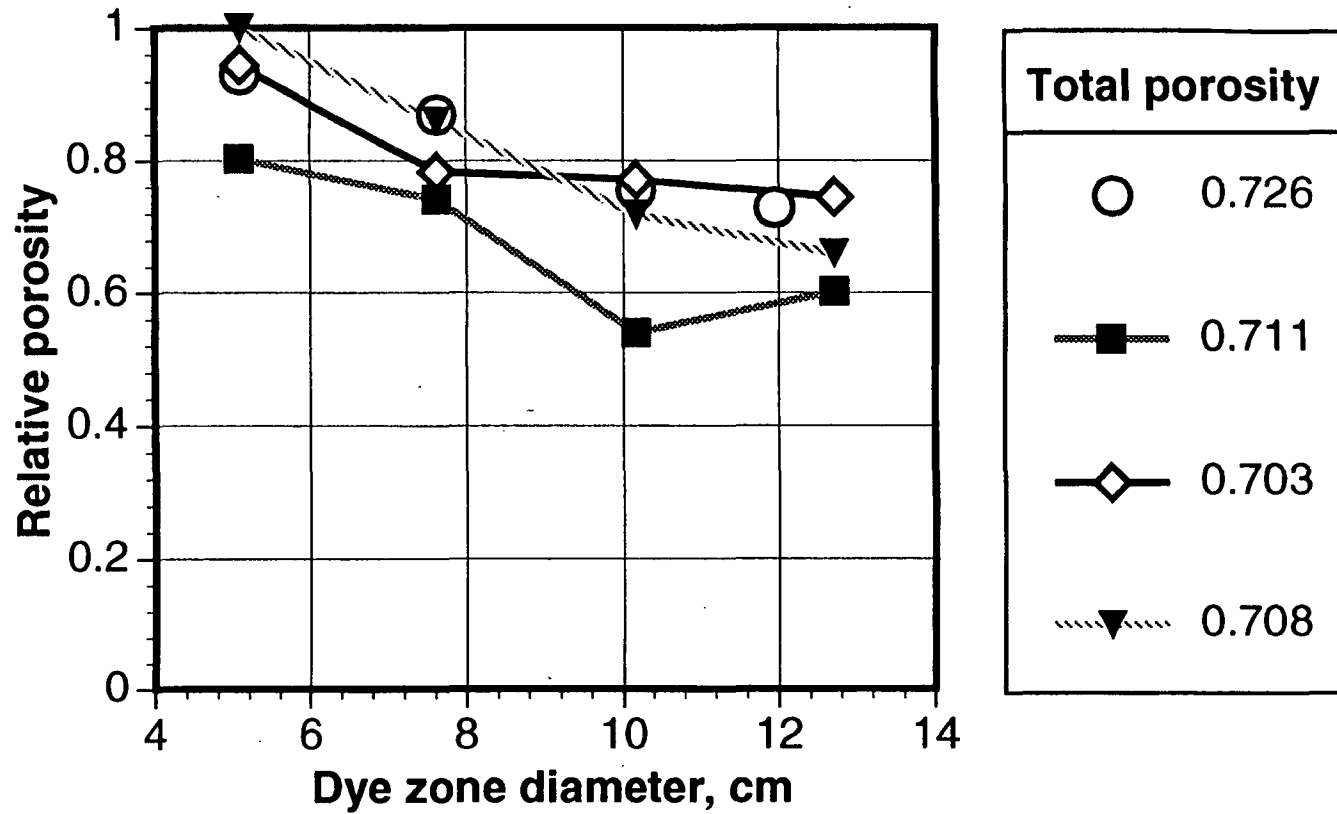
Predicted relative porosity results based on 90% of extrafiber pore space being open to flow.



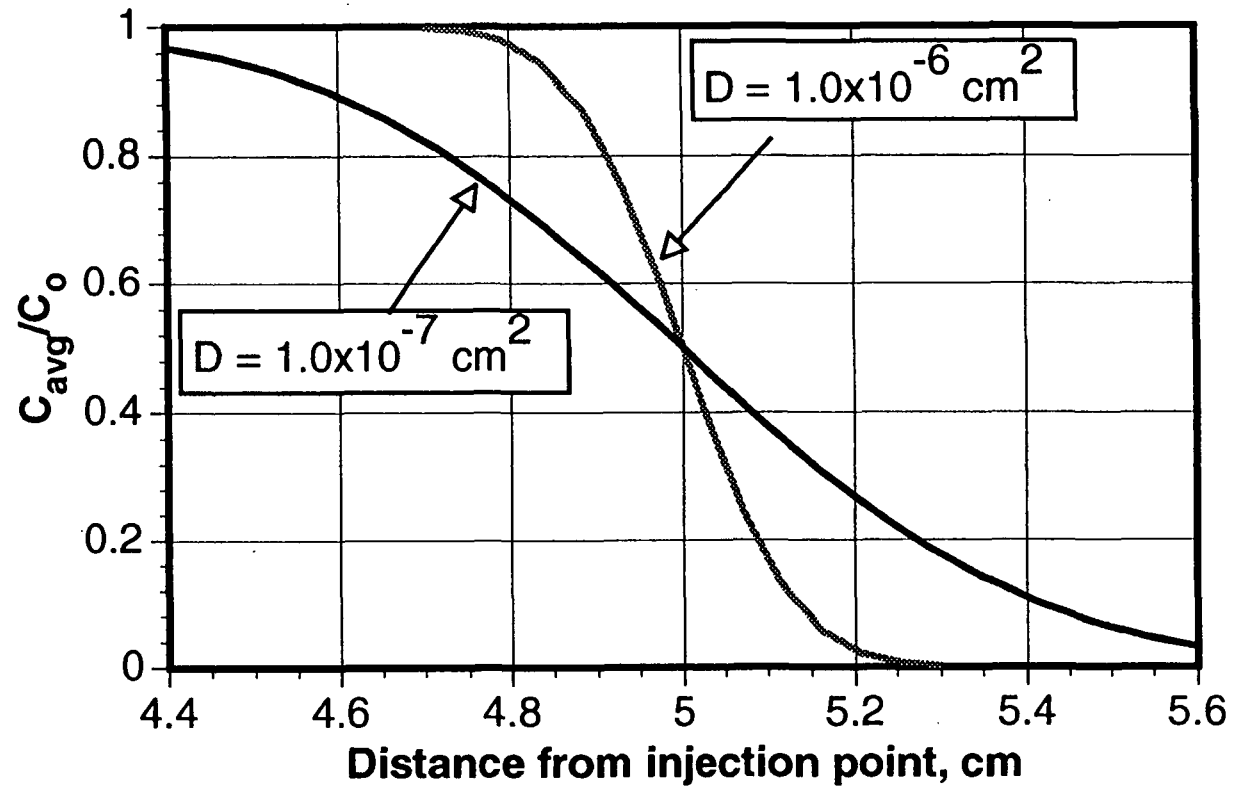
Distortion of a flat dye-water boundary moving in a flow with a parabolic velocity profile. Some of the dye advances faster than the average flow velocity.



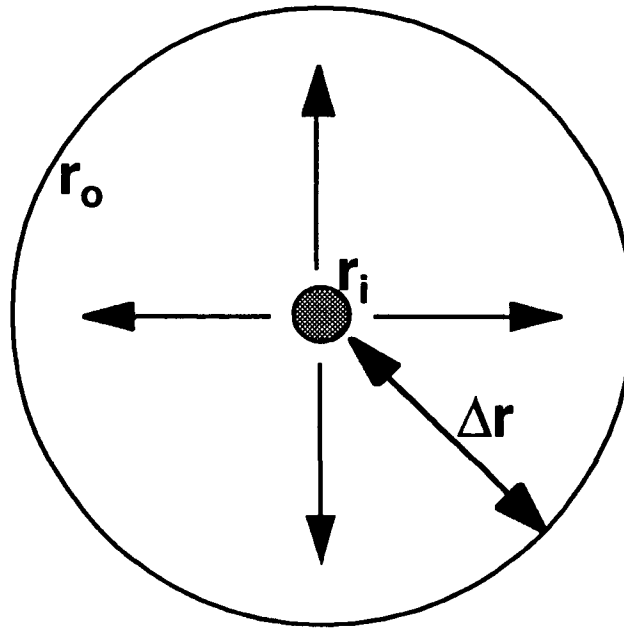
Relative porosity versus dye diameter in bleached kraft handsheets.



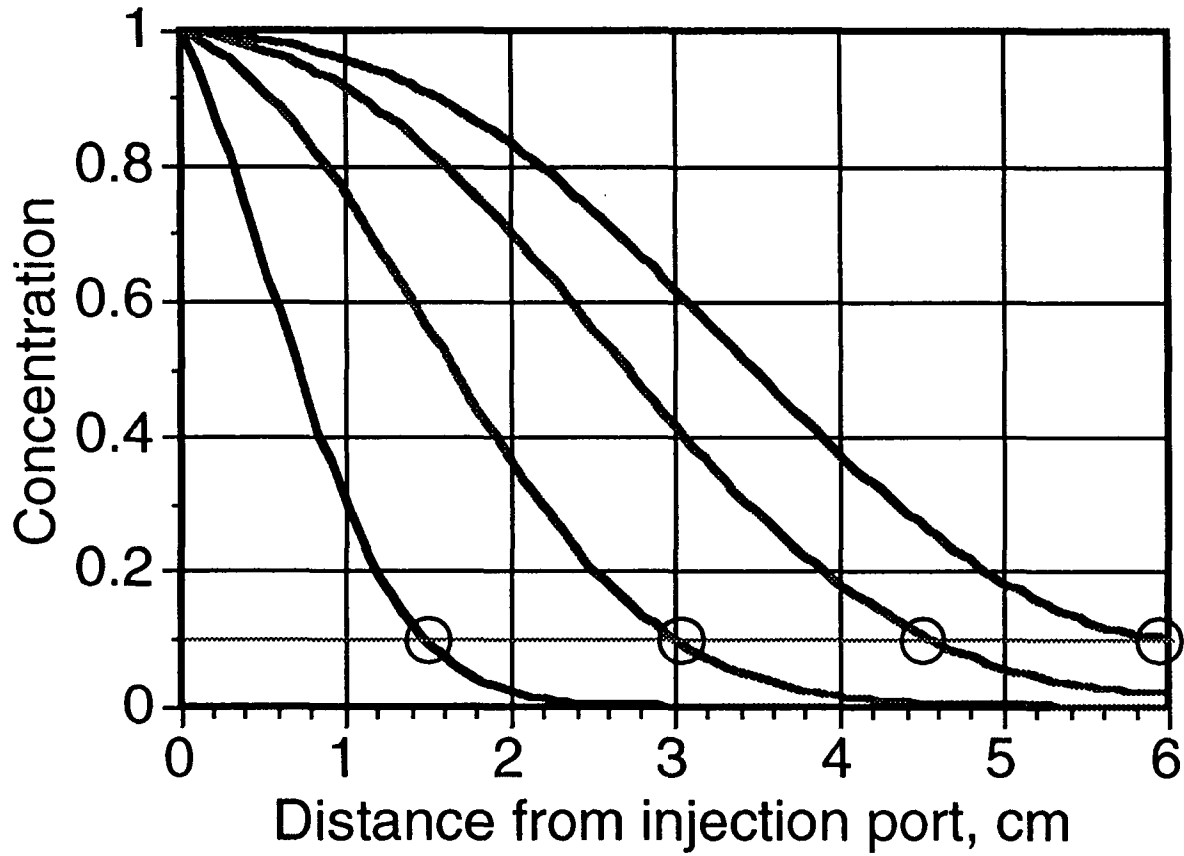
Relative porosity results in saturated blotter paper as a function of dye zone diameter injected into the sheet.



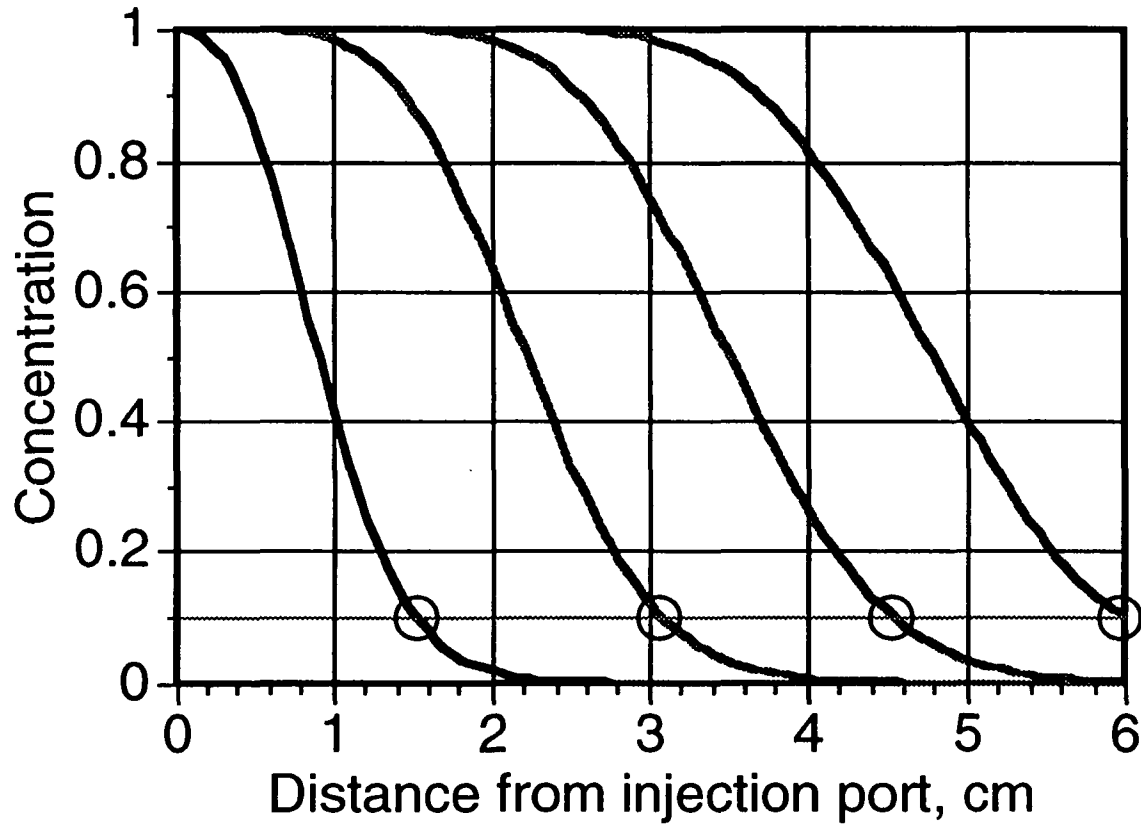
Predicted dispersion of a dye boundary after 5 cm travel in a capillary tube.



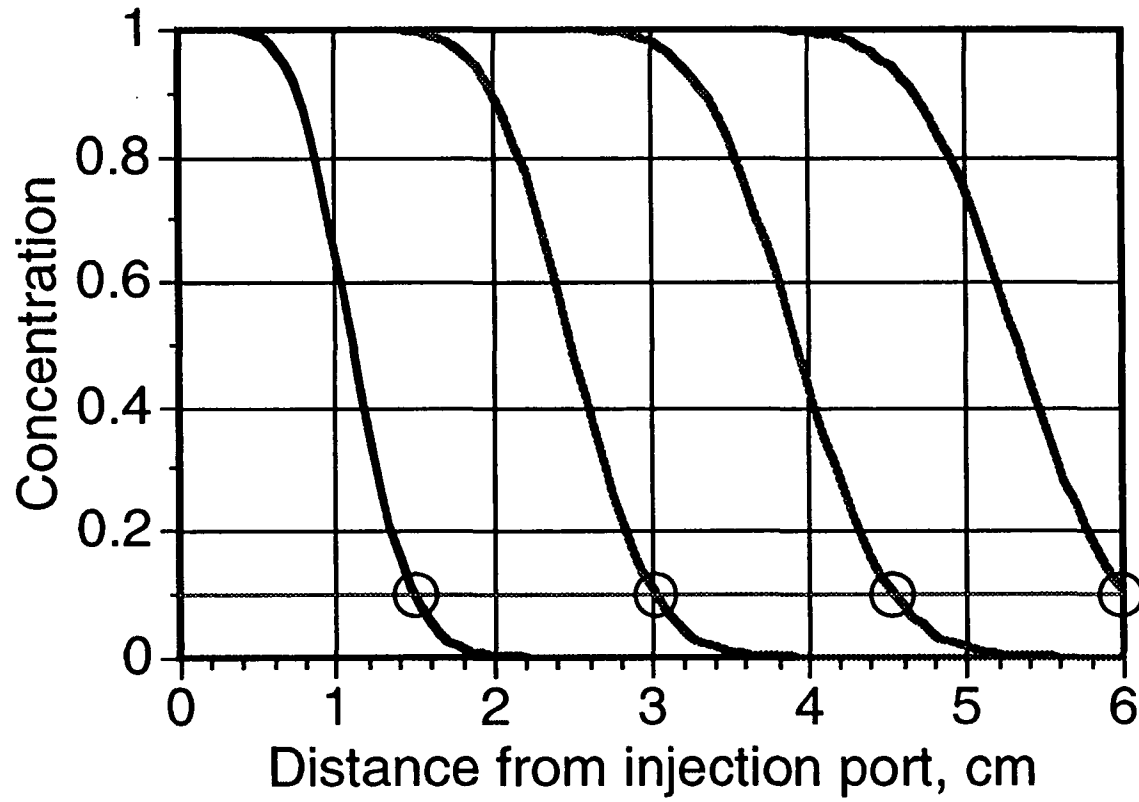
Radial geometry of fibrous mat with dye injection flow.



Computed breakthrough curves for $P = 10$.



Computed breakthrough curves for $P = 100$.



Computed breakthrough curves for $P = 1000$.

Conclusions

- Dead-end pores are relatively insignificant to the extrafiber pore space.
- Kyan's geometrical model significantly underestimates the open pore space in paper and similar fibrous structures.
- The relative porosity in paper is roughly 90% of the extrafiber porosity.

Applications to Consider

- Application of coatings
- Imbibition of fluids (including printing)
- Displacement dewatering in paper
- Displacement washing of pulp mats
- Flow through filters

**CONTROLLED CROWN PRESS
LUBRICATION AND HEAT TRANSFER**

SLIDE MATERIAL

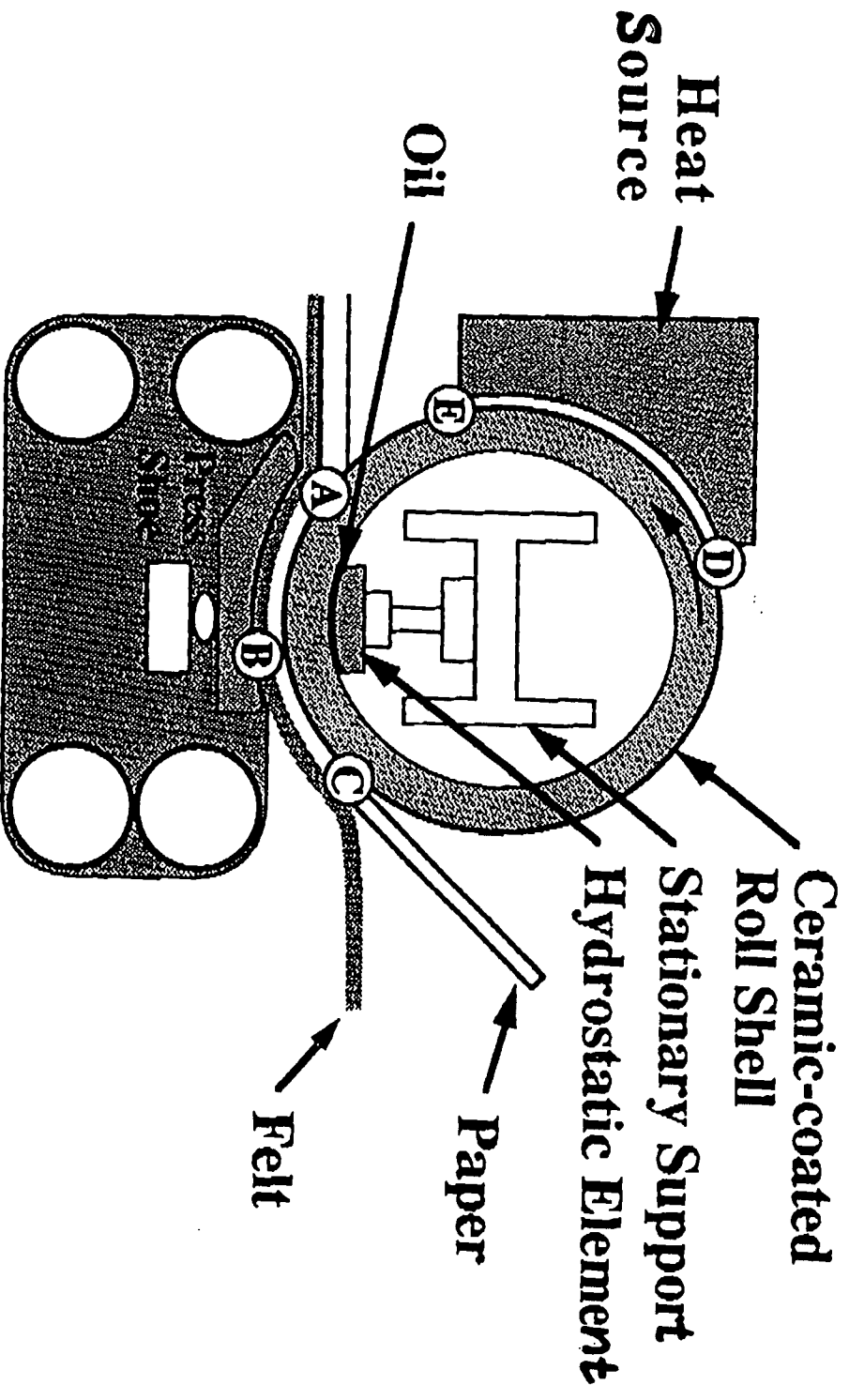
FOR

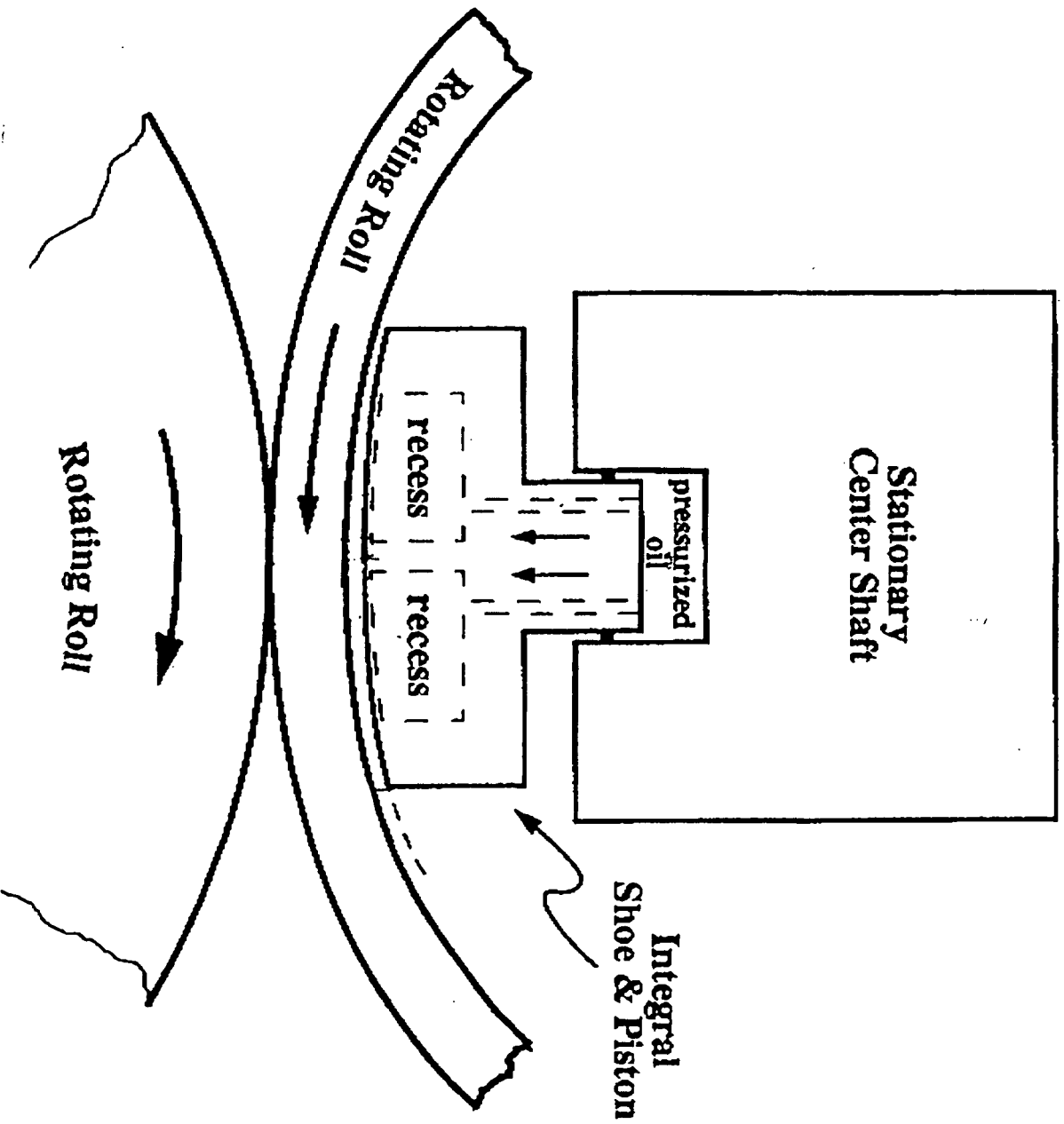
PROJECT 3470

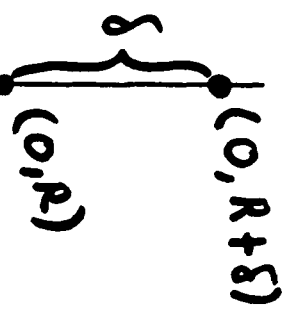
**March 22, 1994
Institute of Paper Science and Technology
Atlanta, Georgia**

MODELING OF FLUID FLOW AND HEAT TRANSFER IN A CROWN
COMPENSATED IMPULSE DRYING PRESS ROLL

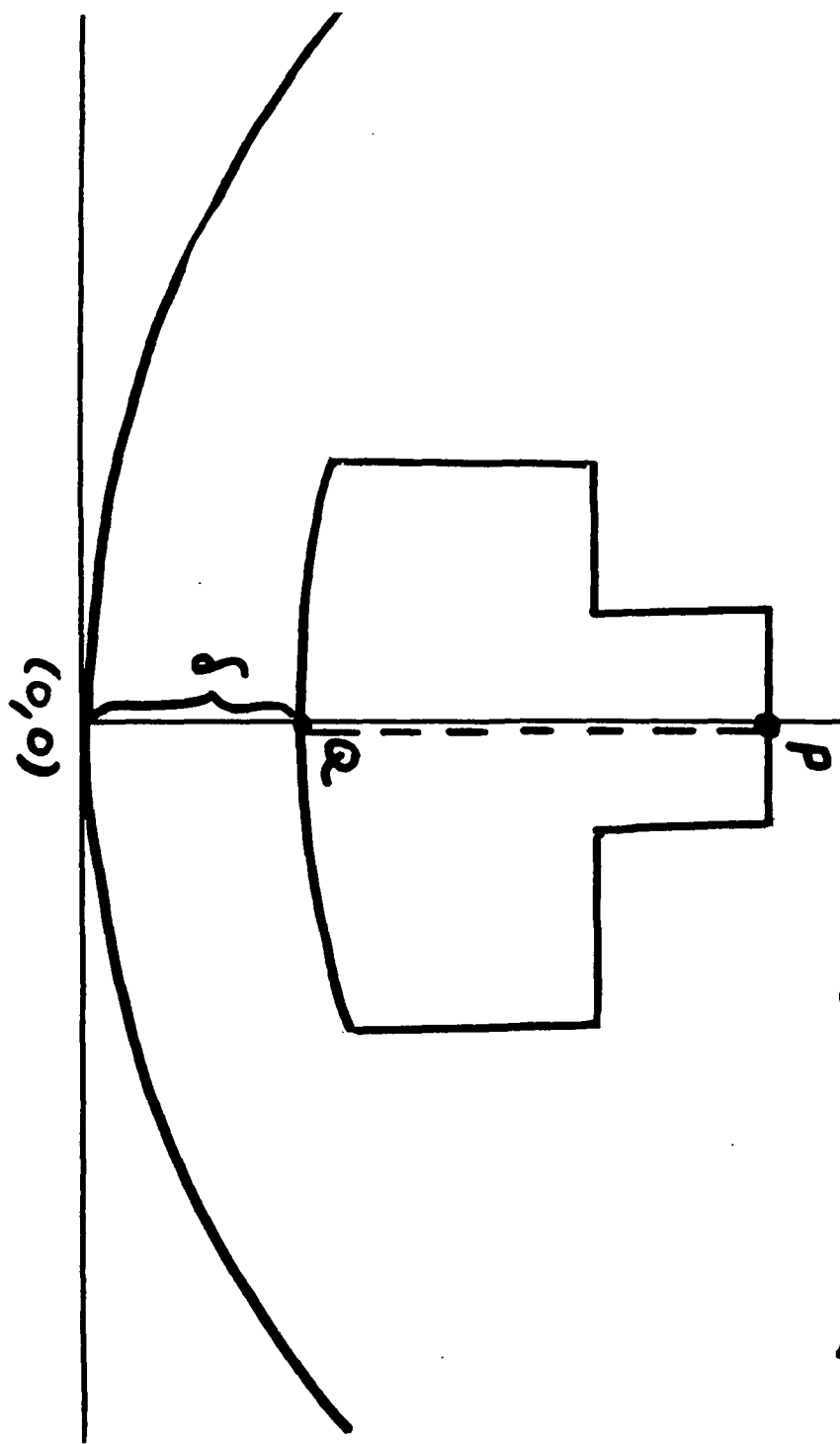
I: The Lubrication Problem

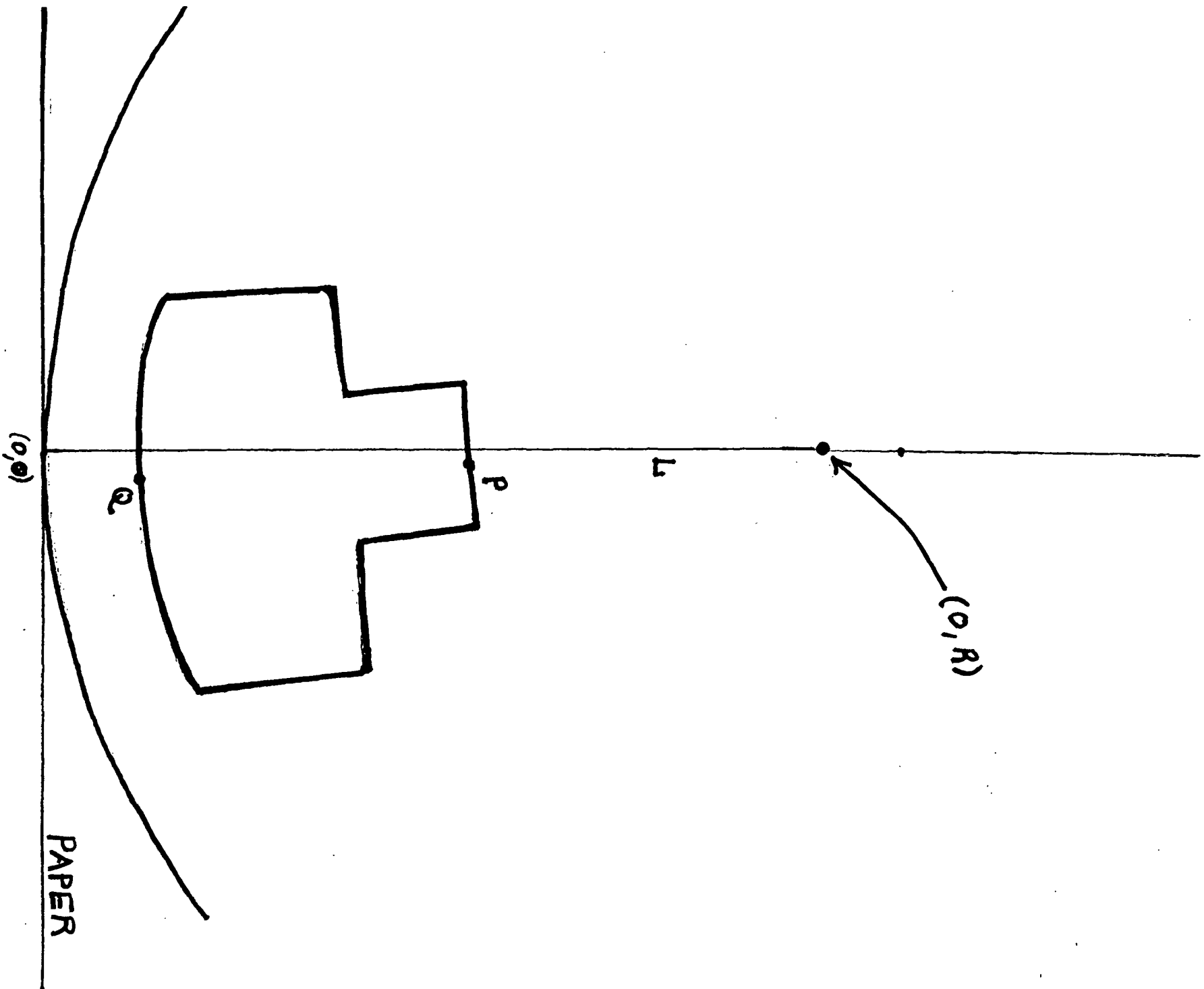


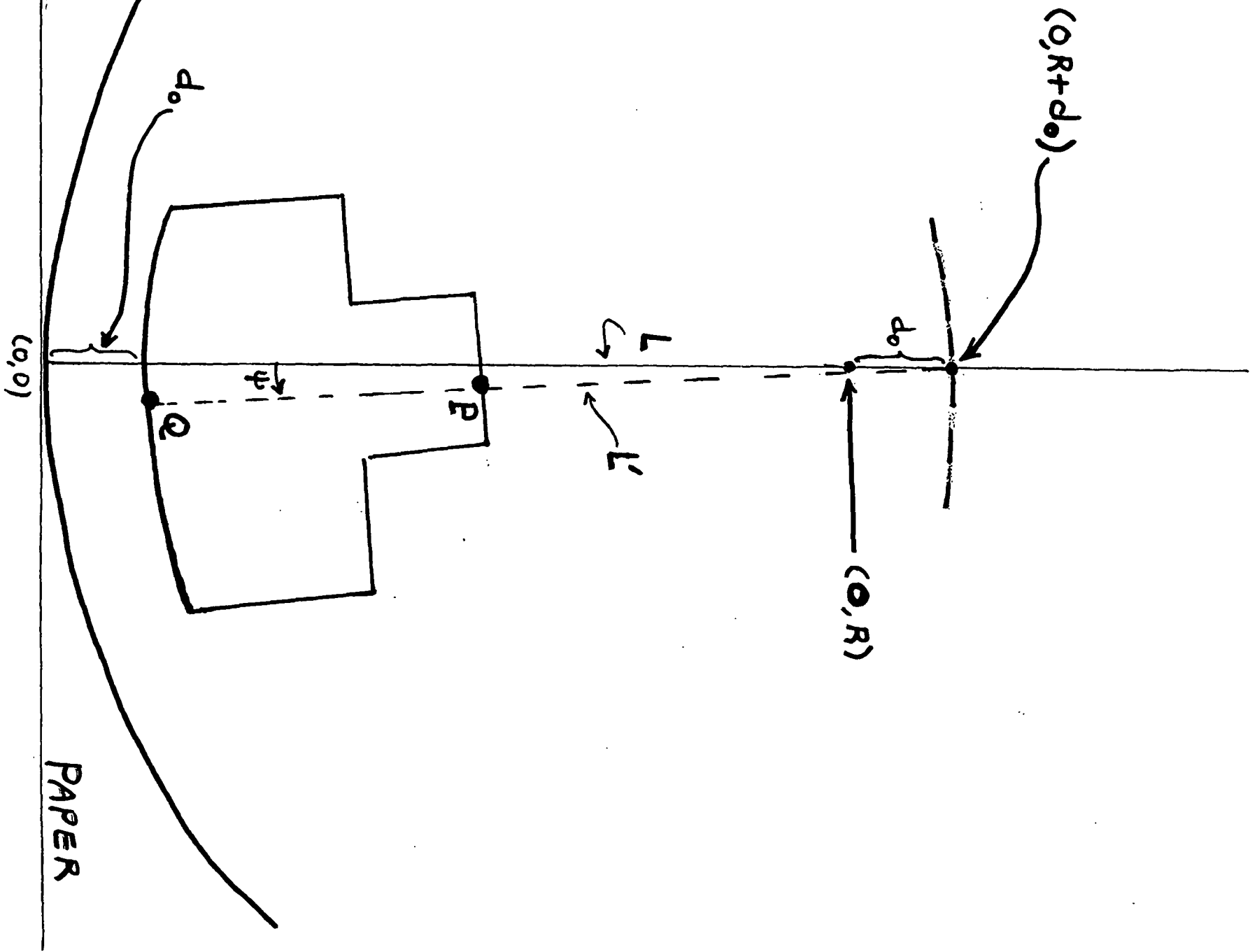


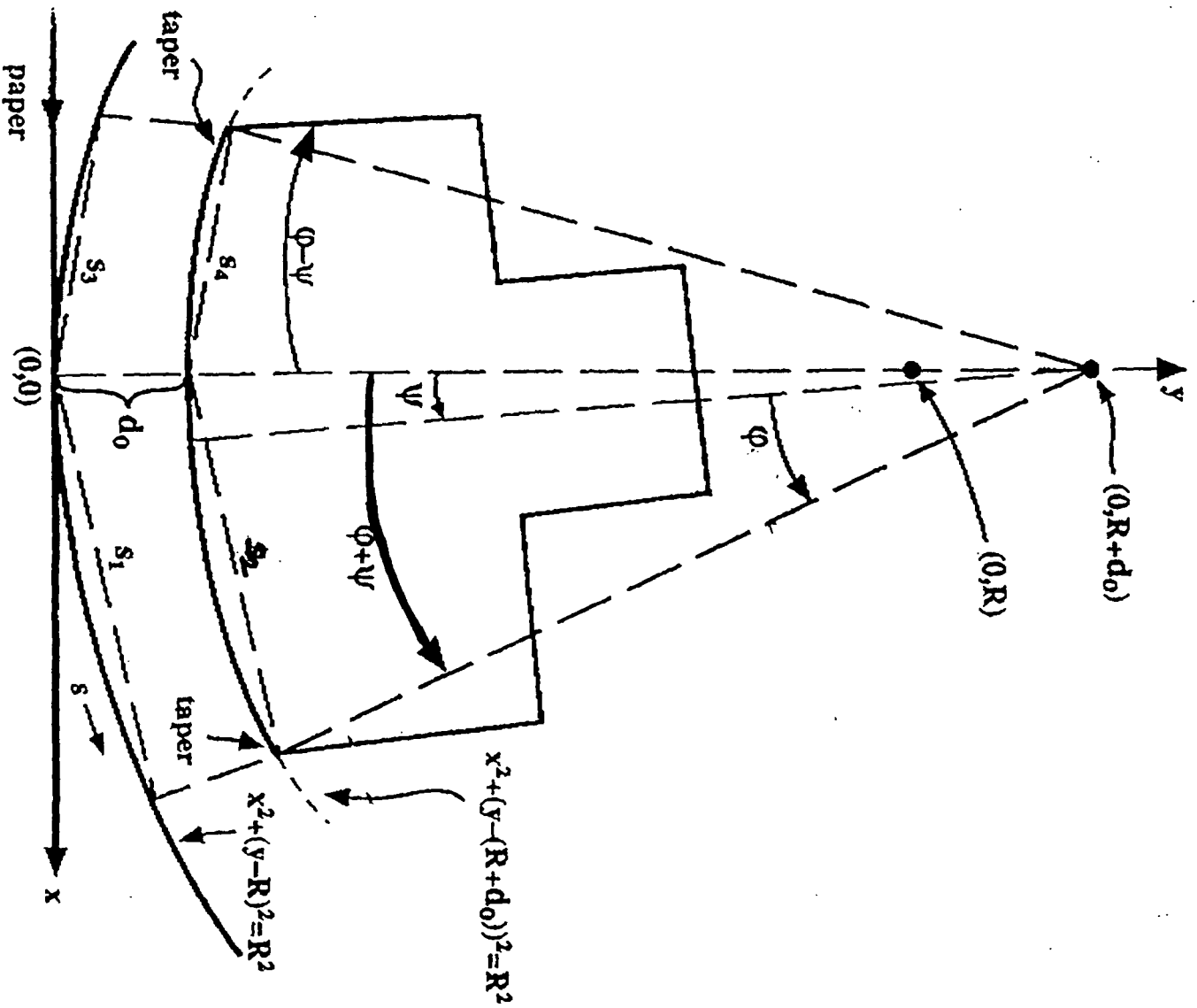


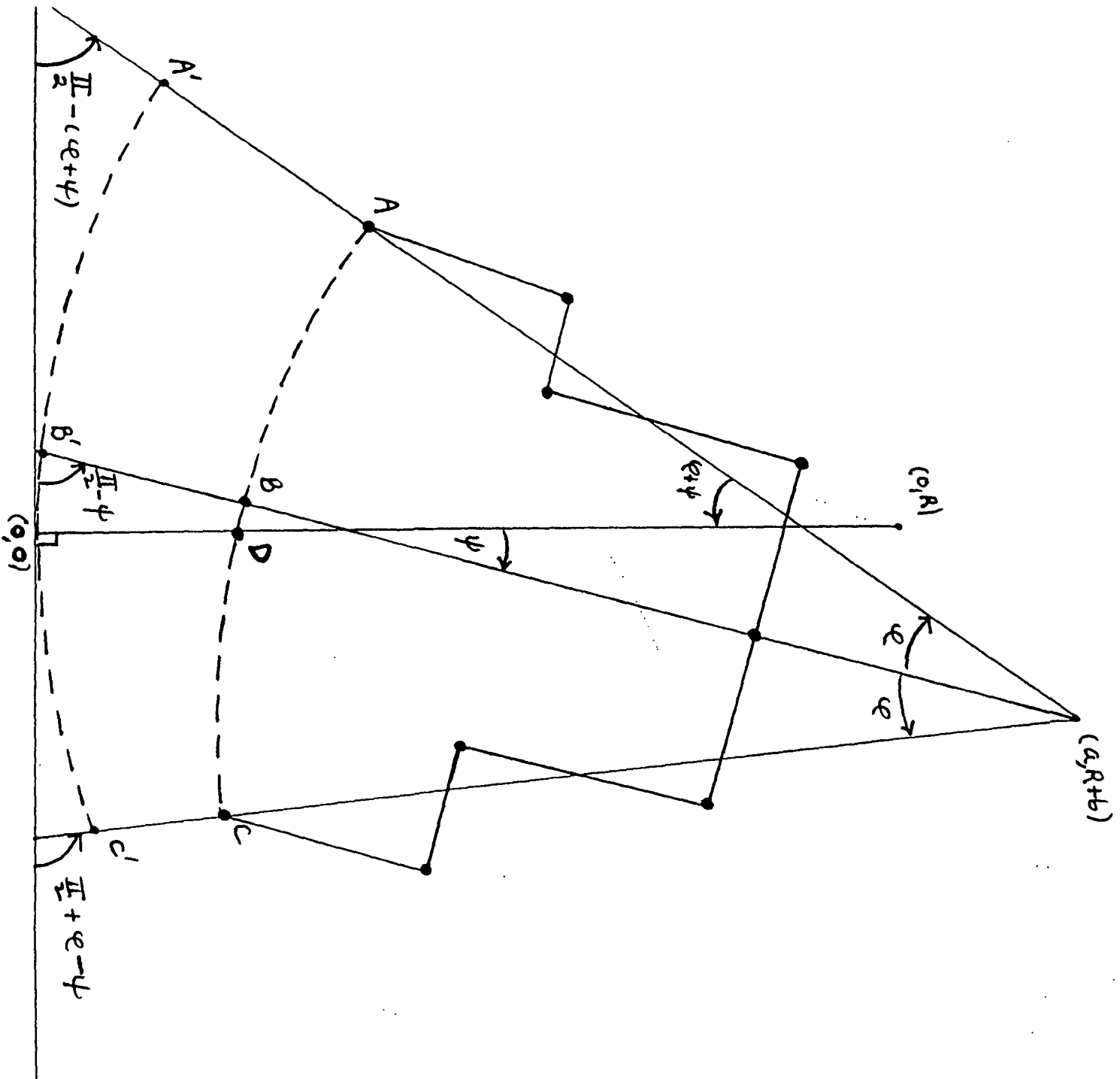
1. $P: \uparrow \downarrow$
2. $P: \rightleftarrows$
3. $\overline{P\mathcal{Q}} \rightarrow$ or $\overline{P\mathcal{Q}} \leftarrow$

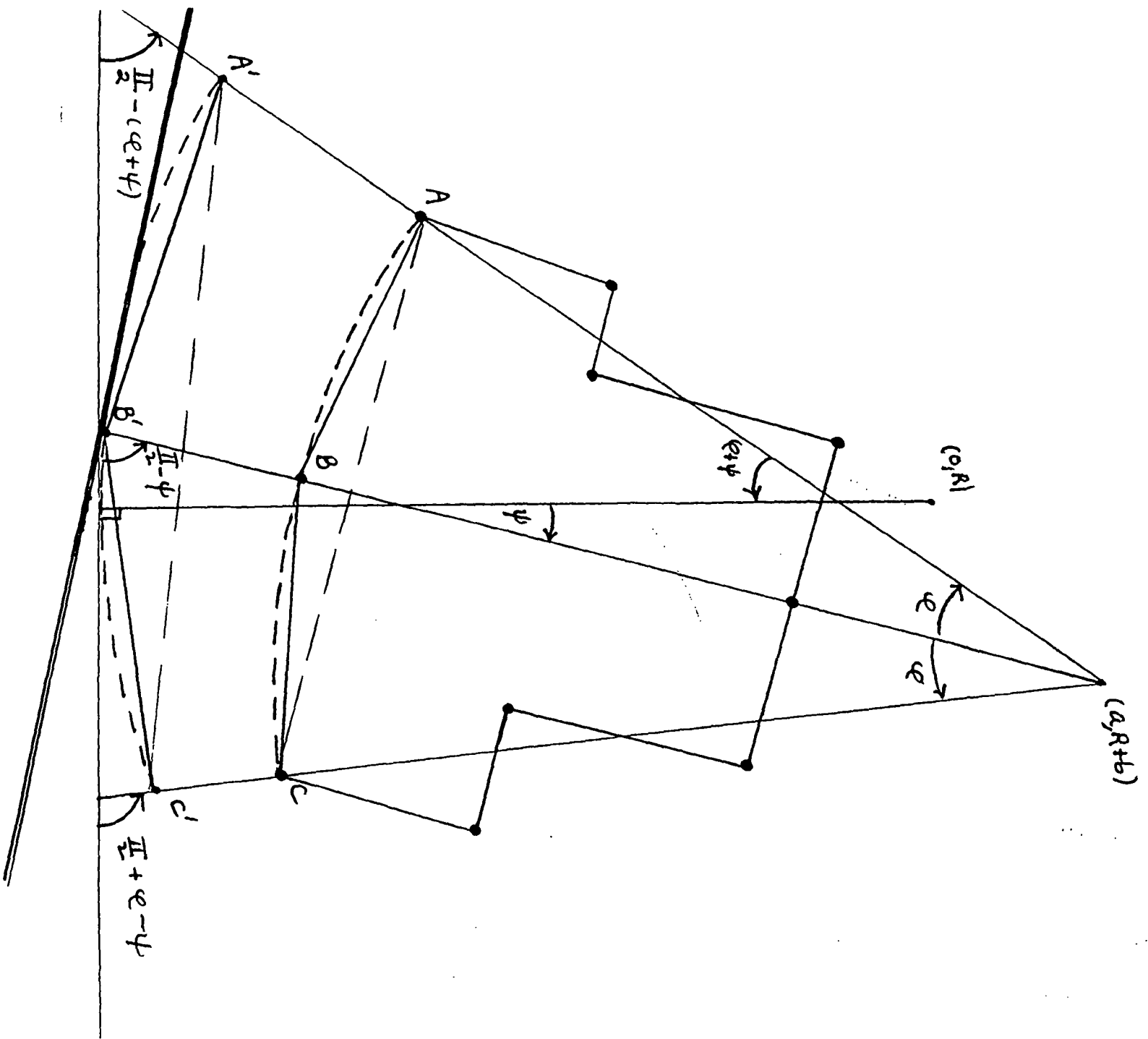


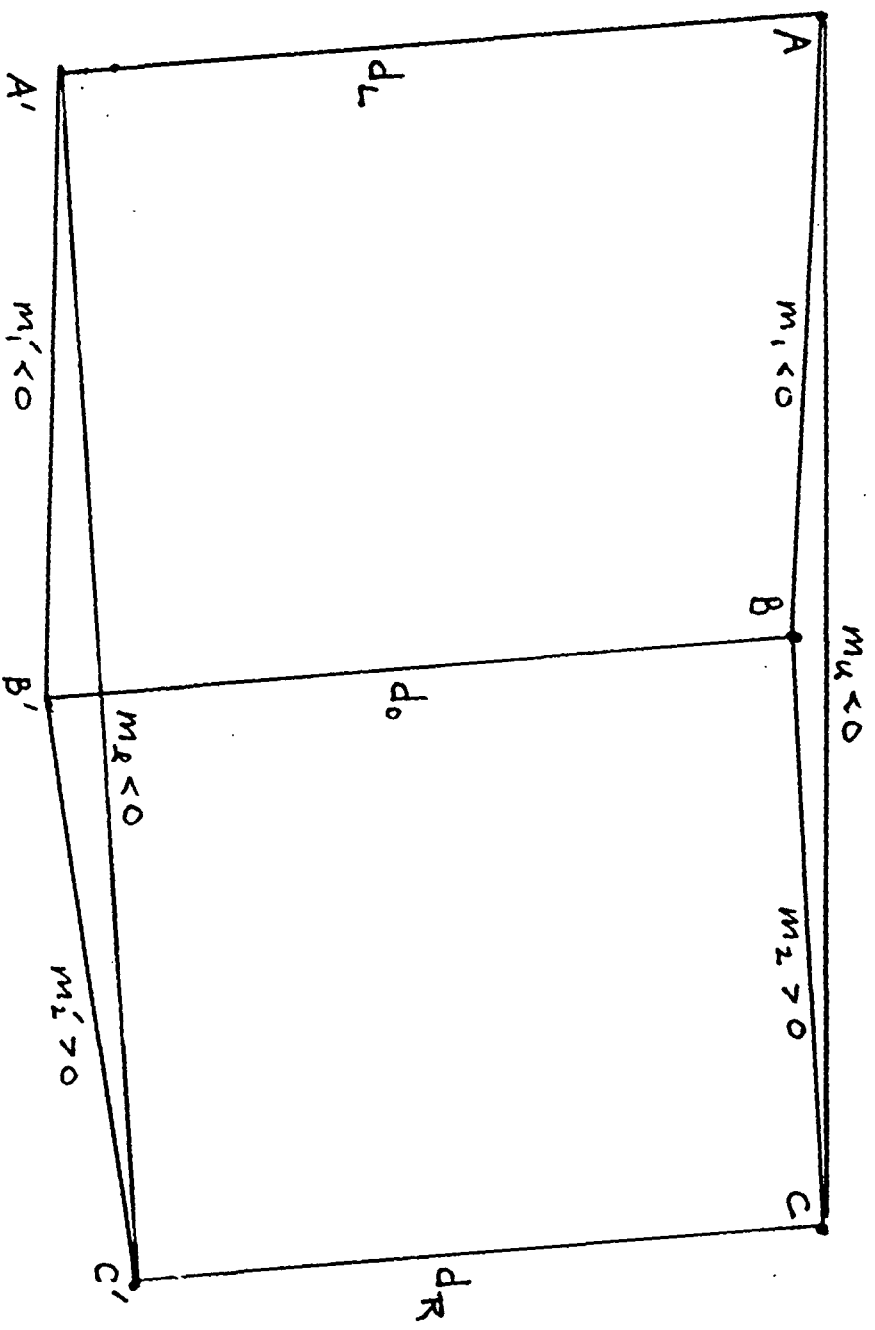




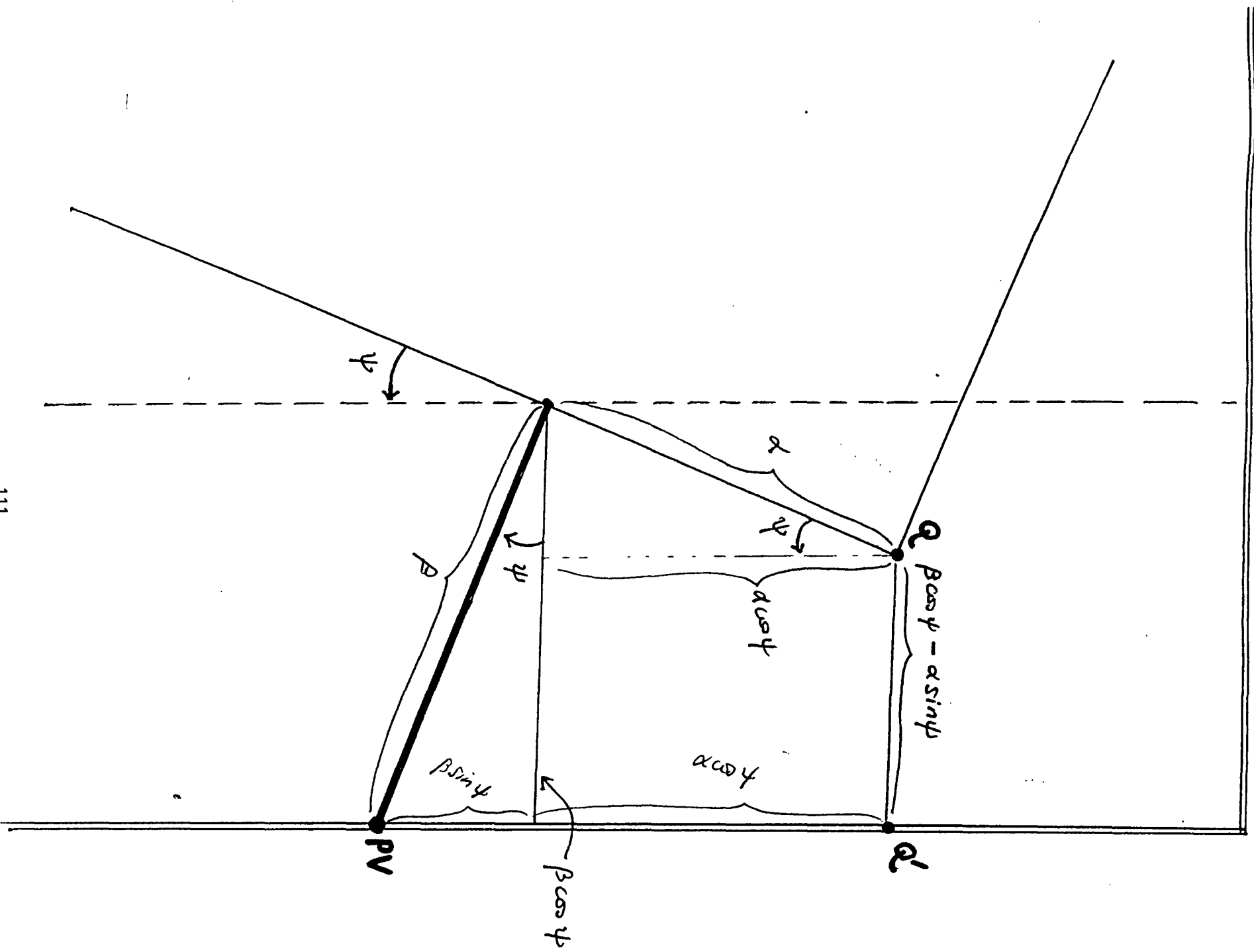


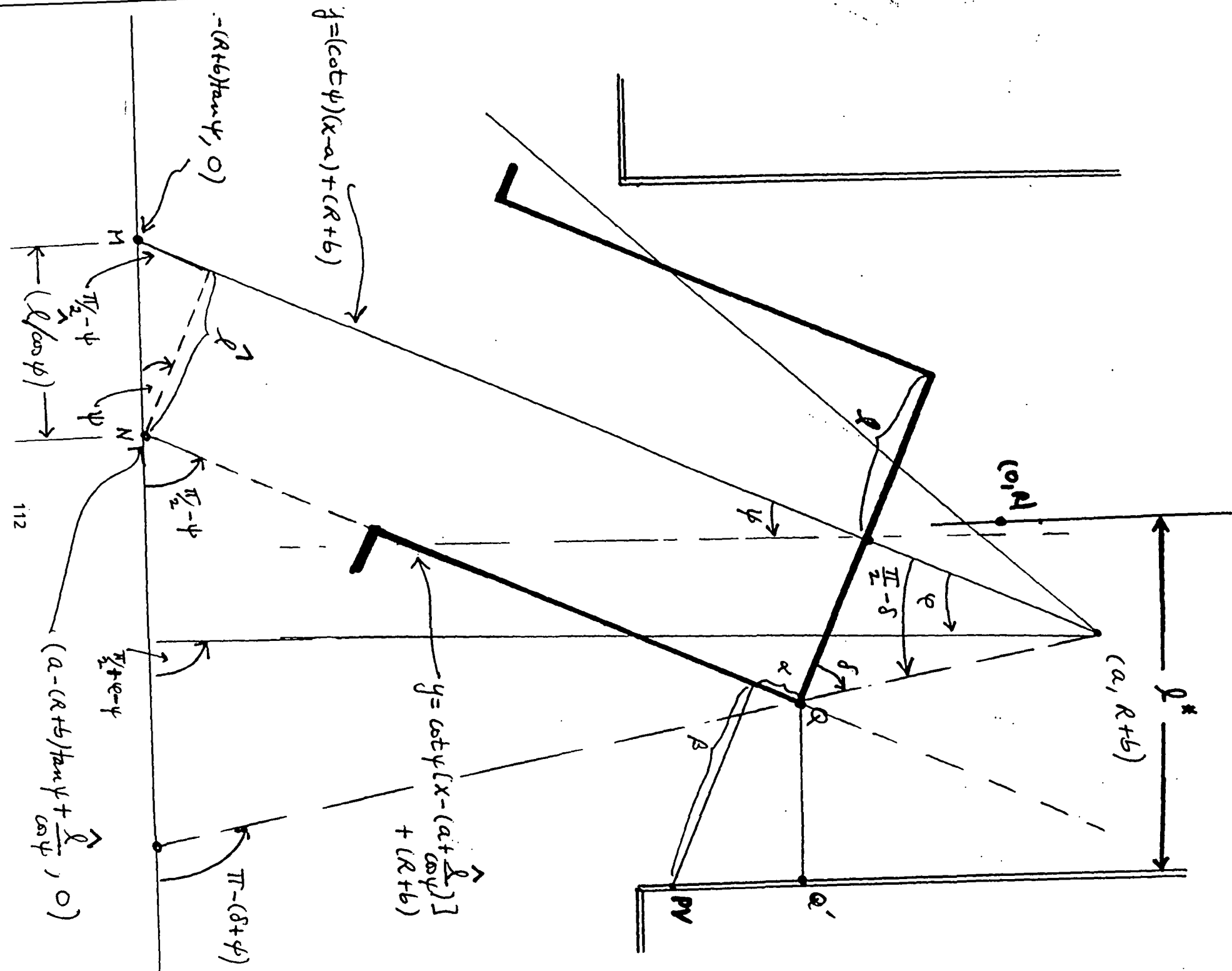






$$d_L > d_0 > d_R$$





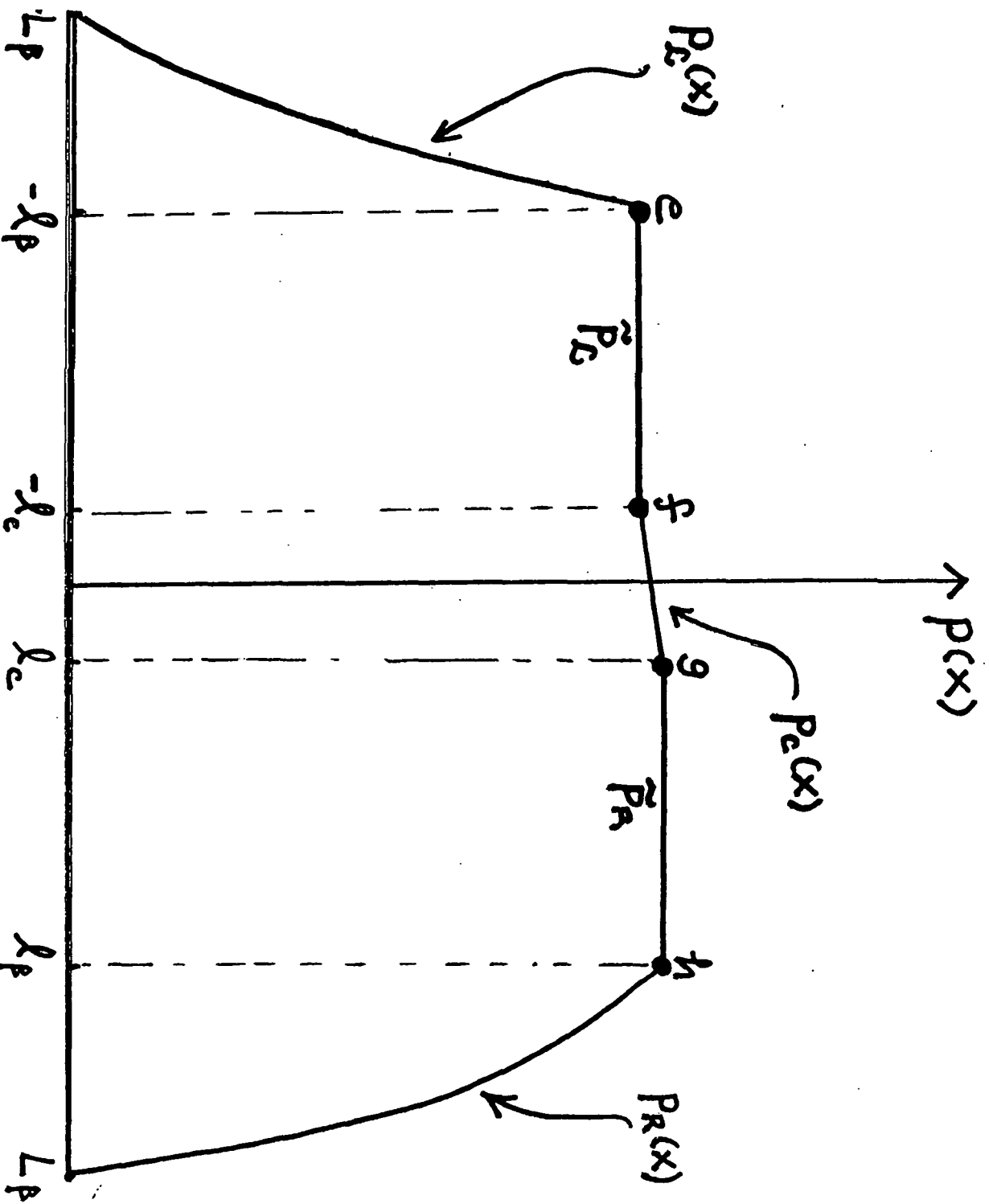
ASSUMPTIONS (AND HOW TO REMOVE THEM!)

APPROXIMATE THE CONVERGENT CURVILINEAR REGION BETWEEN THE BOTTOM OF THE SHOE AND THE INSIDE OF THE ROLL BY A PLANAR-WALLED CHANNEL.

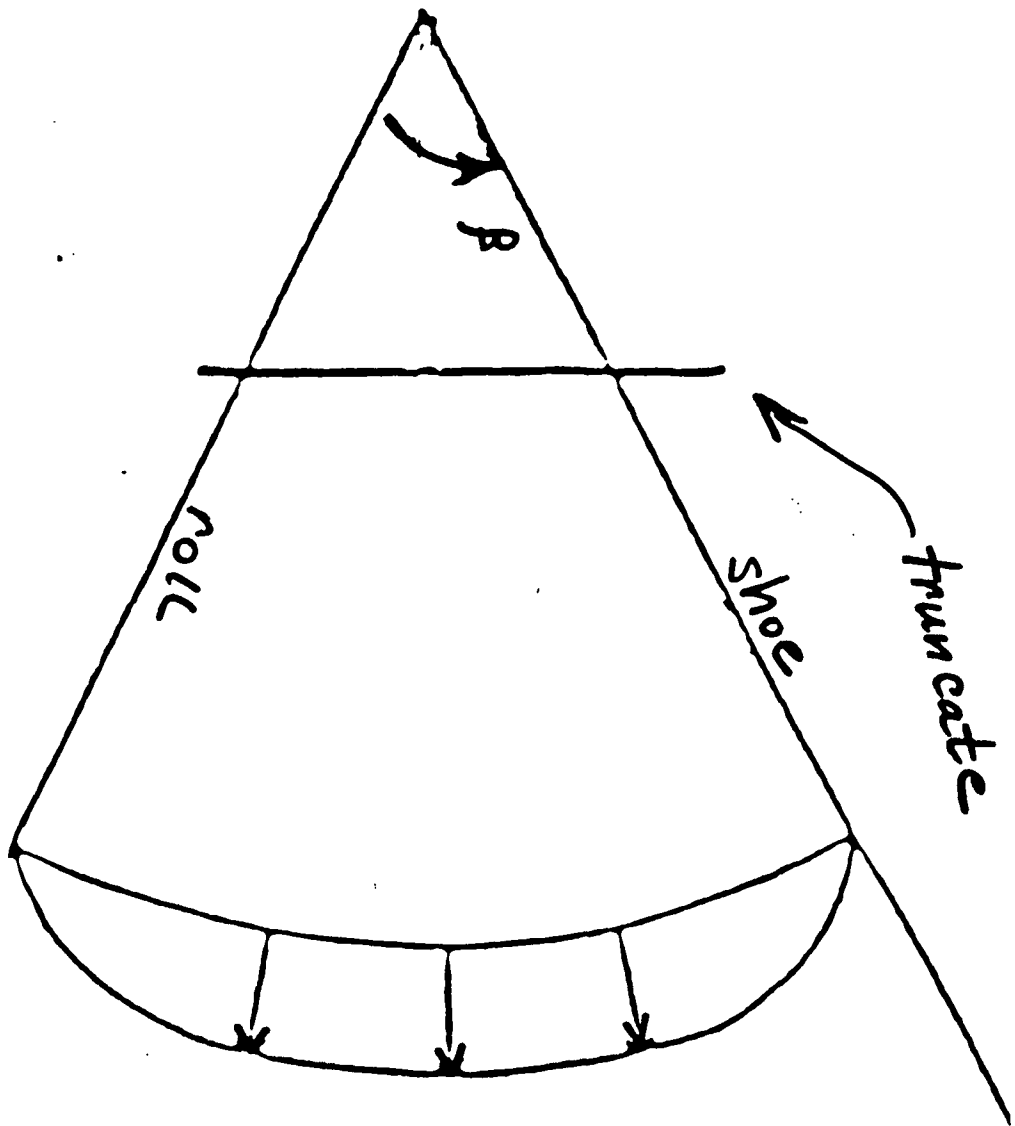
USE CONFORMAL MAPPING TO FIRST MAP THE ACTUAL CHANNEL ONTO A CURVILINEAR CHANNEL WHOSE WALLS LIE ON CONCENTRIC CIRCLES-THEN ANOTHER CONFORMAL MAP TO SEND THIS REGION ONTO A PARALLEL WALL CHANNEL.

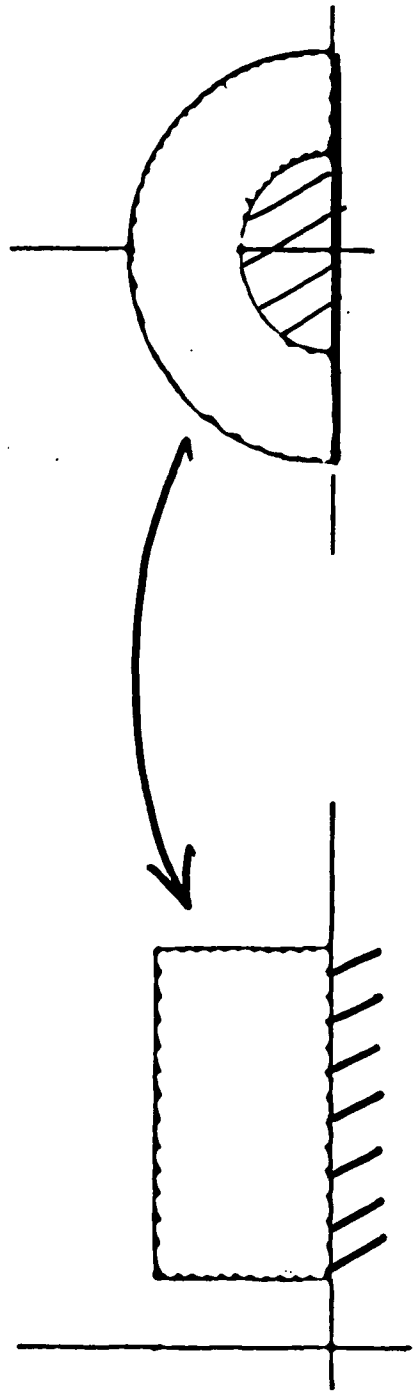
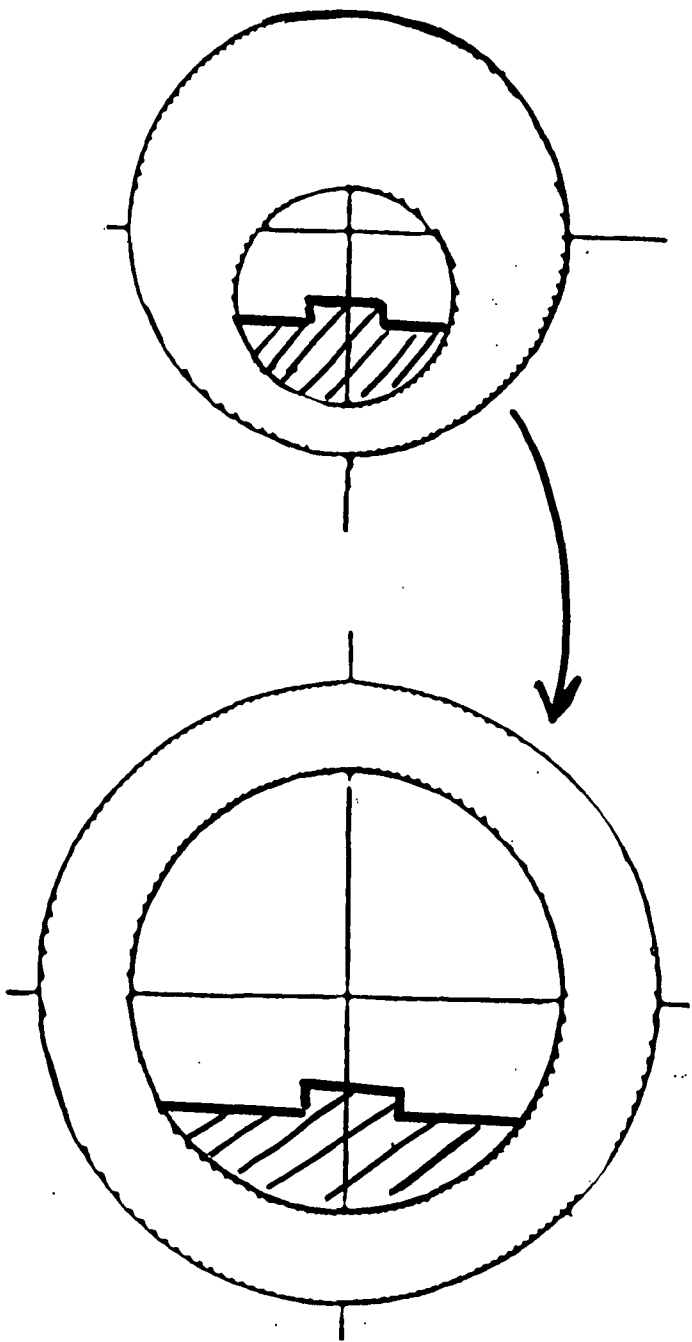
USE A STANDARD LUBRICATION THEORY ASSUMPTION TO WRITE DOWN GENERAL EXPRESSIONS FOR THE VELOCITY FIELDS WHICH MODIFY COUETTE-POISEUILLE FLOW.

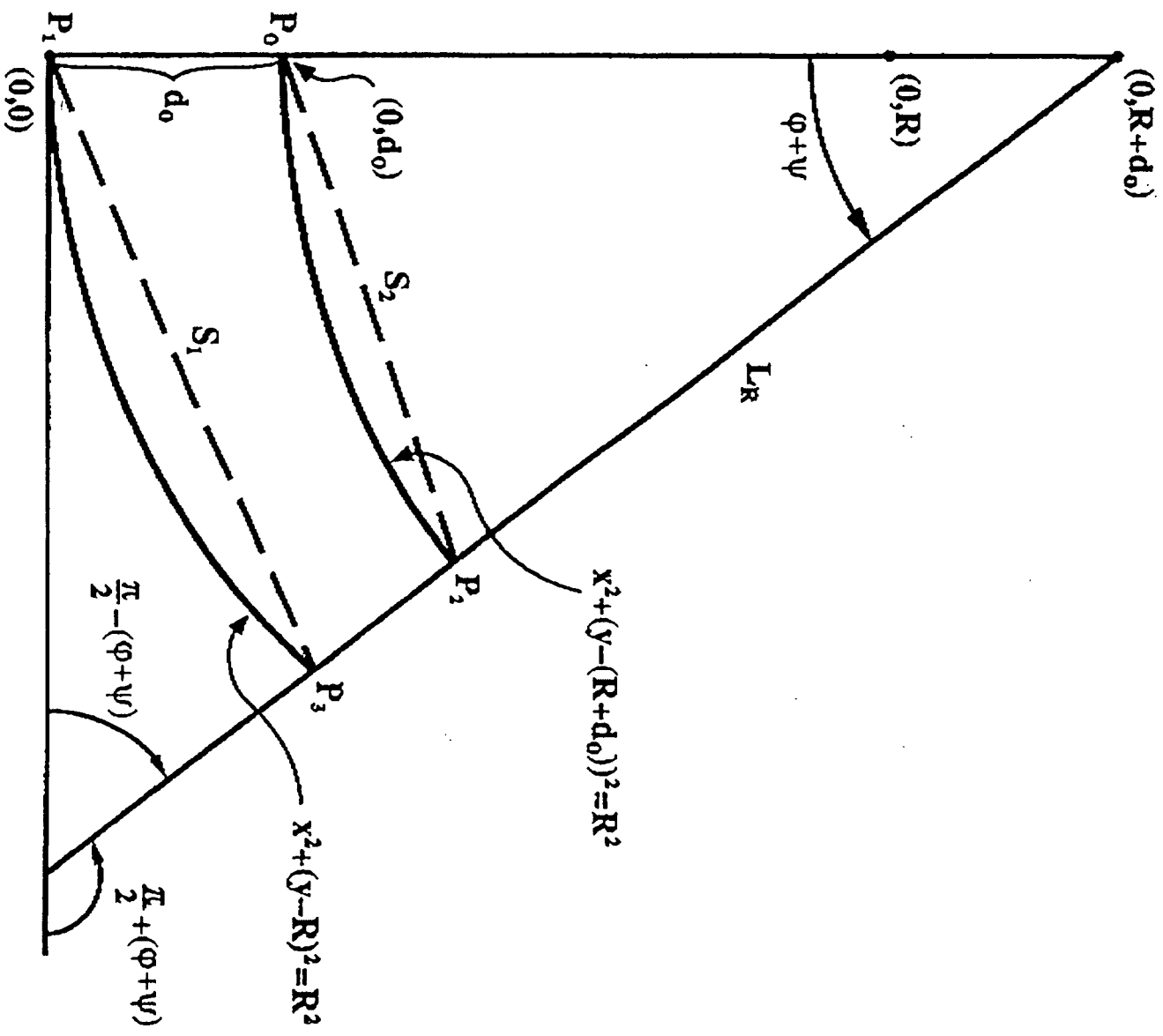
FOR THE APPROXIMATE PLANAR-WALLED CHANNEL INTRODUCED POLAR COORDINATES AND STUDY THE HAMMEL FLOW IN A (TRUNCATED) CONVERGENT WALL CHANNEL.

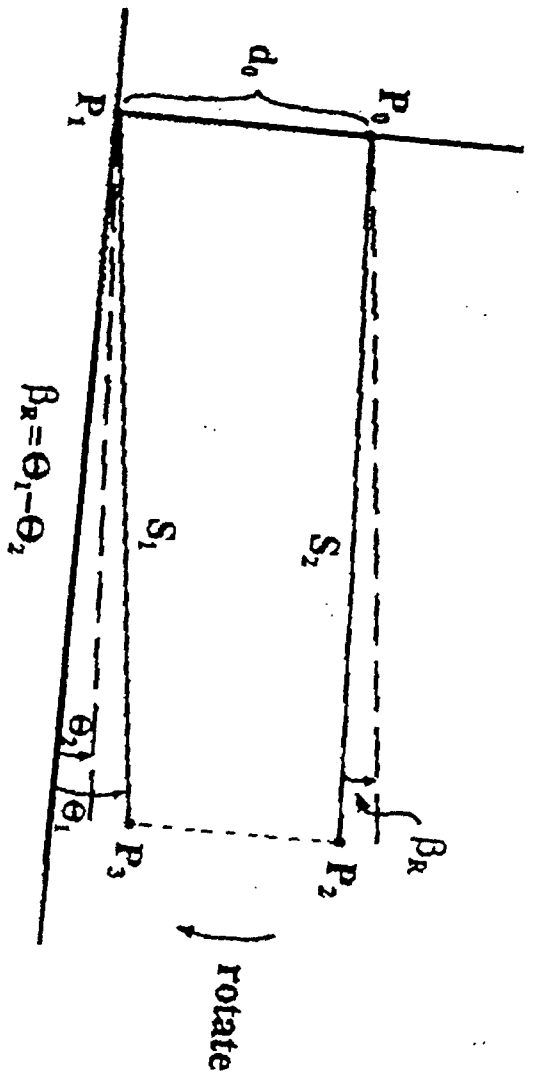


$p(x)$ is discontinuous at $e, f, g, h \Rightarrow$
 $\mathcal{N}(x, y)$ is discontinuous at e, f, g, h .



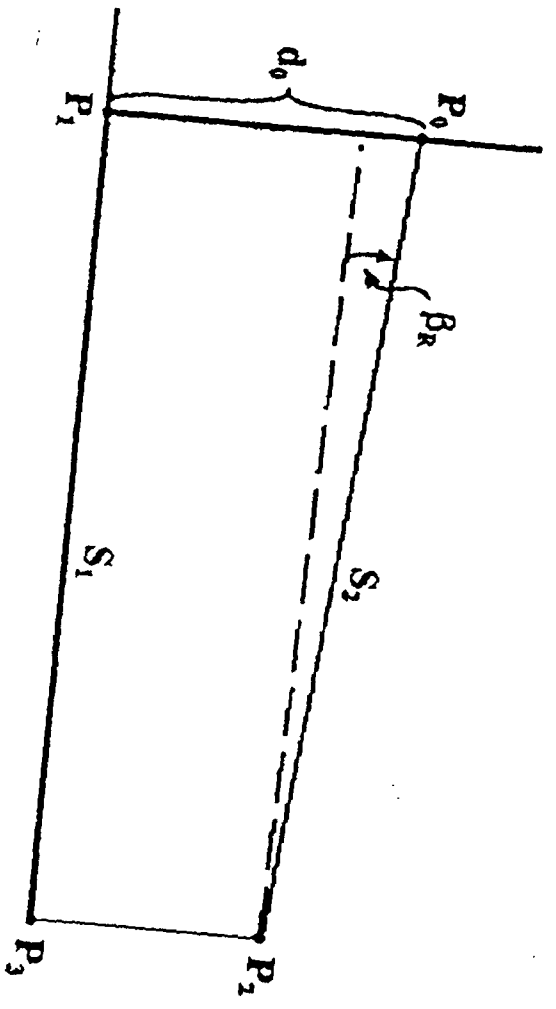






(a)

$$B_r = \theta_1 - \theta_2$$



(b)

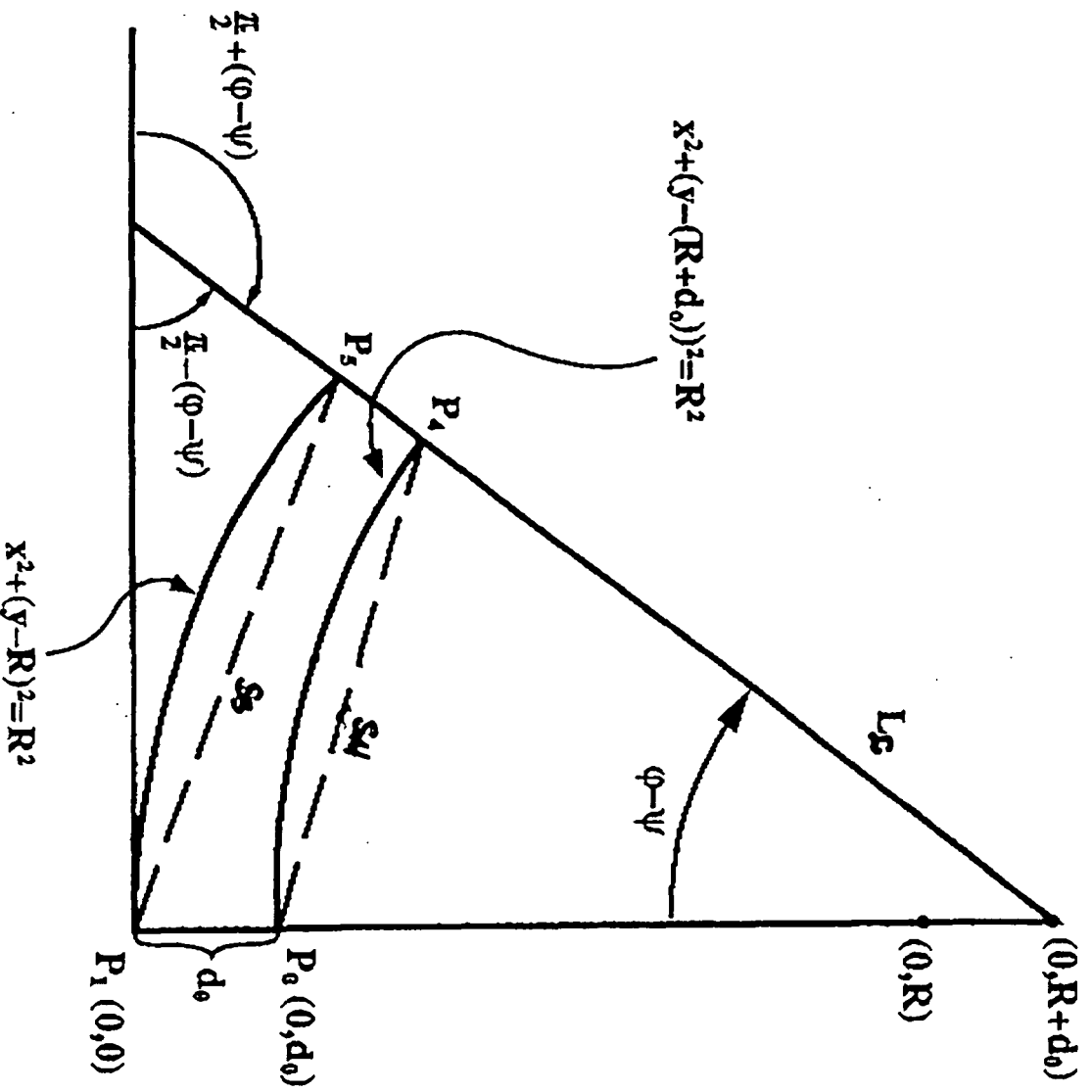
$$\tan \beta_r = \frac{[(mR(\varphi + \psi)x_3 + (R + d_0))/x_3] - \left[\frac{mR(\varphi + \psi) + \sqrt{1 + mR^2(\varphi + \psi)}}{1 + [(mR(\varphi + \psi)x_3 + (R + d_0))/x_3]} [mR(\varphi + \psi) + \sqrt{1 + mR^2(\varphi + \psi)}] \right]}{1 + [(mR(\varphi + \psi)x_3 + (R + d_0))/x_3] \left[\frac{-mRd_0 + \sqrt{mR^2d_0^2 + (1 + mR^2)(R^2 - d_0^2)}}{1 + mR^2} \right]}$$

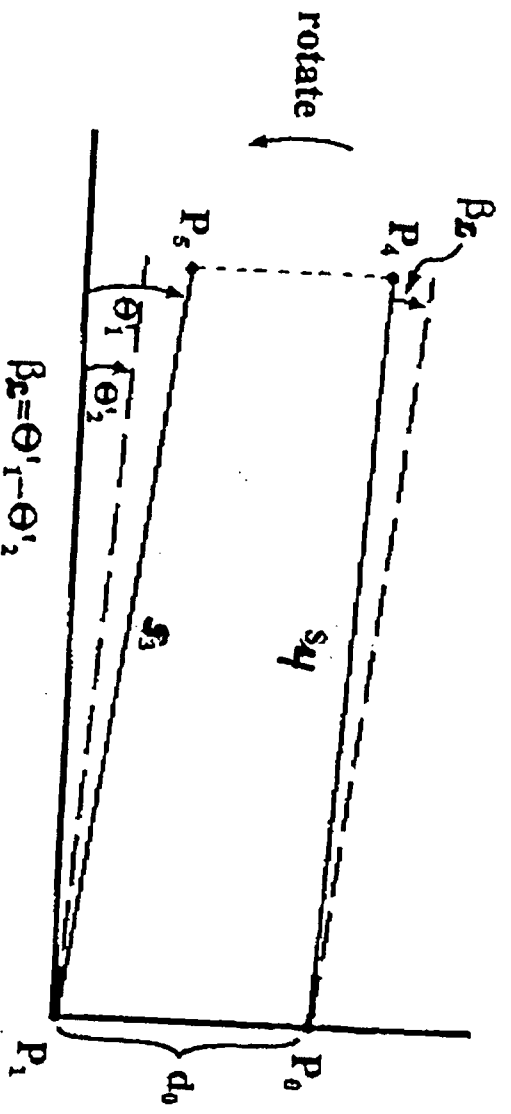
$$\tan \beta_r \simeq \left(\frac{d_0}{2R} \right) \sin(\phi + \psi) \quad (\beta_r = \theta_1 - \theta_2)$$

$$l_r = R\sqrt{2(1 - \cos(\phi + \psi))}$$

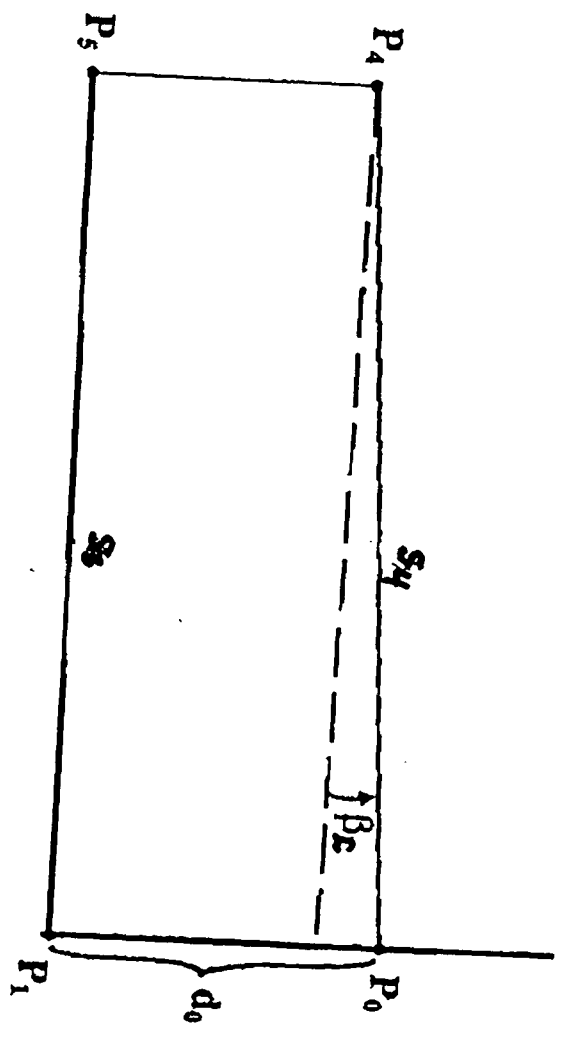
$$L_r = l_r \cos \beta_r$$

$$d_r(x) = d_0 - x \tan \beta_r, \quad 0 \leq x \leq L_r$$





(a)



(b)

$$\tan \beta_C \simeq \left(\frac{d_0}{2R} \right) \sin(\phi - \psi) \quad (\beta_C = \theta'_1 - \theta'_2)$$

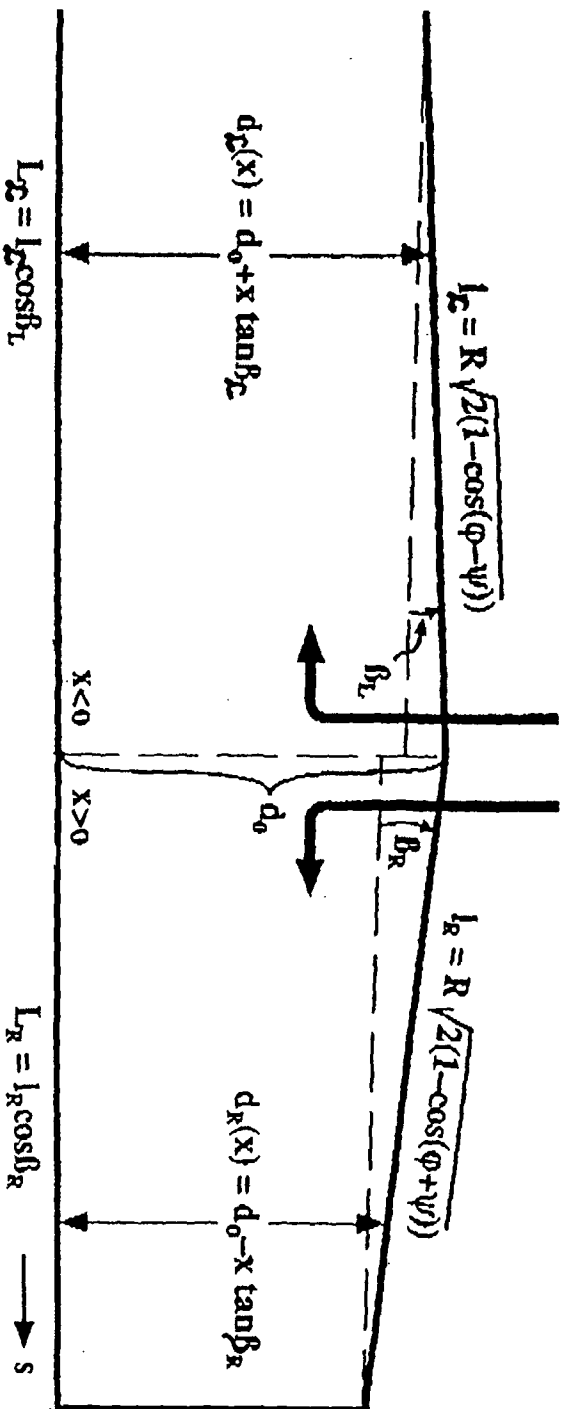
$$l_C = R \sqrt{2(1 - \cos(\phi - \psi))}$$

$$L_C = l_C \cos \beta_C$$

AND

$$d_C(x) = d_0 - x \tan \beta_C, \quad 0 \leq x \leq L_C$$

Lubricant flow



$$\psi = \psi(F, P_{sh}, P_{exit}, s, R, \varphi, \bar{R}, \mu, \rho)$$

$$d_0 = d_0(F, P_{sh}, P_{exit}, s, R, \varphi, \bar{R}, \mu, \rho)$$

$$u_{R}(x, y) = \frac{C_{R}(x)}{2\mu} y (d_{R}(x) - y) + s \left(\frac{d_{R}(x) - y}{d_{R}(x)} \right)$$

$$\dot{m}_{R} = \rho \int_0^{d_{R}(x)} u_{R}(x, y) dy \equiv \frac{\rho C_{R}(x) d_{R}^3(x)}{12\mu} + \frac{1}{2} \rho s d_{R}(x)$$

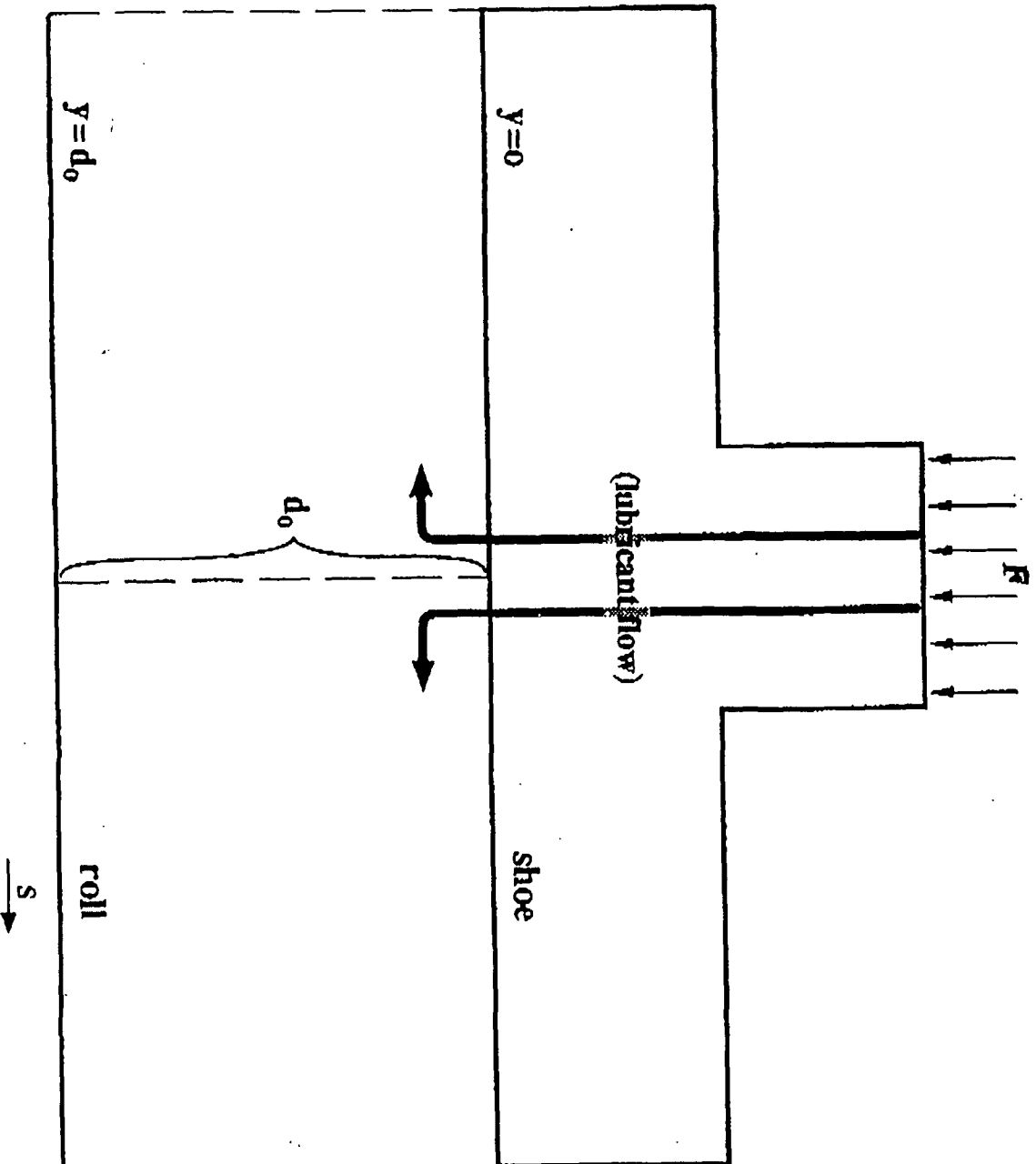
$$p'_{R}(x) = -C_{R}(x) \equiv 6\mu \left(\frac{s}{d_{R}^2(x)} - \frac{2\dot{m}_{R}}{\rho d_{R}^3(x)} \right)$$

$$p_{R}(x) - \tilde{p}_{R} = \frac{6\mu}{\tan \beta_{R}} \left[s \left(\frac{1}{d_{R}(x)} - \frac{1}{d_0} \right) - \frac{\dot{m}_{R}}{\rho} \left(\frac{1}{d_{R}^2(x)} - \frac{1}{d_0^2} \right) \right]$$

Set $x = L_{R}$, $P_{R}^{*} = P_{R}(L_{R})$, $\Delta P_{R} = P_{R}^{*} - \tilde{P}_{R} \Rightarrow$

$$\Delta p_{pr} = \frac{6\mu}{\tan \beta r} \left[s \left(\frac{1}{d_r^*} - \frac{1}{d_0} \right) - \frac{m_r}{\rho} \left(\frac{1}{(d_r^*)^2} - \frac{1}{d_0^2} \right) \right]$$

$$\lim_{\beta r \rightarrow 0} m_r = \frac{1}{2} \rho s d_0 + \frac{\rho \Delta p_{pr} d_0^3}{12 \mu l r}$$



$$u_C(x, y) = \frac{C_C(x)}{2\mu} y(d_C(x) - y) - s \left(\frac{d_C(x) - y}{d_C(x)} \right)$$

$$\dot{m}_C = \rho \int_0^{d_C(x)} u_C(x, y) dy = \frac{\rho C_C(x) d_C^3(x)}{12\mu} - \frac{1}{2} \rho s d_C(x)$$

$$p'_C(x) = -C_C(x) \equiv -6\mu \left(\frac{2\dot{m}_C}{\rho d_C^3(x)} + \frac{s}{d_C^2(x)} \right)$$

$$p_C(x) - \bar{p}_C = \frac{-6\mu}{\tan \beta_C} \left[s \left(\frac{1}{d_C(x)} - \frac{1}{d_0} \right) + \frac{\dot{m}_C}{\rho} \left(\frac{1}{d_C^2(x)} - \frac{1}{d_0^2} \right) \right]$$

set $x = L_C$, $P_C^* = P_C(L_C)$, $\Delta P_C = P_C^* - \bar{p}_C \Rightarrow$

$$\Delta p_C = \frac{-6\mu}{\tan \beta_C} \left[s \left(\frac{1}{d_C^*} - \frac{1}{d_0} \right) + \frac{m_C}{\rho} \left(\frac{1}{(d_C^*)^2} - \frac{1}{d_0^2} \right) \right]$$

N.B. m_z : \leftarrow

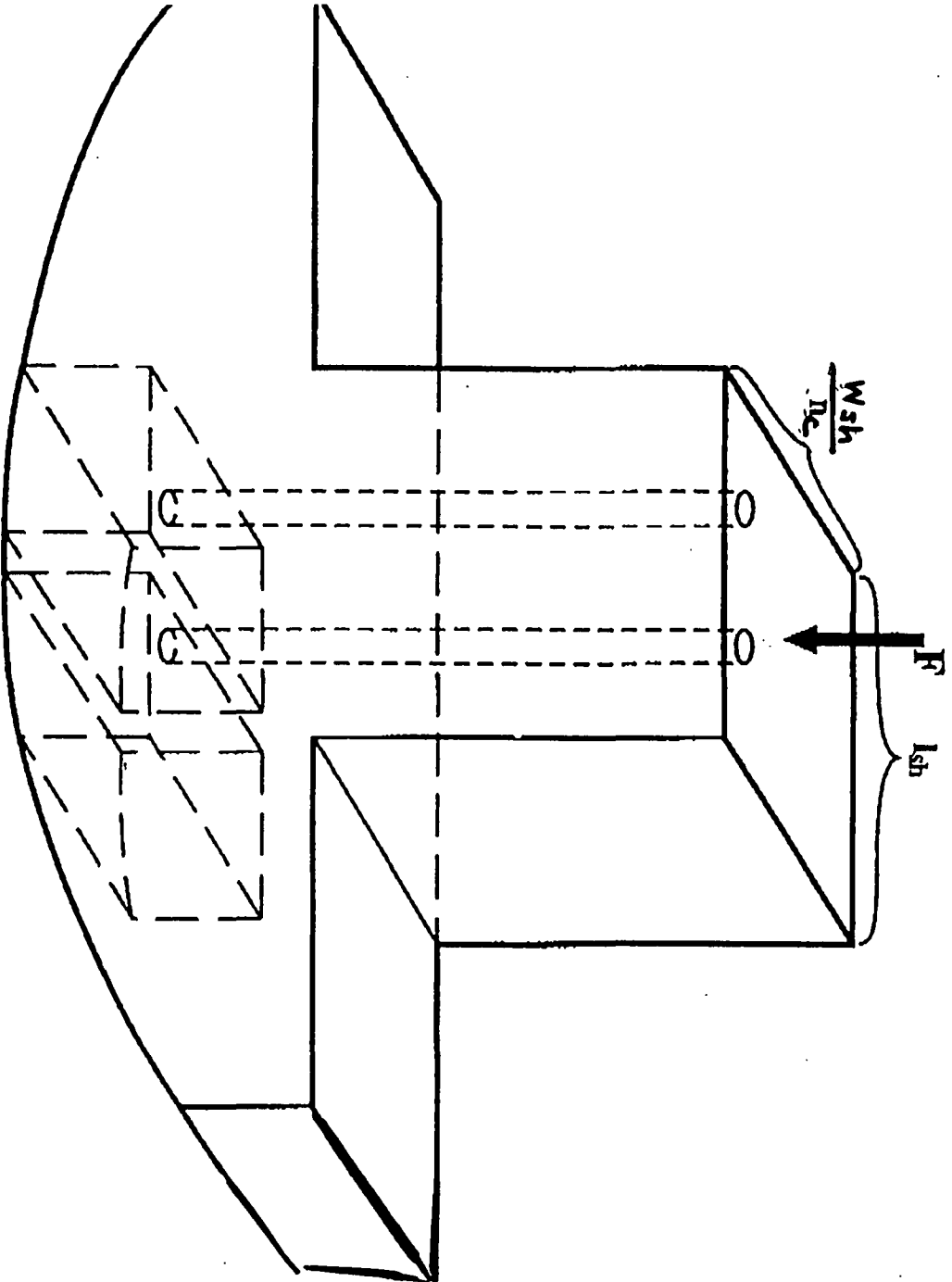
$$m_C \rightarrow -\frac{1}{2} \rho s d_0 + \frac{\rho \Delta p_C d_0^3}{12\mu l} \quad (\text{as } \beta_C \rightarrow 0)$$

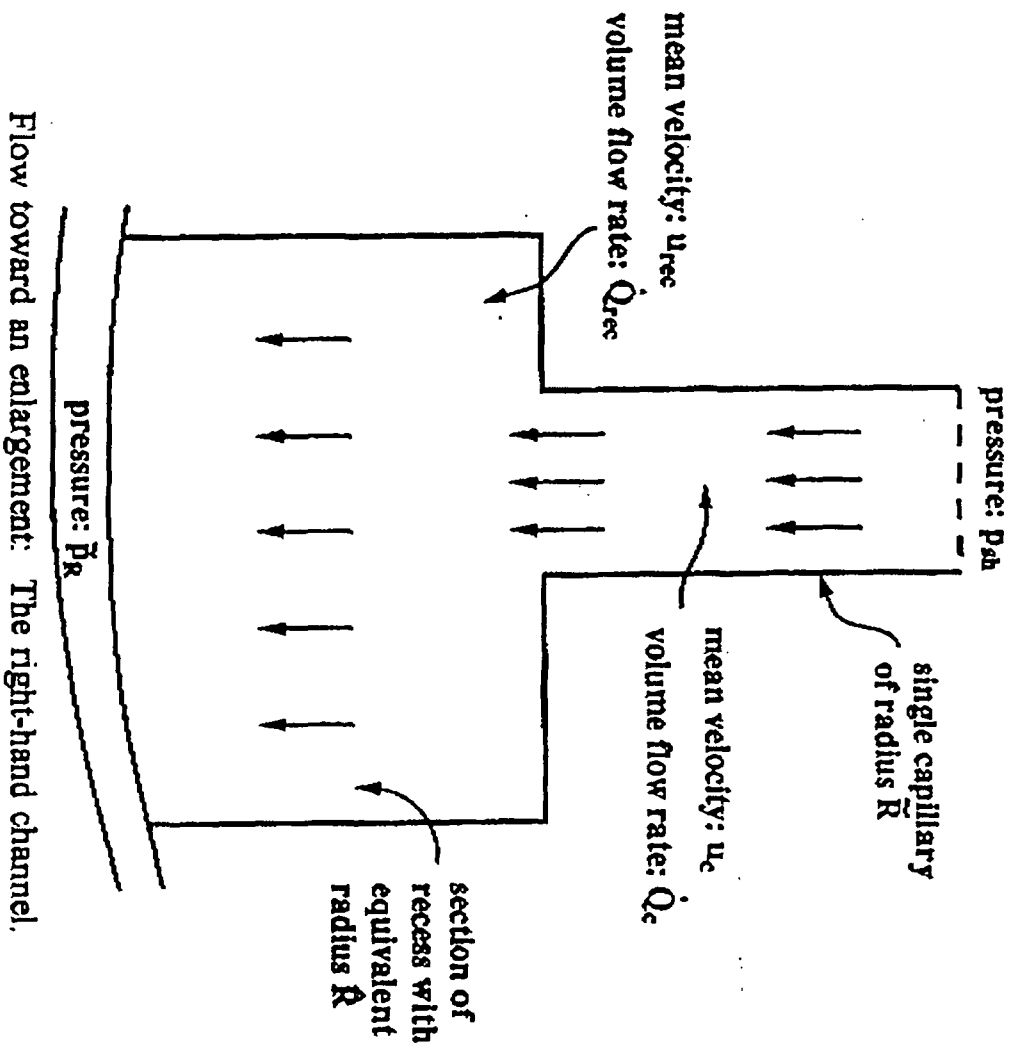
Now need to relate m_C and m_z to

S and $p_{sh} - p_{atm}$. ($p_{atm} = p_R^* = p_C^*$)

$$p_{atm} - \bar{p}_R = \frac{6\mu}{\tan \beta_R} \left[s \left(\frac{1}{d_R^*} - \frac{1}{d_0} \right) - \frac{m_R}{\rho} \left(\frac{1}{d_R^{*2}} - \frac{1}{d_0^2} \right) \right]$$

$$p_{atm} - \bar{p}_C = \frac{-6\mu}{\tan \beta_C} \left[s \left(\frac{1}{d_C^*} - \frac{1}{d_0} \right) + \frac{m_C}{\rho} \left(\frac{1}{(d_C^*)^2} - \frac{1}{d_0^2} \right) \right]$$





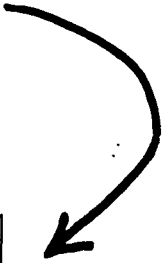
$$\bar{p}_R = p_{sh} + \rho u_{rec}(u_c - u_{rec})$$

$$\dot{Q}_c = \pi R^2 u_c, \quad \dot{Q}_{rec} = \pi R^2 u_{rec}$$

$$\dot{Q}_c = \dot{Q}_{rec}$$

$$\alpha = \rho \left(\frac{\bar{R}}{\hat{R}} \right)^2 \left(1 - \left(\frac{\bar{R}}{\hat{R}} \right)^2 \right)$$

$$\bar{p}_R = p_{sh} + \left(\frac{\dot{m}_R}{\rho} \right)^2 \cdot \frac{100\alpha}{\pi^2 \bar{R}^4}$$

$$p_{atm} - \bar{p}_R = \frac{6\mu}{\tan \beta_R} \left[s \left(\frac{1}{d_R^*} - \frac{1}{d_0} \right) - \frac{\dot{m}_R}{\rho} \left(\frac{1}{d_R^{*2}} - \frac{1}{d_0^2} \right) \right]$$


$$\frac{\dot{m}_R}{\rho} \simeq s\lambda_R + \frac{\tan \beta_R}{6\mu} \cdot \delta_R (p_{sh} - p_{atm})$$

$$\lambda_R = \frac{d_0 d_R^*}{d_0 + d_R^*}$$

$$\delta_R = \frac{d_0^2 d_R^{*2}}{d_0^2 - d_R^{*2}}$$

TANGENTIAL AND NORMAL FORCES

ON THE SHOE AND ROLL

$$\int_0^{L_R} (p_R(x) - \bar{p}_R) dx \equiv N_{sl}^R = \frac{6\mu L_R}{\tan \beta_R} \left(\frac{\eta_R}{d_R^2} - \frac{s}{d_0} \right) + \frac{6\mu s}{\tan^2 \beta_R} \ln \left(\frac{d_0}{d_R^*} \right) - \frac{6\mu \eta_R}{\tan^2 \beta_R} \left(\frac{1}{d_R^*} - \frac{1}{d_0} \right)$$

$$\eta_R = m_R / s$$

$$\int_0^{L_C} (p_C(x) - \bar{p}_C) dx \equiv N_{sl}^C = \frac{6\mu L_C}{\tan \beta_C} \left(\frac{s}{d_0} + \frac{\eta_C}{d_0^2} \right) - \frac{6\mu s}{\tan^2 \beta_C} \ln \left(\frac{d_0}{d_C^*} \right) - \frac{6\mu \eta_C}{\tan^2 \beta_C} \left(\frac{1}{d_C^*} - \frac{1}{d_0} \right)$$

$$\eta_C = m_C / s$$

$$N_{sh}^R = -N_{sl}^R, \quad N_{sh}^C = -N_{sl}^C$$

$$N_{sl}^{net} = N_{sl}^R + N_{sl}^C$$

$$\left\{ \begin{aligned} \mathcal{J}_{sh}^R &= -\mu \int_0^{l_R \cos \beta_R} \left(\frac{\partial u_R}{\partial y}(x, y) \Big|_{y=d_R(x)} \right) dx \\ \frac{\partial u_R}{\partial y} &= \frac{C_R(x)}{2\mu} (d_R(x) - 2y) - \frac{s}{d_R(x)} \\ \mathcal{J}_{sh}^R &= \frac{6\mu n_R}{\rho \tan \beta_R} \left[\frac{1}{d_R^*} - \frac{1}{d_0} \right] - \frac{2\mu s}{\tan \beta_R} \ln \left[\frac{d_0}{d_R^*} \right] \end{aligned} \right.$$

$$\left\{ \begin{aligned} \mathcal{J}_{sh}^C &= -\mu \int_0^{l_C \cos \beta_C} \left(\frac{\partial u_C}{\partial y}(x, y) \Big|_{y=d_C(x)} \right) dx \\ \frac{\partial u_C}{\partial y} &= \frac{C_C(x)}{2\mu} (d_C(x) - 2y) + \frac{s}{d_C(x)} \\ \mathcal{J}_{sh}^C &= \frac{6\mu n_C}{\rho \tan \beta_C} \left(\frac{1}{d_C^*} - \frac{1}{d_0} \right) + \frac{2\mu s}{\tan \beta_C} \ln \left[\frac{d_0}{d_C^*} \right] \end{aligned} \right.$$

n.b. : $\dot{m}_C \leftarrow$

TO ADD : $\dot{m}_C \rightarrow -\dot{m}_C$

$$\begin{aligned}
\mathcal{J}_{\text{sh}}^{\text{net}} &= \mathcal{J}_{\text{sh}}^{\mathcal{R}} + \mathcal{J}_{\text{sh}}^{\mathcal{C}} \\
&= 2\mu\text{s} \ln \left[\left(\frac{d_0}{d_c^*} \right)^{\frac{1}{\tan \beta_{\mathcal{C}}}} / \left(\frac{d_0}{d_r^*} \right)^{\frac{1}{\tan \beta_{\mathcal{R}}}} \right] \\
&\quad + \frac{6\mu\text{m}\tau}{\rho \tan \beta_{\mathcal{R}}} \left[\frac{1}{d_r^*} - \frac{1}{d_0} \right] - \frac{6\mu\text{m}\tau}{\rho \tan \beta_{\mathcal{C}}} \left[\frac{1}{d_c^*} - \frac{1}{d_0} \right]
\end{aligned}$$

$$\mathcal{J}_{\text{sl}}^{\mathcal{R}} = -\frac{6\mu\text{m}\tau}{\rho \tan \beta_{\mathcal{R}}} \left[\frac{1}{d_r^*} - \frac{1}{d_0} \right] + \frac{4\mu\text{s}}{\tan \beta_{\mathcal{R}}} \ln \left[\frac{d_0}{d_r^*} \right]$$

$$\mathcal{J}_{\text{sl}}^{\mathcal{C}} = -\frac{6\mu\text{m}\tau}{\rho \tan \beta_{\mathcal{C}}} \left(\frac{1}{d_c^*} - \frac{1}{d_0} \right) - \frac{4\mu\text{s}}{\tan \beta_{\mathcal{C}}} \ln \left[\frac{d_0}{d_c^*} \right]$$

$i_{\mathcal{L}} \rightarrow -i_{\mathcal{L}}$

$$\begin{aligned}
\mathcal{J}_{\text{sl}}^{\text{net}} &= \mathcal{J}_{\text{sl}}^{\mathcal{R}} + \mathcal{J}_{\text{sl}}^{\mathcal{C}} \\
&= 4\mu\text{s} \ln \left[\left(\frac{d_0}{d_r^*} \right)^{\frac{1}{\tan \beta_{\mathcal{R}}}} / \left(\frac{d_0}{d_c^*} \right)^{\frac{1}{\tan \beta_{\mathcal{C}}}} \right] \\
&\quad - \frac{6\mu\text{m}\tau}{\rho \tan \beta_{\mathcal{R}}} \left[\frac{1}{d_r^*} - \frac{1}{d_0} \right] + \frac{6\mu\text{m}\tau}{\rho \tan \beta_{\mathcal{C}}} \left[\frac{1}{d_c^*} - \frac{1}{d_0} \right]
\end{aligned}$$

$$\mathcal{J}_{sh} + \mathcal{J}_{s1} = 6\mu s \ln \left[\left(\frac{d_0}{d_c^*} \right)^{\frac{1}{\tan \beta_R}} / \left(\frac{d_0}{d_c^*} \right)^{\frac{1}{\tan \beta_R}} \right]$$

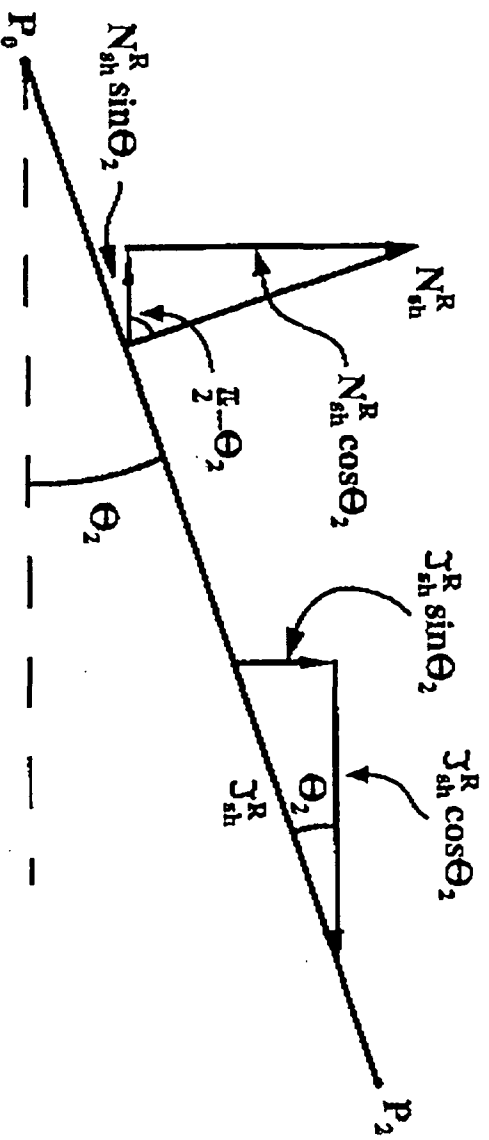
$$\begin{aligned} \mathcal{J}_{sh}^R &= \frac{2\mu s}{\tan \beta_R} \left[3 \left(\frac{d_0 - d_c^*}{d_0 + d_c^*} \right) - \ln \left(\frac{d_0}{d_c^*} \right) \right] \\ &+ \left(\frac{d_0 d_c^*}{d_0 + d_c^*} \right) (\bar{p}_R - P_{atm}). \end{aligned}$$

agrees with Batchelor if $\bar{p}_R = P_{atm}$

$$\mathcal{J}_{sh}^R|_{s=0} = \left(\frac{d_0 d_c^*}{d_0 + d_c^*} \right) (\bar{p}_R - P_{atm})$$

$$\left\{ \begin{aligned} \mathcal{J}_{sh}^L &= \frac{2\mu}{\tan \beta_C} \left[3 \left(\frac{d_0 - d_c^*}{d_0 + d_c^*} \right) + \ln \left(\frac{d_0}{d_c^*} \right) \right] s \\ &- \frac{d_0 d_c^*}{d_0 + d_c^*} (\bar{p}_C - P_{atm}) \\ \mathcal{J}_{sh}^L|_{s=0} &= - \frac{d_0 d_c^*}{d_0 + d_c^*} (\bar{p}_C - P_{atm}) \end{aligned} \right.$$

THE EQUILIBRIUM EQUATIONS



$$F = N_{sh}^R \cos \theta_2 + N_{sh}^L \cos \theta_2' + \mathcal{J}_{sh}^R \sin \theta_2 + \mathcal{J}_{sh}^L \sin \theta_2'$$

$$N_{sh}^L \sin \theta_2' + \mathcal{J}_{sh}^R \cos \theta_2 = -\mathcal{J}_{sh}^L \cos \theta_2' + N_{sh}^R \sin \theta_2$$

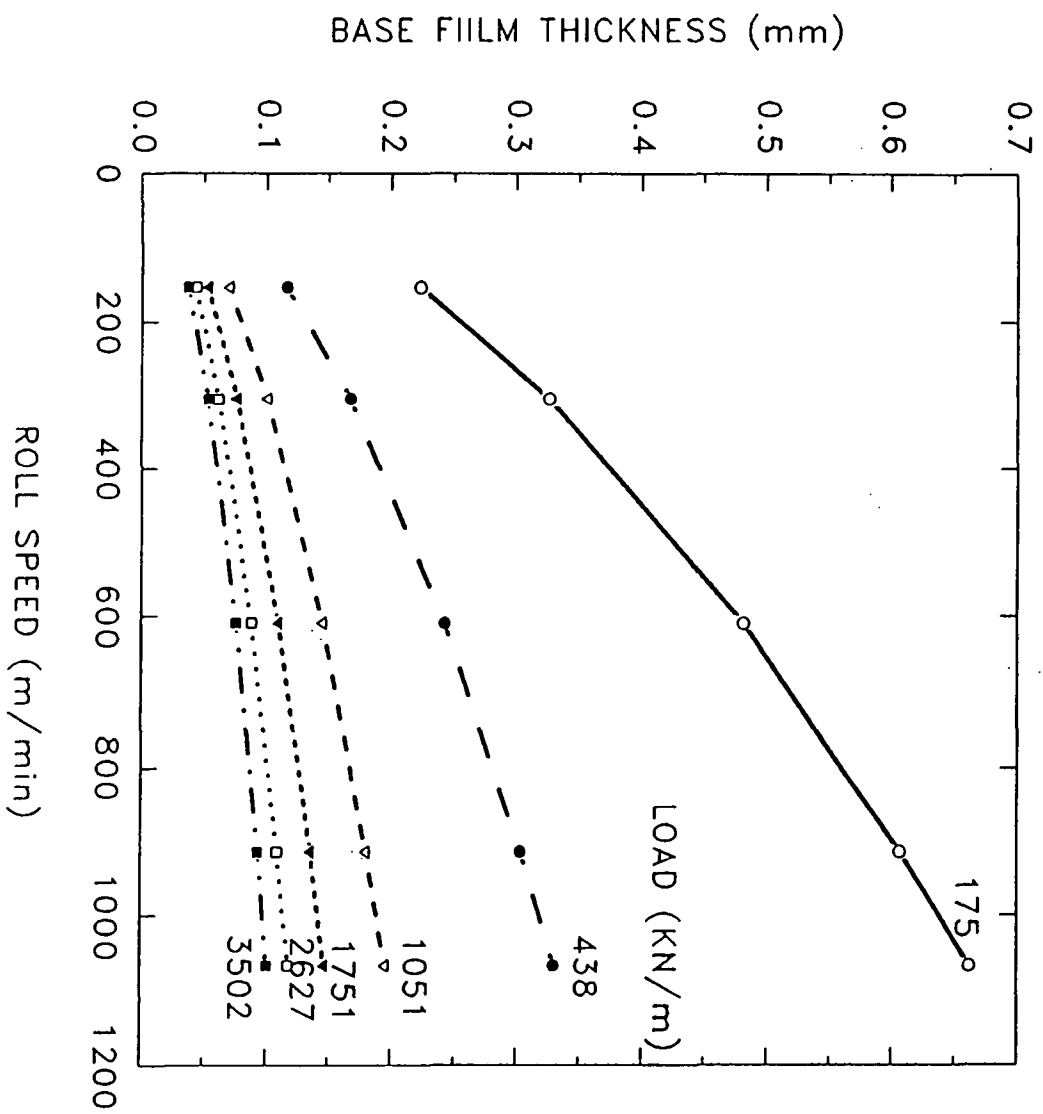
$$G_V(F, s, p_{sh} - p_{atm}, R, \phi, \tilde{R}, \hat{R}, \mu, \rho; d_0, \psi) = 0$$

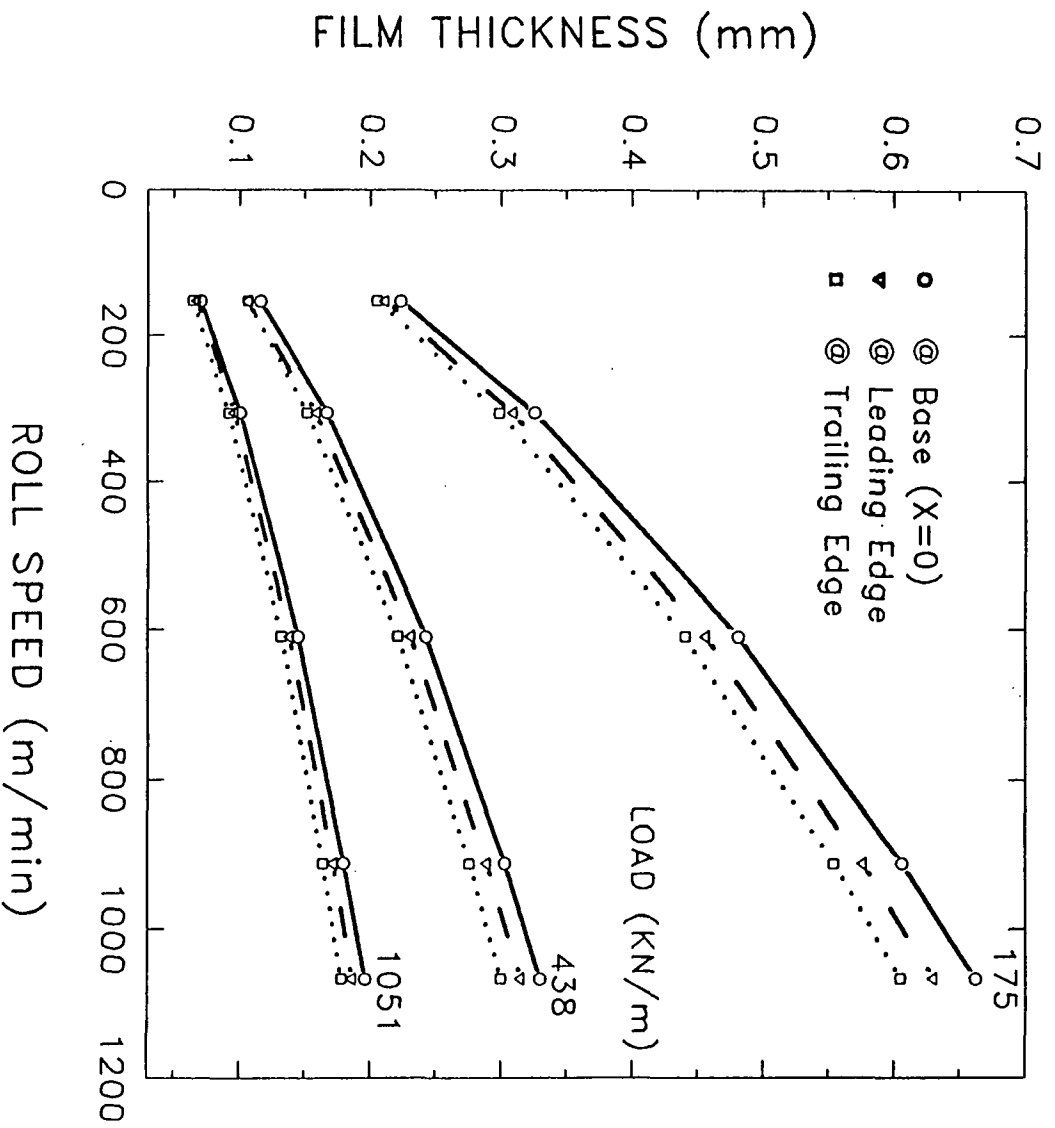
$$G_H(F, s, p_{sh} - p_{atm}, R, \phi, \tilde{R}, \hat{R}, \mu, \rho; d_0, \psi) = 0$$

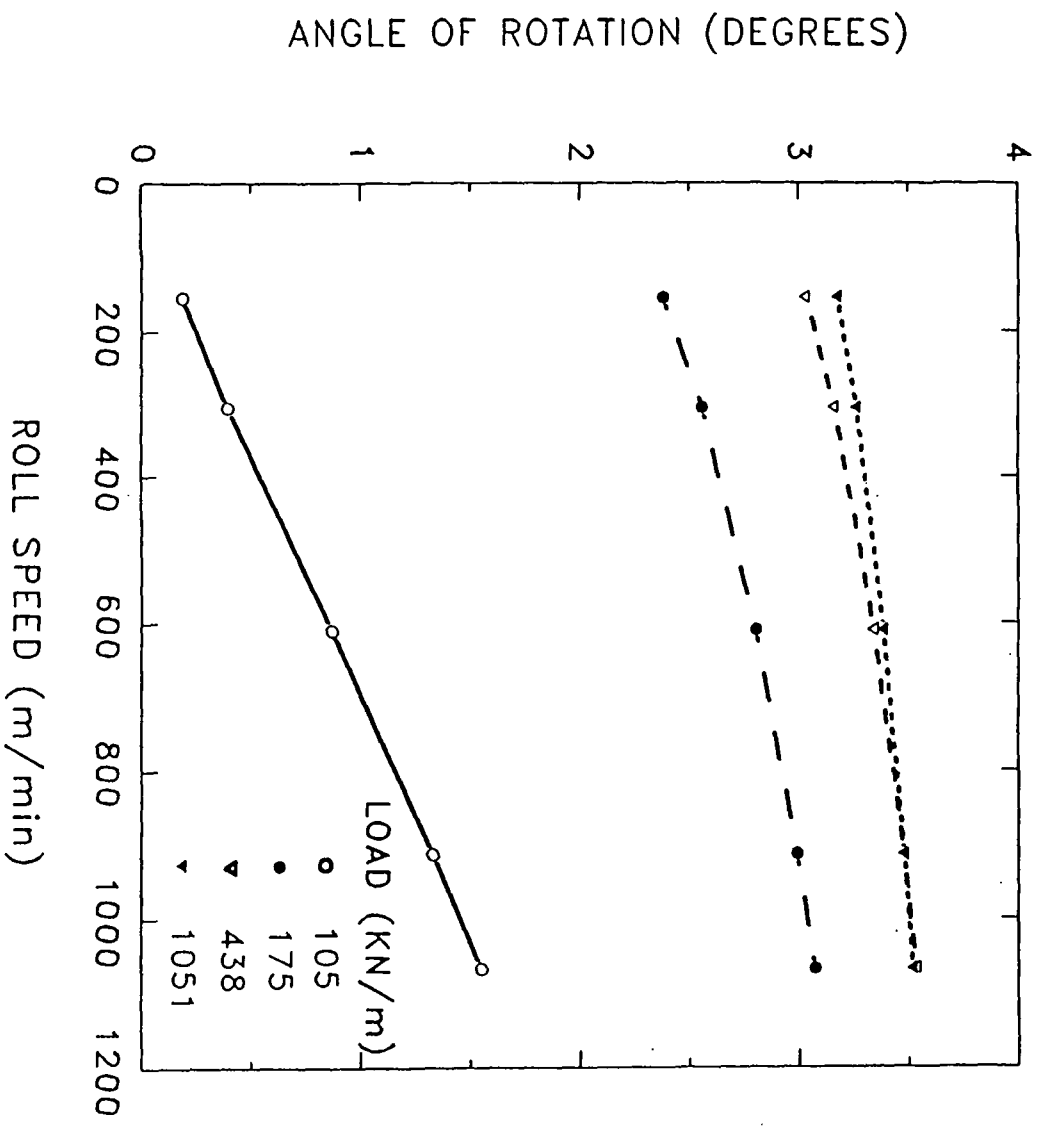
$$\mathcal{P} = \{F, s, p_{sh} - p_{atm}, R, \phi, \tilde{R}, \hat{R}, \mu, \rho\}$$

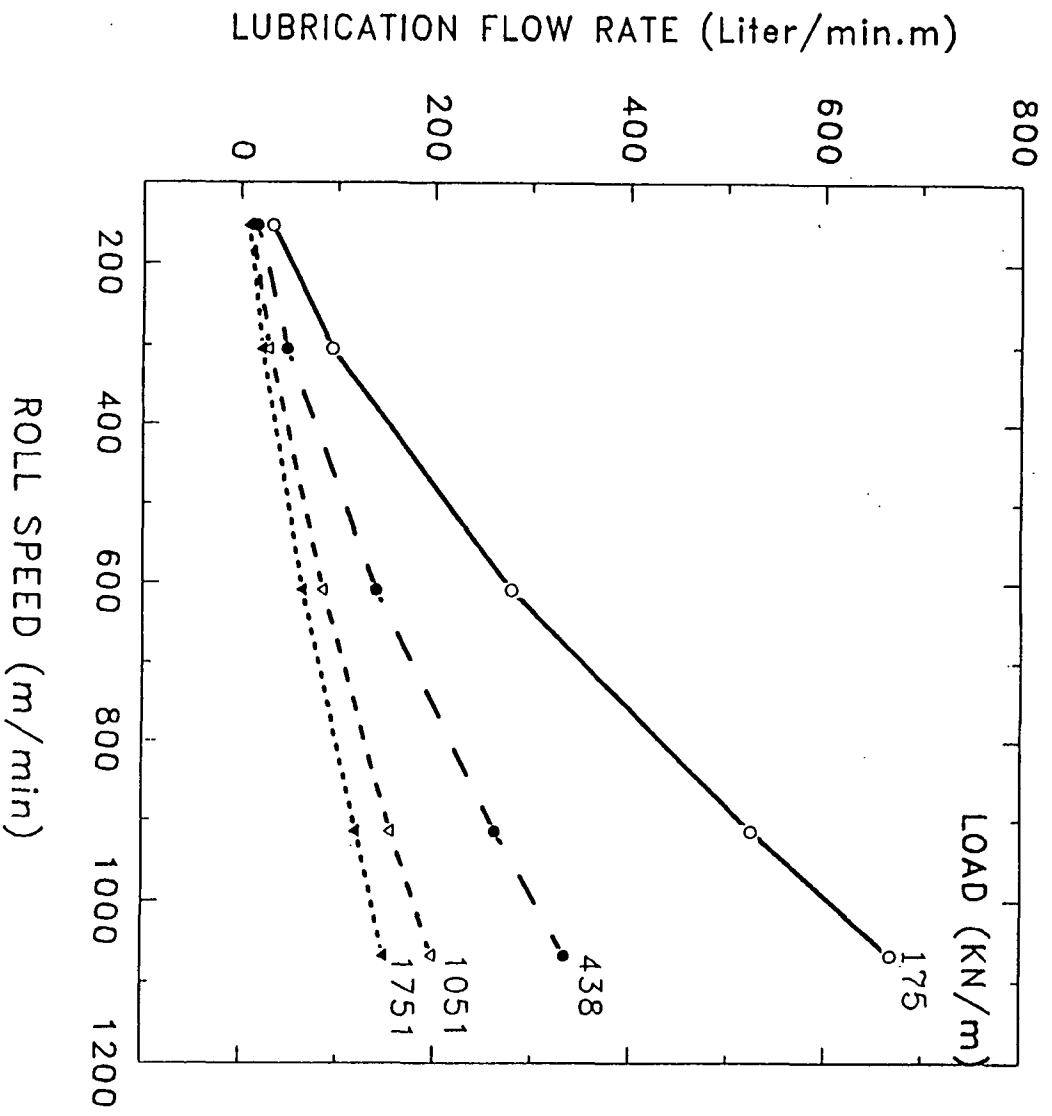
$$\begin{aligned}
u_{\mathcal{R}}(x, y) &= \frac{C_{\mathcal{R}}(x)}{2\mu} y(d_{\mathcal{R}}(x) - y) + s \left(\frac{d_{\mathcal{R}}(x) - y}{d_{\mathcal{R}}(x)} \right) \\
&= \frac{1}{2\mu} \left[\frac{12\mu\dot{m}_{\mathcal{R}}}{\rho} d_{\mathcal{R}}^{-3}(x) - 6\mu s d_{\mathcal{R}}^{-2}(x) \right] y(d_{\mathcal{R}}(x) - y) \\
&\quad + s(1 - y d_{\mathcal{R}}^{-1}(x)) \\
&= -\frac{6\dot{m}_{\mathcal{R}}}{\rho} y^2 d_{\mathcal{R}}^{-3}(x) + \left[\frac{6\dot{m}_{\mathcal{R}}}{\rho} y + 3s y^2 \right] d_{\mathcal{R}}^{-2}(x) \\
&\quad - 4s y d_{\mathcal{R}}^{-1}(x) + s
\end{aligned}$$

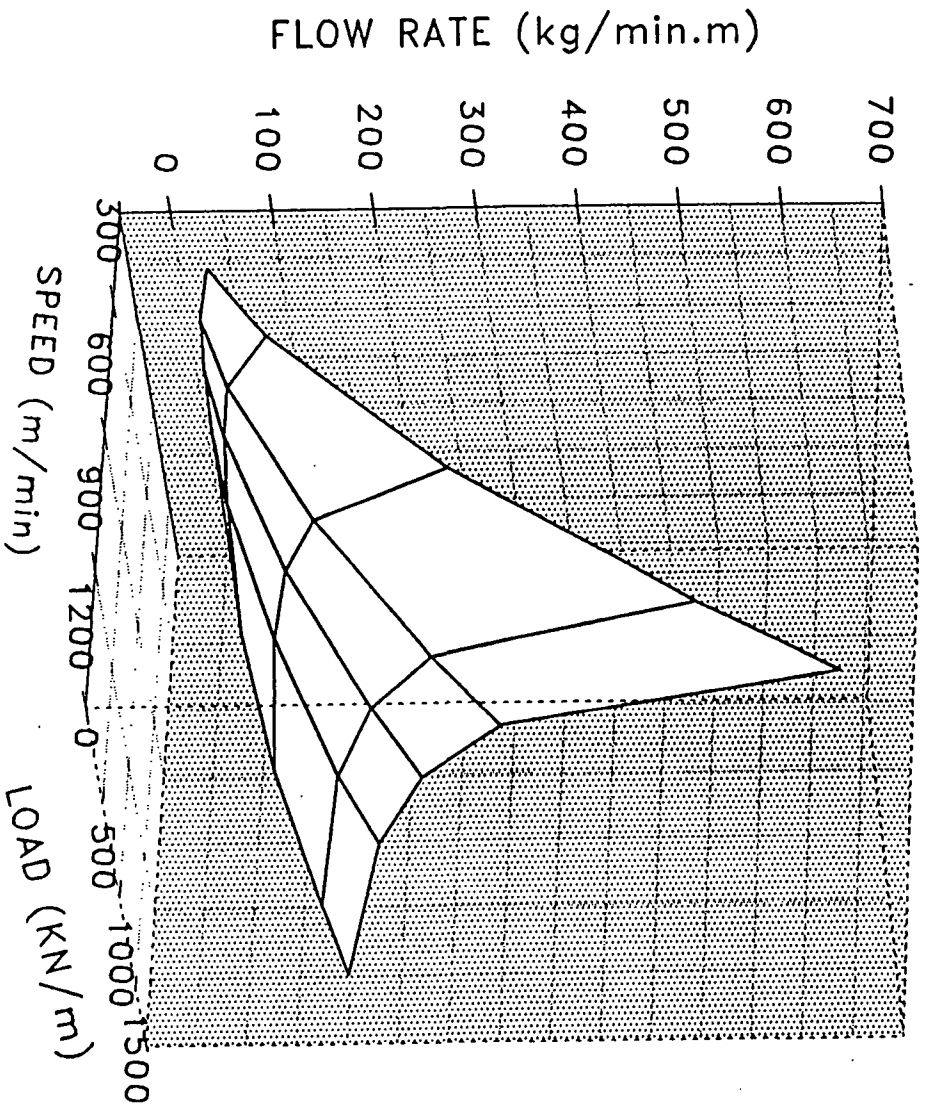
$$\begin{aligned}
u_{\mathcal{L}}(x, y) &= \frac{C_{\mathcal{L}}(x)}{2\mu} y(d_{\mathcal{L}}(x) - y) - s \left(\frac{d_{\mathcal{L}}(x) - y}{d_{\mathcal{L}}(x)} \right) \\
&= \frac{1}{2\mu} \left[\frac{12\mu\dot{m}_{\mathcal{L}}}{\rho} d_{\mathcal{L}}^{-3}(x) + 6\mu s d_{\mathcal{L}}^{-2}(x) \right] y(d_{\mathcal{L}}(x) - y) \\
&\quad - s(1 - y d_{\mathcal{L}}^{-1}(x)) \\
&= -\frac{6\dot{m}_{\mathcal{L}}}{\rho} y^2 d_{\mathcal{L}}^{-3}(x) + \left[\frac{6\dot{m}_{\mathcal{L}}}{\rho} y - 3s y^2 \right] d_{\mathcal{L}}^{-2}(x) \\
&\quad + 4s y d_{\mathcal{L}}^{-1}(x) - s
\end{aligned}$$

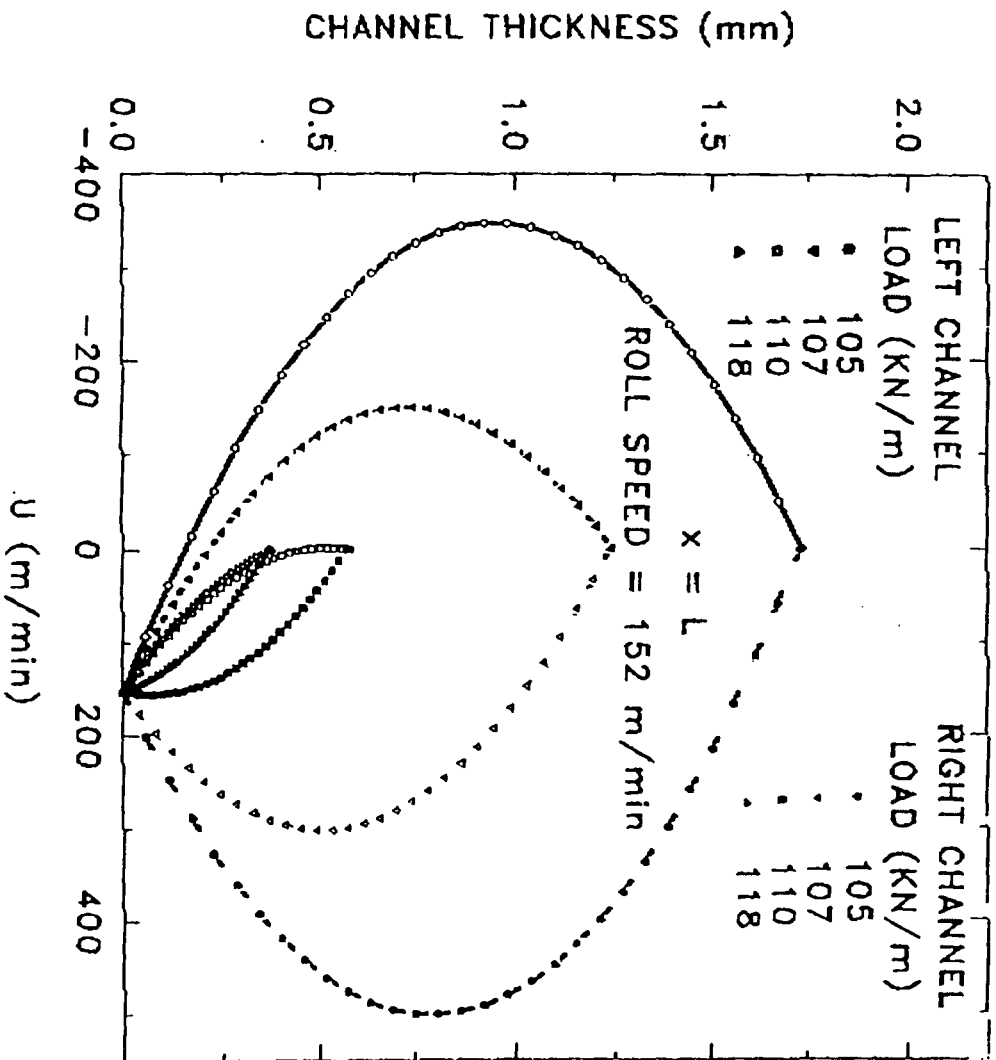


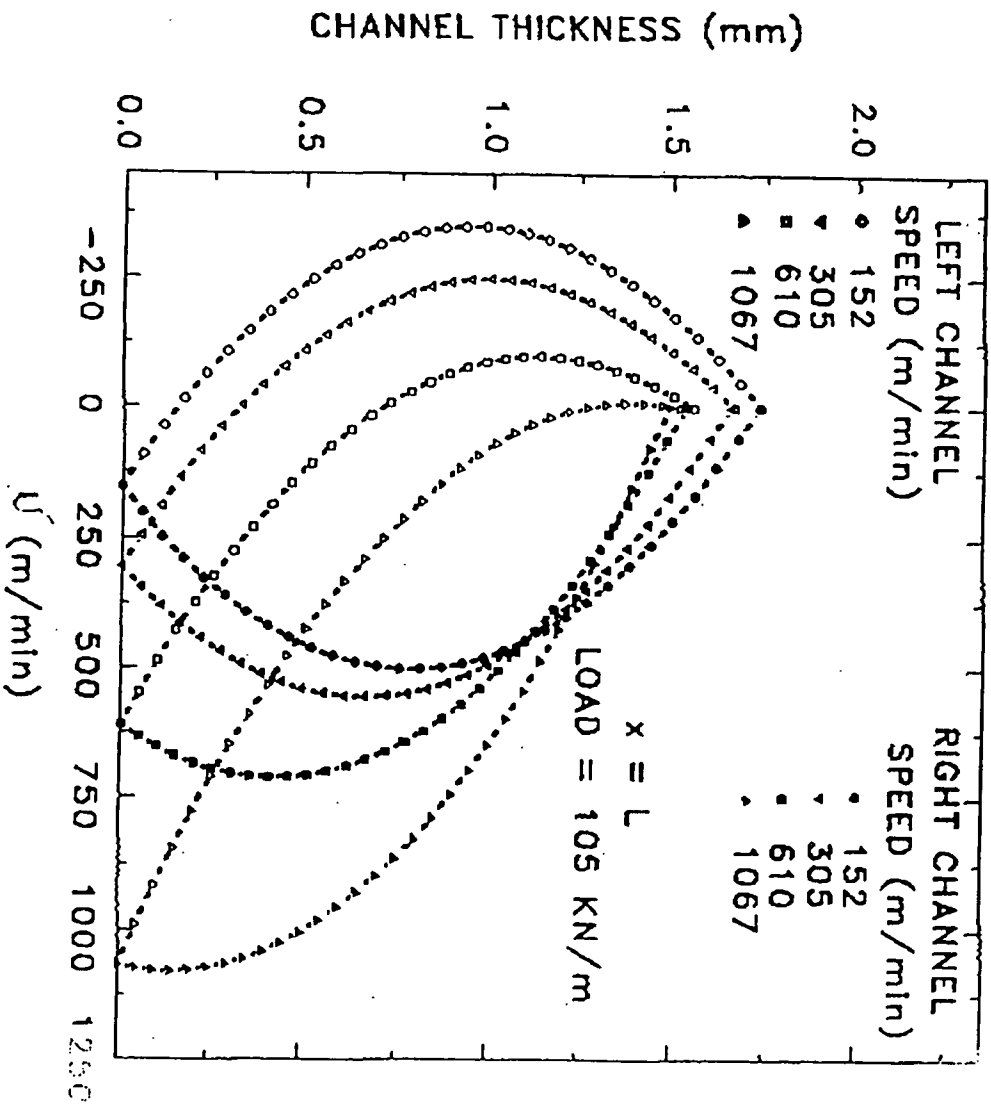


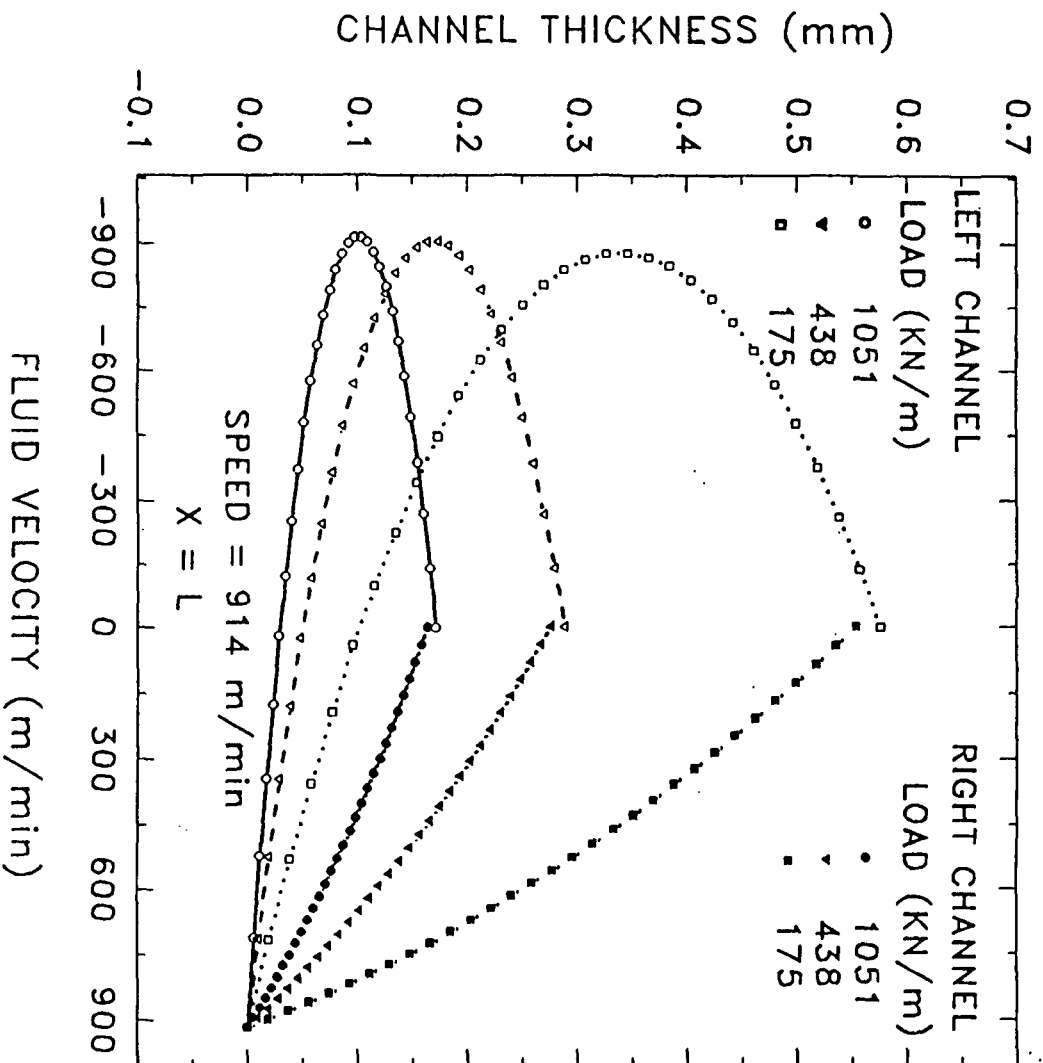


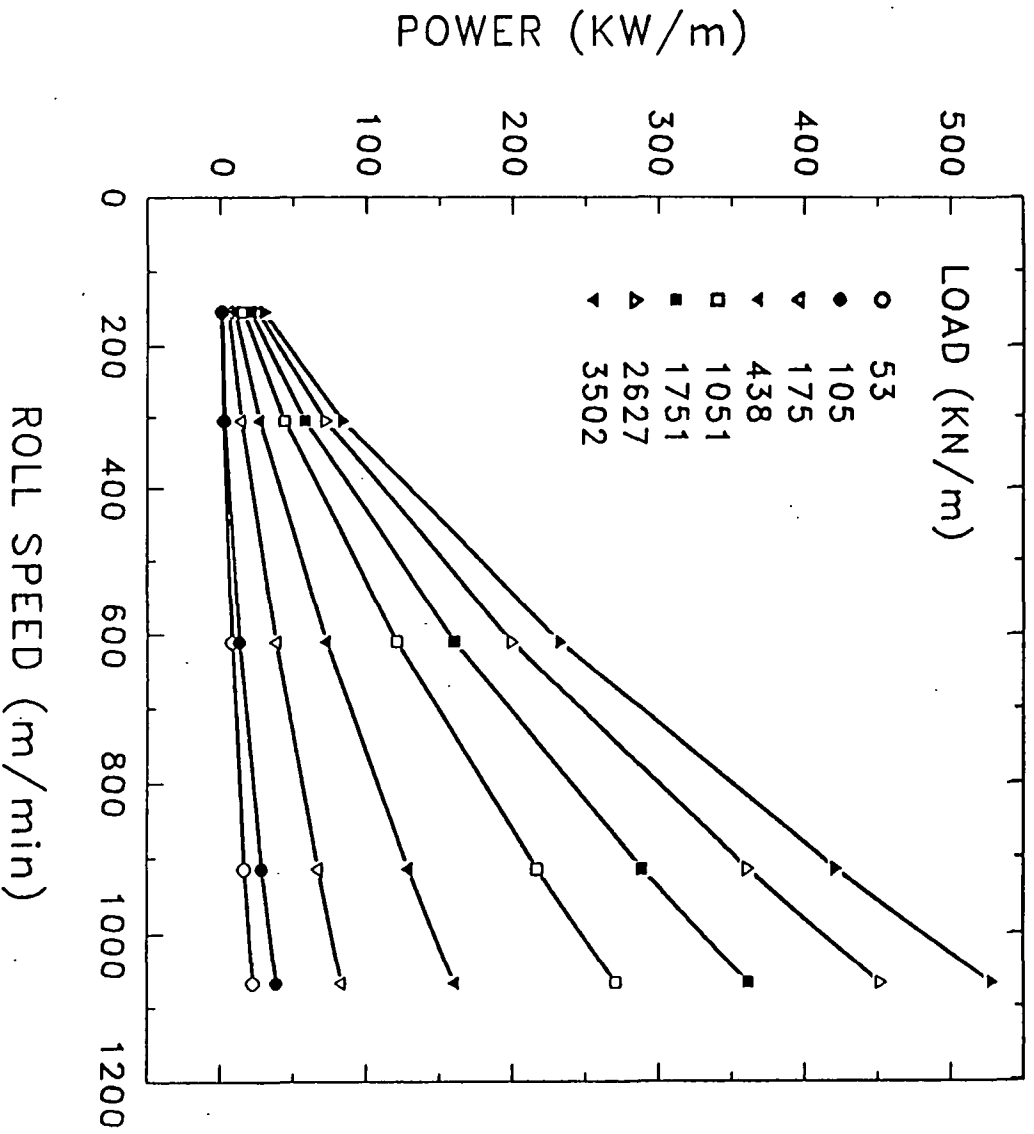


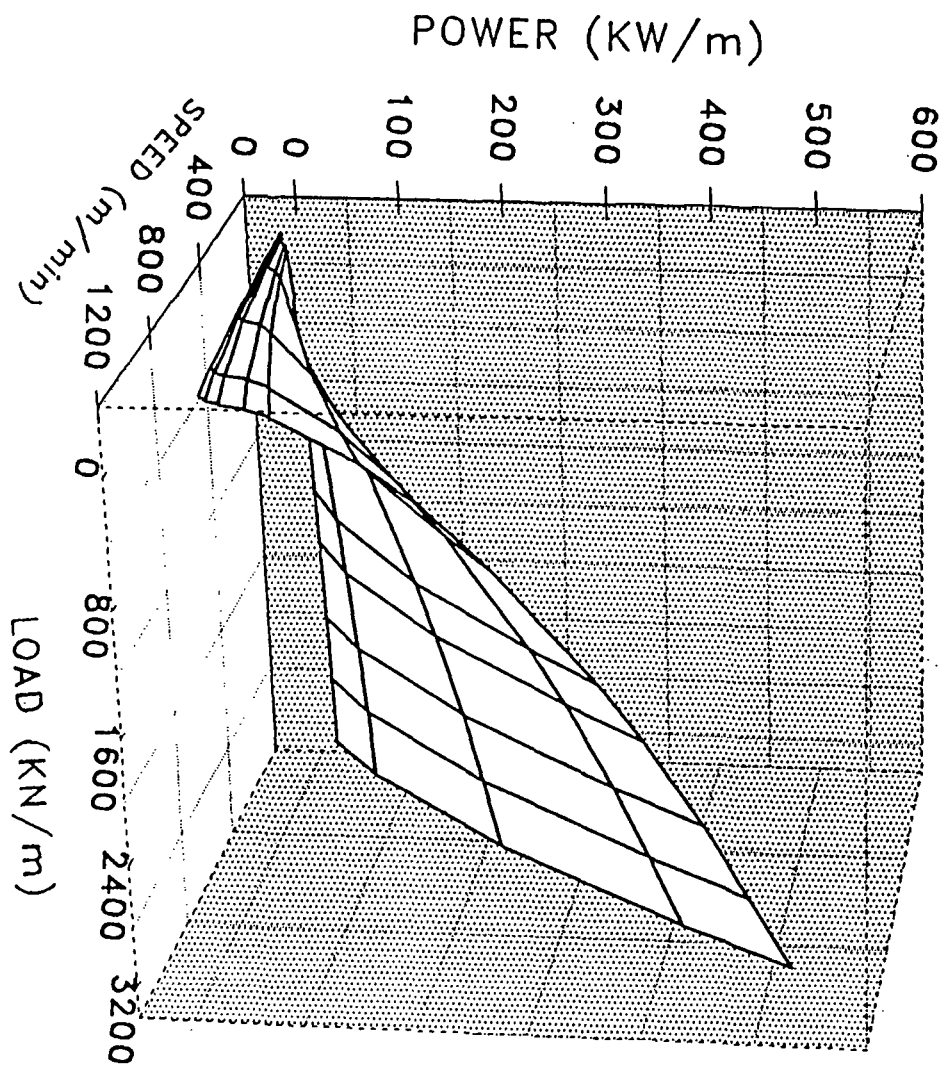


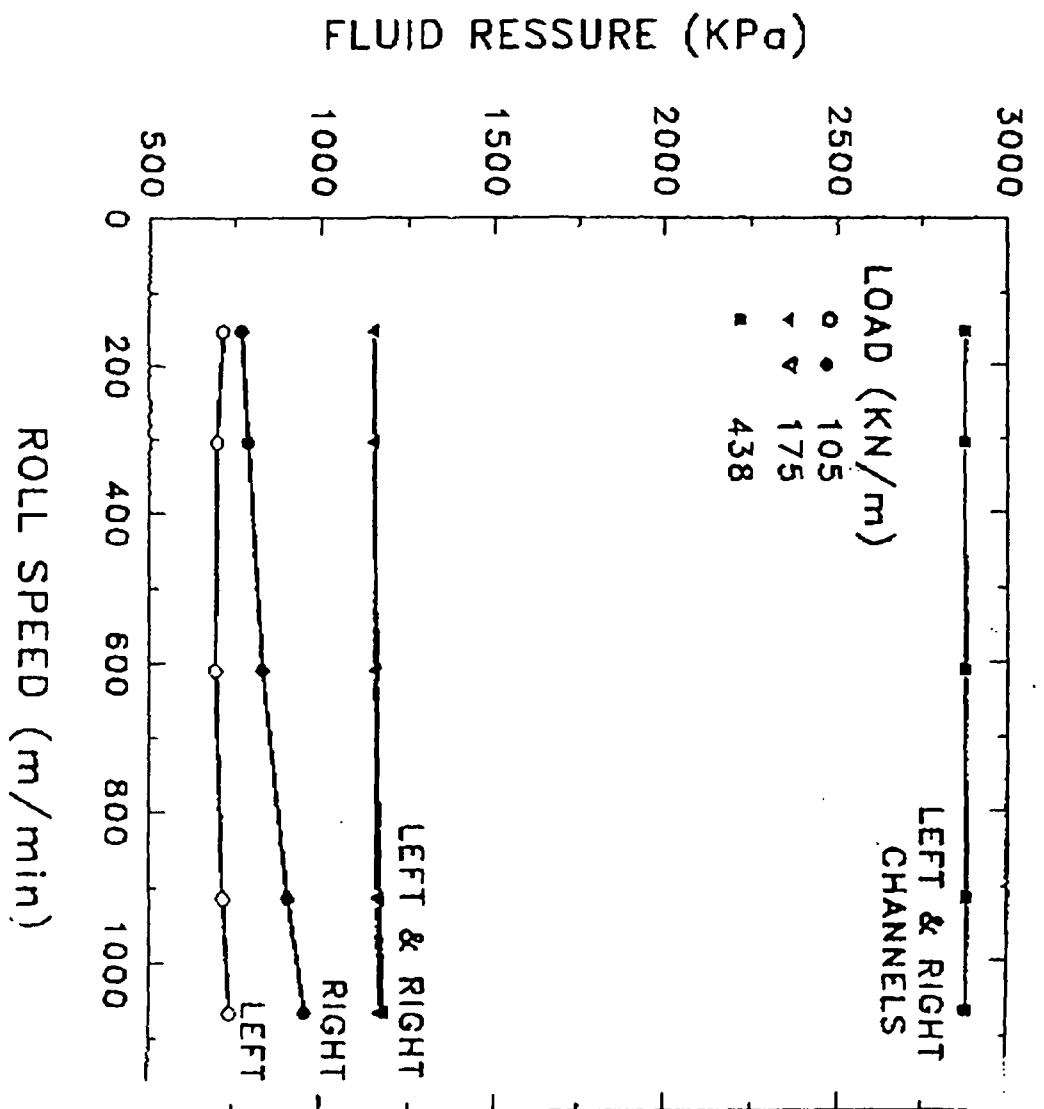












\tilde{P}_R AND \tilde{P}_C

